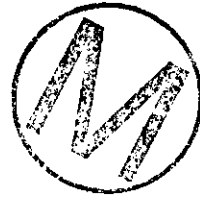# Title 40 CFR Part 191
Compliance Certification
Application
for the
Waste Isolation Pilot Plant

MASS Attachment 18-1

THIS PAGE INTENTIONALLY LEFT BLANK

Sandia National Laboratories

Albuquerque, New Mexico 87185-1341

date: March 20, 1996

to: Martin Tierney, MS 1328, Dept. 6741

from: Geoff Freeze, MS 1324, Dept. 6115 (INTERA)
Kurt Larson, MS 1341, Dept. 6751

subject: Initial Pressure in the Castile Brine Reservior

The initial brine pressure in the Castile brine reservoir to be used in BRAGFLO calculations for the 1996 WIPP Compliance Certification Application calculations is specified in this memorandum. The pressure was determined in a meeting held March 19, 1996. In attendance were Rip Anderson, Palmer Vaughn, Jon Helton, Peter Davies, Al Lappin, Peter Swift, Geoff Freeze, and Kurt Larson, and perhaps others. The pressure specified in this memorandum supercedes the pressure specified in an earlier memorandum. The pressures are being changed because the range specified in the earlier memorandum has been considered further and is now thought to be unduly conservative because it is inconsistent with available evidence on the pressures encountered in anhydrite intervals in the region of the WIPP.

The group reached consensus on the approach to be used for determining the pressures, as well as the pressures to be used. These will be described in a separate document that is in preparation at the time of this memorandum.

The pressure in the brine reservoir is to be sampled in the range of 11.1 to 17 MPa (1.11×10^7 to 1.7×10^7 Pa). The distribution is triangular with a mode at 12.7 MPa (1.27×10^7 Pa).

Distribution:
Lori Dotson   MS 1341
Kurt Larson   Day File
SWCF-A:WBS1.2.07.1:PDD:QA:Non-Salado:PKG#19B:Castile Brine Reservior Pressure (WPO #31072) (2)

Title 40 CFR Part 191
Compliance Certification
Application
for the
Waste Isolation Pilot Plant

MASS Attachment 18-2

THIS PAGE INTENTIONALLY LEFT BLANK

Package received from Kurt Larson 960524/un

Sandia National Laboratories

Albuquerque, New Mexico 87185

date: May 20, 1996

to: SWCF-A Records Center
SWCF-A:WBS1.2.07.1:PDD:QA:NONSALADO:
PKG#19:CASTILE BRINE RESERVOIR PRESSURE

In Kurt - this has been approved and supersedes the earlier records pkg. 960529/un

from: Geoff Freeze, INTERA
Kurt Larson, SNL

subject: Castile Brine Reservoir Pressure Record Package

This memo describes a two-step process for assignment of initial fluid pressure in the Castile brine reservoir for use in BRAGFLO simulations. The first step is to examine the relationship between fluid pressures and lithostatic pressures in anhydrite units in the Salado and Castile formations. The second step is to examine observed Castile brine reservoir pressures and adjust them to WIPP-12 depth, representative of the depth of the BRAGFLO Castile brine reservoir. Adjustments assume either a hydrostatic or near lithostatic (as determined in step 1) correction. The resulting adjusted pressures are used to develop a range for use in performance assessment.

Table 1 compares observed (measured and interpreted) Castile brine reservoir fluid pressures with corresponding lithostatic pressures. Observed pressures are from TME-3153 (Table H.1) except where indicated. Lithostatic pressures are from SAND92-0700/3 (based on WIPP-11 density log shown in Figure 2.3-13).

Table 1. Fluid and Lithostatic Pressures for Castile Brine Reservoirs

Location	Fluid Pressure at Reservoir Depth (MPa)	Lithostatic Pressure at Reservoir Depth (MPa)	Fluid Pressure as a % of Lithostatic Pressure
Pogo	17.4	21	83
Tidewater	16.0	22	64
Union	10.1	18	56
H&W Danford 1	7.0	14	50
Bilbrey	11.2	19	59
Culbertson	12.8	21	56
Mascho 1	12.4	21	57
Mascho 2	12.0	21	59
Shell	13.4	22	54
WIPP-12	12.7*	20	64
ERDA-6	14.1	18	78
Belco	14.3	20	72
Gulf Covington	13.6	22	62

* from SAND89-7069, Appendix A

Additional estimates of anhydrite fluid pressure are available from the Salado (SWCF-A:WBS 1.2.07.1:PDD:QA:SALADO:PKG12:Anhydrite Pressure). The lithostatic pressure at the measurement depth is 15 MPa. Interpreted values are 12.9, 12.4, 12.3, 11.1, and 9.4 MPa. The corresponding percentages of lithostatic pressure are 86, 83, 82, 74, and 63, respectively.

For the 18 fluid pressures (13 Castile, 5 Salado), the percentage of lithostatic rages from 50 to 86% with an average value of 67% and a median value of 64%. Based on this data, and on the fact that some of Castile measured pressures are minimum pressures (flow was above ground surface), the maximum fluid pressure in the Castile brine reservoir is assumed to be 85% of lithostatic.

For the 4 locations where measured or interpreted values best represent formation pressure (i.e., not minimums), the measured values are adjusted to reflect formation pressure at the depth of the WIPP-12 reservoir (140 masl). The pressure adjustment requires an assumption about pressure variation with depth in the Castile. Two bounding cases are used, hydrostatic and 85% of lithostatic, with the adjusted pressures calculated as follows:

$$P_a = P + \rho g \,(h - 140) / 1 \times 10^{-6}$$

where:

P_a = adjusted pressure [Mpa]
P = measured/estimated pressure [Mpa]
ρ = assumed density [kg/m^3]
g = gravitational constant [9.8 N/kg]
h = brine reservoir elevation [masl]

A brine density of 1,240 kg/m^3 (SAND89-7069; p. 2-12) was assumed for the hydrostatic variation, an average formation density of 0.85*2,400 kg/m^3 (SAND92-0700/3; p 4-14) was assumed for the lithostatic variation. The adjusted pressures are shown in Table 2.

Table 2. Adjusted Castile Brine Reservoir Formation Pressures

Location	Pressure at Reservoir Depth (MPa)	Pressure at WIPP-12 Depth with Hydrostatic Adjustment (MPa)	Pressure at WIPP-12 Depth with 85% Lithostatic Adjustment (MPa)
WIPP-12	12.7[b]	12.7	12.7
ERDA-6	14.1[a]	15.5	16.4
Belco	14.3[a]	14.5	14.5
Gulf Covington	13.6[a]	12.1	11.1
[a]from TME-3153, Table H.1 [b]from SAND89-7069, Appendix A			

All of these measured and adjusted values should be considered in the range of values used in performance assessment calculations. Because the BRAGFLO brine reservoir is assumed to have

WIPP-12 properties, the best measured value is the interpreted WIPP-12 pressure of 12.7 MPa. Minimum and maximum pressures are 11.1 MPa and 16.4 MPa, respectively. At WIPP-12 reservoir depth 85% of lithostatic pressure (20 MPa) is 17 MPa. Because this value is greater than the maximum value from Table 2, it is used to define the upper end of the brine reservoir pressure range.

Based on the above information, the following distribution is proposed Castile brine reservoir initial pressure:

Distribution: Triangular
Minimum: 11.1 MPa
Mode: 12.7 MPa
Maximum 17.0 MPa

Title 40 CFR Part 191
Compliance Certification
Application
for the
Waste Isolation Pilot Plant

MASS Attachment 18-3

THIS PAGE INTENTIONALLY LEFT BLANK

WPO 37971

Sandia National Laboratories

Albuquerque, New Mexico 87185-1341

Memorandum of Record

date: May 27, 1996

to: SWCF-A:WBS1.2.07.1:PDD:NON-SALADO:PKG#19C:Castile Brine, Reservoir Volume (WPO #31082)

from: Kurt Larson   Dept. 6822   MS 1341
      Geoff Freeze   Dept. 6115   INTERA

subject: Castile Brine Reservoir Volume Revision

This memorandum records the rationale for selection of a revised brine volume contained in a hypothetical Castile brine reservoir for the 1996 performance assessment calculations for the Compliance Certification Application. This rationale was developed during a meeting held March 19, 1996, as documented in a memorandum to Martin Tierney from Kurt Larson and Geoff Freeze, March 20, 1996, which was submitted to the same records package as this Memorandum of Record.

The volume of brine in the Castile brine reservoir is used in BRAGFLO, and is one of several parameters necessary for estimating the fluid flow in the intrusion borehole resulting from its penetration of the waste panels and a hypothetical brine reservoir. Discussion of other parameters for the brine reservoir is documented elsewhere. The volume of brine used is based on the conceptual model of brine reservoirs, analogy to a tested brine reservoir penetrated within the land withdrawal area by the WIPP-12 borehole, and consideration of the possible effects of deep boreholes assumed to be drilled in the vicinity of WIPP during the regulatory period.

Brine reservoirs in the northern Delaware Basin are believed to be fractured systems, with predominantly vertical or nearly-vertical fractures, and with those fractures spaced widely enough that a borehole can penetrate through a volume of rock containing a brine reservoir without intersecting any fractures and therefore not produce brine. They usually occur in the upper portion of the Castile, in an interval interpreted to be from 7 to 24 meters thick (Reeves et al., 1991). The interconnectivity of fractures is uncertain. Appreciable brine volumes have been produced from several reservoirs, but there is little direct information on the areal extent of the reservoirs. The WIPP-12 data indicates that fractures in the network have a variety of apertures and permeabilities, and their pressure and brine volume decrease at different rates. Brine occurrences in the Castile behave as reservoirs, i.e., they are bounded systems - rather than as aquifers such as groundwater in the Culebra and Magenta. The average porosity of fractures of the WIPP-12 reservoir from which brine can be

Exceptional Service in the National Interest

produced, over its areal extent, is approximately 0.008. This porosity is not the porosity of intergranular voids (although that is likely low as well), but rather is the porosity of a fractured network containing some large-aperture fractures and a large volume of (conceptually) non-porous blocks. Thus, the fracture porosity is not distributed evenly through the medium.

The volume contained within the WIPP-12 reservoir has been estimated by a method described in the previous record package specifying reservoir volumes. Using the values and methods specified there, estimated reservoir pore volumes (bulk volume multiplied by porosity) and their areal extent assuming a circular boundary have been calculated, as shown in Table 1.

Table 1: Estimated brine volume (m³) and effective radius (m) (areal extent assuming a circular boundary) of the brine reservoir encountered at WIPP-12 as a function of interpreted compressibilities and thicknesses.

	$C = 5 \times 10^{-12} \, Pa^{-1}$	$C = 1 \times 10^{-10} \, Pa^{-1}$	$C = 1 \times 10^{-8} \, Pa^{-1}$
7 m thickness	$3.2 \times 10^4 \, m^3$ 430 m	$3.2 \times 10^6 \, m3$ 4300 m	$6.4 \times 10^7 \, m^3$ 19000 m
24 m thickness	$3.2 \times 10^4 \, m^3$ 230 m	$3.2 \times 10^6 \, m^3$ 2300 m	$6.4 \times 10^7 \, m^3$ 10300 m

Table 1 shows that there is uncertainty in both the volume of the brine reservoirs and their areal extent.

The smaller interpreted volumes of the brine reservoir from WIPP-12 are associated with effective radii on the order of several hundred meters. These dimensions are somewhat smaller than the waste panels; this interpretation of the extent of reservoirs is generally but not quantitatively supported by geophysical survey data. The interpreted large volumes are associated with effective radii much larger than the waste panel dimensions, or even the site dimensions. For performance assessment, it is assumed that reservoirs that may exist under the waste panels have limited extent and interconnectivity, with brine volumes consistent with the lower values estimated from the WIPP-12 encounter. The basis for this assumption is discussed in the following paragraphs.

Consistent with regulatory criteria regarding the rate of drilling to be used in performance assessment, it is assumed that 47 deep boreholes may be drilled per square kilometer in the next 10,000 years. Scoping calculations indicate that this drilling rate yields approximately 50-acre spacing of boreholes in the vicinity of the WIPP in 1,000 years, and nearly 5 acre spacing of boreholes at the end of 10,000 years. Even with limited probability of intersecting a brine reservoir, in 1,000 years there should be approximately one intersection per 500 acres, and in 10,000 years approximately 1 intersection per 50 acres. Thus,

penetrations will occur at closely-spaced intervals. In current practice, when a problematic brine reservoir is encountered drillers allow the well to flow until it is safe to continue drilling; total volumes produced and the time allowed for flow vary, depending on the driller and conditions. Even if the driller does continue to drill, the reservoir will be partially depleted by flow that occurs during drilling. Thus, every time a reservoir is penetrated, it is partially depleted. If reservoirs are well-interconnected, they will be penetrated and partially depleted many times during 10,000 years, until at some time penetrating a reservoir no longer produces flow. If reservoirs are poorly-interconnected, regions of undisturbed pressure and volume could persist, although these would have lower producible brine volumes due to their limited extent.

There is an area in which potential brine reservoirs cannot be penetrated and depleted for some time - under the waste panels while passive institutional controls are effective. The passive institutional controls shield a region of the Castile from exploratory drilling. If brine reservoirs are well-interconnected, the sheltered region could be depleted by the effects of multiple penetrations occurring in unprotected areas. If brine reservoirs are poorly-interconnected, they could persevere under undisturbed conditions under the panels. It is considered that there are two reasonable conceptual models consistent with regulatory guidance for the future condition of brine reservoirs in the WIPP region: (1) they are interconnected over large areas and penetrated and partially depleted many times; or (2) they are interconnected over small areas and not affected by the penetrations that occur far away. It is considered that penetrating a undisturbed pressure and volume, smaller reservoir through the waste panels has potentially greater consequences than penetrating a depleted large reservoir. Therefore, the latter model is assumed: brine in the Castile potentially under the waste panels is hydraulically poorly-interconnected (with extent similar to the lower estimates from WIPP-12), not much affected by penetrations occurring far away, and can persevere with pristine conditions until it is penetrated by a borehole drilled within the panel area.

The minimum pore volume of the brine reservoir used in BRAGFLO should be the minimum volume obtained from WIPP-12 analysis, 32000 cubic meters. Because this volume WIPP-12 reservoir is associated with an estimated effective area of about 1/3 of the waste panel area, and because a reservoir with a volume larger than the minimum WIPP-12 volume could reasonably exist under the waste panels, larger reservoir volumes should also be used. A total of five different volumes of brine should be used in performance assessment for determining the consequence of first penetration of a brine reservoir: 32000, 64000, 96000, 128000, and 160000 cubic meters.

Reference:
Reeves, M., G.A. Freeze, V.A. Kelley, J.F. Pickens, D.T. Upton, and P.B. Davies, 1991. Regional Double-Porosity Solute Transport in the Culebra Dolomite under Brine-Reservoir-Breach Conditions: An Analysis of Parameter Sensitivity and Importance. SAND89-7069. Sandia National Laboratories: Albuquerque, N.M.
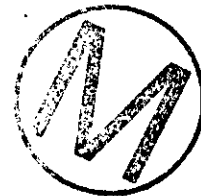
Copy To:

Peter Swift	MS 1341
Lori Dotson	MS 1341
Kurt Larson	Day File
Rip Anderson	MS 1328
Jon Helton	MS 1328
Palmer Vaughn	MS 1328
Peter Davies	MS 1324
Al Lappin	MS 1324

Title 40 CFR Part 191
Compliance Certification
Application
for the
Waste Isolation Pilot Plant

MASS Attachment 18-4

THIS PAGE INTENTIONALLY LEFT BLANK

Sandia National Laboratories

Albuquerque, New Mexico 87185-MS1328

INFORMATION ONLY

date: March 21, 1996

to: Martin Tierney

from: Jon Helton

subject: Addition of Discrete Parameter

Please add a discrete parameter to the data base that takes on values 1 to 32, with equal probability (i.e., 1/32) assigned to each value. This parameter will be used to select brine pocket fields for use in calculations with BRAGFLO, CCDFGF and GRIDFLO. Possible brine pocket locations (l= 1,2,3,4,5) are shown in Attachment A. A single brine pocket field in designated by a vector of the form $(l_1, l_2, l_3, l_4, l_5)$, where $l_i = 0$ implies the absence of pressurized brine at location i and $l_i = 1$ implies the presence of pressurized brine at location i. The following correspondence exists between the integers 1, 2, ..., 32 and the brine pocket fields:

	1	2	3	4	5	TOTAL # of Brine Pockets
1~	0	0	0	0	0	0
2~	0	0	0	0	1	1
3~	0	0	0	1	0	1
4~	0	0	0	1	1	2
5~	0	0	1	0	0	1
6~	0	0	1	0	1	2
7~	0	0	1	1	0	2
8~	0	0	1	1	1	3
9~	0	1	0	0	0	1
10~	0	1	0	0	1	2
11~	0	1	0	1	0	2
12~	0	1	0	1	1	3
13~	0	1	1	0	0	2
14~	0	1	1	0	1	3
15~	0	1	1	1	0	3
16~	0	1	1	1	1	4
17~	1	0	0	0	0	1
18~	1	0	0	0	1	2
19~	1	0	0	1	0	2
20~	1	0	0	1	1	3
21~	1	0	1	0	0	2
22~	1	0	1	0	1	3
23~	1	0	1	1	0	3
24~	1	0	1	1	1	4
25~	1	1	0	0	0	2
26~	1	1	0	0	1	3
27~	1	1	0	1	0	3
28~	1	1	0	1	1	4
29~	1	1	1	0	0	3
30~	1	1	1	0	1	4
31~	1	1	1	1	0	4
32~	1	1	1	1	1	5

EN1: Definition of Distribution D_L for Drilling Location

- Discretize repository into finite number of locations
- Define D_L on basis of area associated with each location
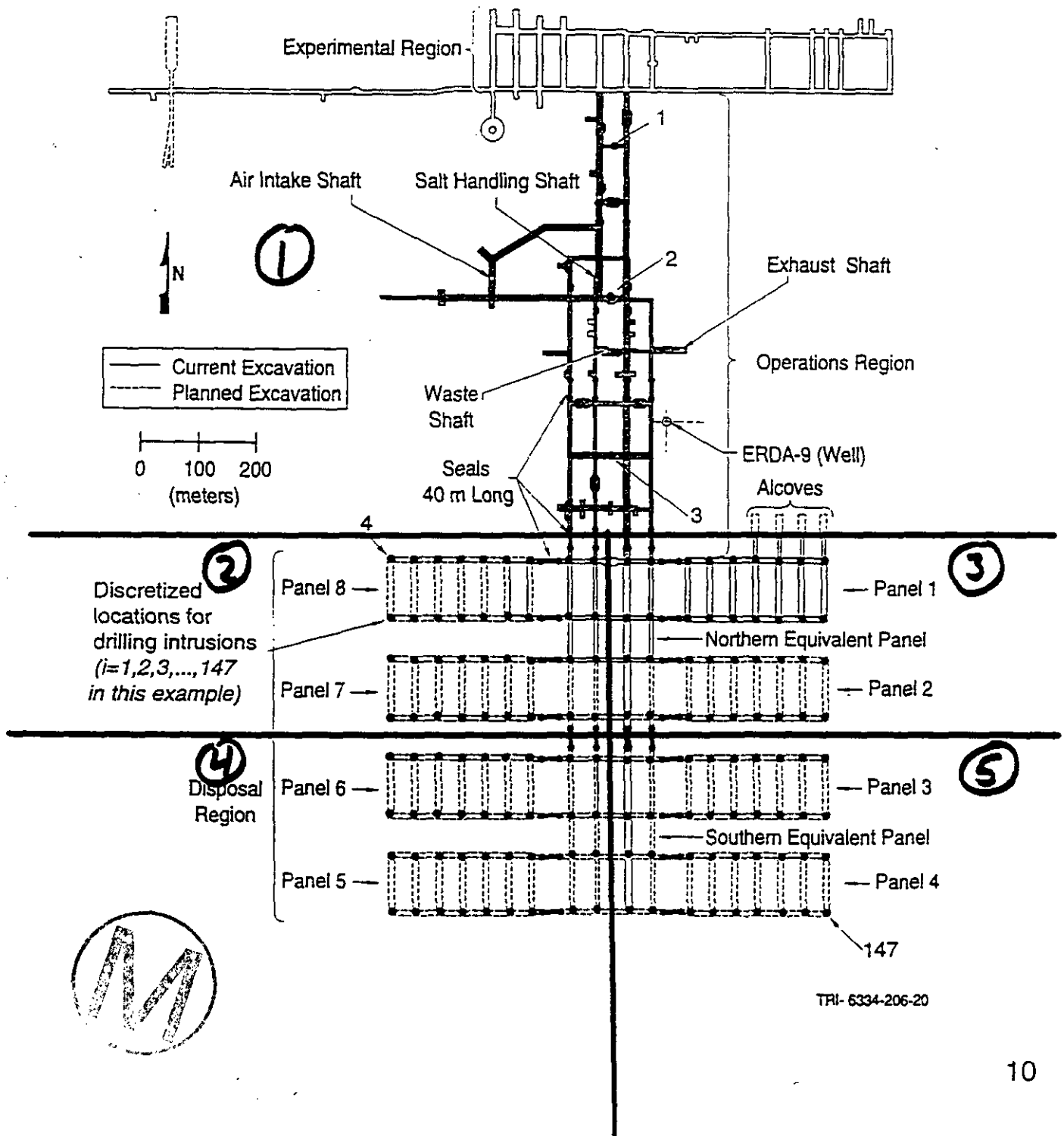
TRI- 6334-206-20

10

Title 40 CFR Part 191
Compliance Certification
Application
for the
Waste Isolation Pilot Plant

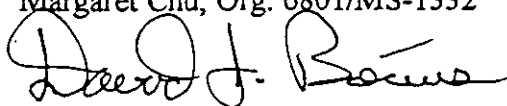# MASS Attachment 18-5

THIS PAGE INTENTIONALLY LEFT BLANK

Sandia National Laboratories

Operated for the U.S. Department of Energy by
Sandia Corporation

LOCKHEED MARTIN

INFORMATION ONLY

Albuquerque, New Mexico 87185-0750

date: 20 February 1996

to   Margaret Chu, Org. 6801/MS-1332

from: David J. Borns, Org. 6116/MS-0750

subject: Proportion of the waste panel area, WIPP site, that is underlain by brine reservoirs in the Castile Formation as Inferred from Transient Electromagnetic Method (TEM or TDEM) Surveys

Reference:
The Earth Technology Corporation, 1988, Final report for time domain electromagnetic (TDEM) surveys at the WIPP Site, Sandia Report, SAND87-7144, Sandia National Laboratories, Albuquerque, NM

In 1987, Sandia National Laboratories and the Earth Technology Corporation conducted a series of 38 time domain electromagnetic (TDEM) soundings at the WIPP Site. Thirty-six (36) of these sounding were taken over an approximately 1x2 km area. These soundings were spaced on a rectangular grid with a separation of 250 m for each station. This area overlaps the surface projection of the WIPP waste panel area at that time (see attached Figure 1).

In brief, the ability of the TEM methods to determine resistivity and depth stems from the field configuration of the method. The transmitter is a square surface loop of insulated wire (500 m on a side for the WIPP surveys) and produces a time varying magnetic field as the current in the loop is turned rapidly on and off. As the current is turned off, electromagnetic induction results in eddy currents in the subsurface. In horizontally layered ground as at WIPP, the eddy currents are horizontally closed rings parallel to the surface. With time after the transmitter loop is turned-off, the currents migrate to greater depth (these can be envisioned as smoke-rings leaving a smoker's mouth). The use of the word, "sounding" for the measurement stems from this migration of the eddy currents. A multicoil receiver lies in the middle of the transmitter loop. This receiver measures the electromotive forces due to the eddy currents which *with time reflect deeper layers in the earth.* In short, the magnitude of the electromotive force measured with increasing time reflects the conductivity at increasing depth. The resulting data aquisition and data analysis obtains a numerical solution for the resistivity distribution with depth that will produce the observed decay in electromotive forces with time (see Fig. 2). These one dimensional inversion matching a model of the resistivity data to the observed data utilize the industry standard ARRTI program of INTERPEX LTD.

From the WIPP measurements, series of one-dimensional inversions were made and profiles of electrical resistivity (or its inverse-conductivity) with depth were made. These profiles indicate whether zones of high electrical conductivity are present at depths of the Castile Formation. The inference is that these zones of high conductivity reflect the presence of brine reservoirs. This inference was supported by taking similar measurements at areas known absence and presence of brine (e.g., boreholes WIPP-12 and DOE-1). The resolution of the method and inversion is discussed by the Earth Technology Corporation (1988). The depth resolution for the method is plus/minus 75 m.

The effect of this resolution is that at the *minimum depth* within the range (e.g., minus 75 m) the proportion of brine reservoirs beneath the surface area is *greater,* since a *greater extent* of the subsurface conductors are above the Bell Canyon Formation (approximately 1200 m depth in the area) and within the Castile Formations. At the *maximum depth* in the range (e.g., plus 75 m), the proportion of brine reservoirs is *less.* Based on the thirty-six sounding in the waste panel area, I have estimated the possible distribution of brine reservoirs beneath the 2 km^2 area in Table 1.

Table 1: Proportion of the Surface Area above the Waste Panel Area that is Underlain by Brine Reservoir in the Castile Formation

	Minimum Depth/ Maximum Reservoir in Castile Formation	*Mean Calculated Depth/Average Reservoir in Castile Formation*	*Maximum Depth/ Minimum Reservoir in Castile Formation*
Percentage of Area Underlain by Brine Reservoirs	55%	25%	10%

Distribution   Org.   MS
W. D. Weart   6000   1335
K. Larson   6847   1341
SWCF: 6800   1330
0517.201310
"WIPP Regulatory"

WBS   RD 7/11/96
SWCF: 1.1.05; Castile Brine Reservoir/Waste Panel
w/cc A: RQA)

CD

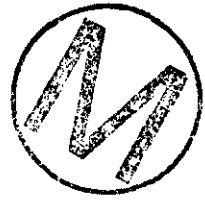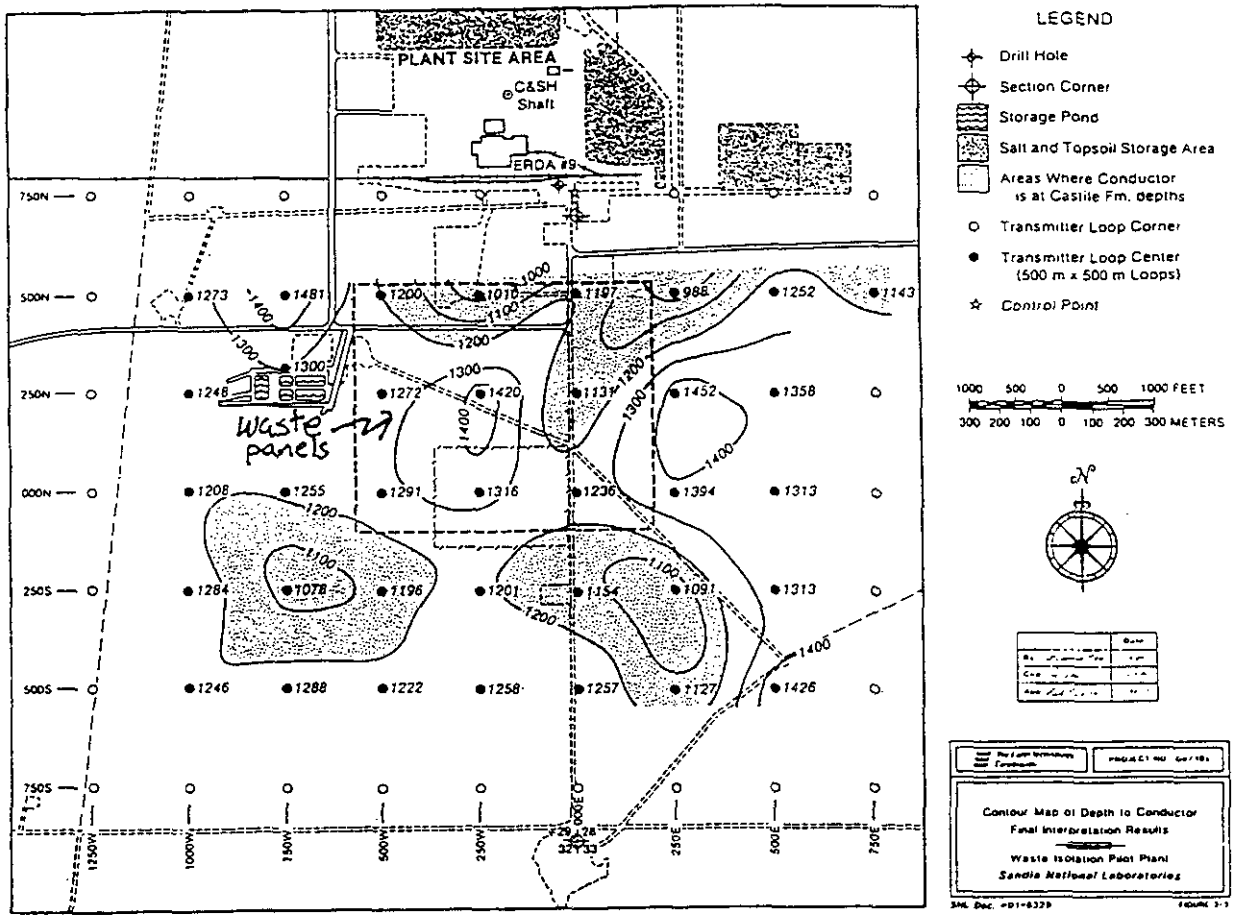SWCFWBS 1.2.07.1.3: CO/CC A/APPENDIX MASS/QA: Castile
- Brine Reservoir

Figure 1. Contour Map of Depth to Conductor from Earth Technology Corporation (1988),
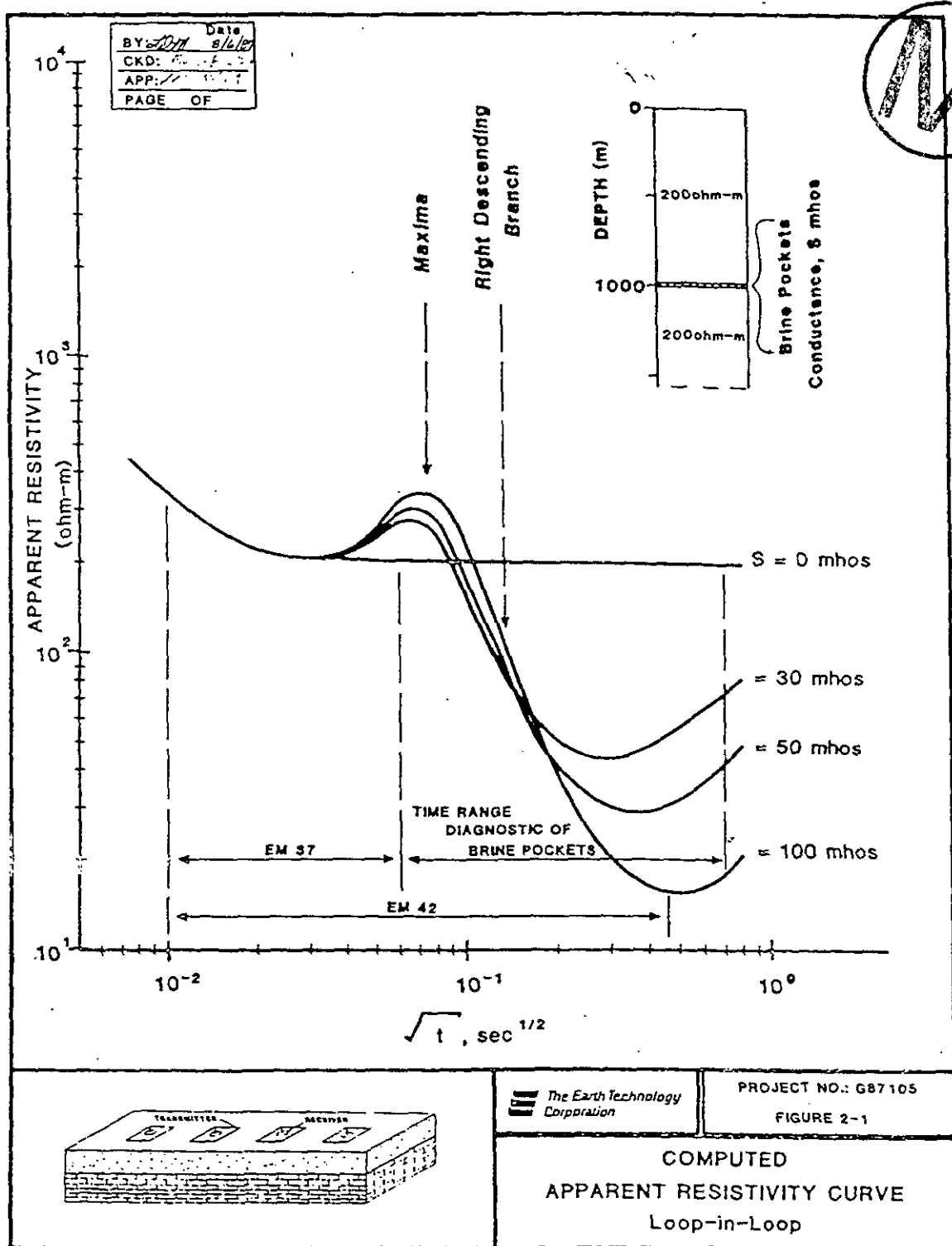*Inner dashed rectangle is the surface projection of the underground waste panels*

Figure 2. Computed Apparent Resistivity Curve

Title 40 CFR Part 191
Compliance Certification
Application
for the
Waste Isolation Pilot Plant

MASS Attachment 18-6

THIS PAGE INTENTIONALLY LEFT BLANK

Probability of Intercepting a Pressurized Brine

Reservoir Under the WIPP

Dennis W. Powers

John M. Sigda

Robert M. Holt

July 10, 1996

ABSTRACT

Twenty-seven drillholes in the Delaware Basin are accepted as showing intercepts of pressurized brine in the Permian Castile Formation. Using an indicator function (brine = 1, no brine = 0) and location data for these and other drillholes in the area around WIPP, semi-variograms were constructed. Parameters from selected semi-variograms were input to an ordinary kriging algorithm to estimate the probabilities of intercepting brine in a drillhole within the Castile Formation beneath the WIPP site. For the area of the disposal panels, the estimated probabilities at computational nodes range between 0.078 and 0.084. For the shaft and access area, probabilities at nodes range between 0.078 and 0.221. Nodes within the experimental area ranged from 0.078 to 0.371. An areally-weighted average for the waste panel area is 0.080.

Structure contour and isopach maps of selected stratigraphic contacts and intervals over part of the nine township area around WIPP show deformed evaporites in areas where most brine occurrences are mapped. No data were obtained from a few drillholes where brine was encountered. The Castile is deformed at WIPP 12, the nearest brine encounter to the WIPP. Stratigraphic data from the Castile are few at WIPP, but there appears to be no significant deformation in the vicinity of the waste panels. This is consistent with generally low probabilities for a drillhole encountering brine as calculated by geostatistical techniques. The estimated thickness from base of Castile to base of Cowden Anhydrite at ERDA 9 is considerably less than the minimum thickness for any known brine encounter, indicating there may be a threshold value for reservoir formation.

1.0 INTRODUCTION

A scenario for the Waste Isolation Pilot Plant (WIPP) includes a drillhole intercept of pressurized brine in the Permian Castile Formation below WIPP underground workings. The analysis of this scenario requires estimates of the probability that a drillhole at WIPP will encounter pressurized Castile brine.

2.0 PURPOSE

This report describes the process that was followed to estimate the probability that a drillhole will intercept brine in the Castile below the underground workings at WIPP. This report also describes how geological data were acquired and analyzed as complementary evidence of the distribution of pressurized Castile brine.

3.0 APPROACH

Several steps were followed to estimate the probabilities of encountering brine in a drillhole:

1)   The reported encounters of pressurized brine were listed, including relevant information about location, depth, drillhole name, and stratigraphic basis for assigning the encounter to the Castile.

2)   A file of locations of oil and gas drillholes penetrating the Castile compiled by the Compliance Department of Westinghouse was provided by Westinghouse as a database for analysis. AUTOCAD software was used to establish locations and prepare data files for use. (See Appendix A).

3)   The UNCERT geostatistics software package was used to prepare semi-variograms utilizing an indicator function (brine report = 1; no brine report =0) and location data for each drillhole. Rbase 5.5 and Excel 4.0 were used to format ASCII data files from AUTOCAD for use by UNCERT.

4)   The semi-variograms were evaluated for sensitivity to data cluster effects and classification errors.

5)   The ordinary kriging module of UNCERT was used to prepare comparable maps showing the estimated conditional probabilities of intercepting brine and to obtain nodal values for points within three defined areas including the underground workings at WIPP.

6)   This analysis report was prepared to show data sources, techniques, estimated conditional probabilities, results and limitations.

Several steps were also followed to analyze how geological features or processes (mainly Castile deformation) are related to the distribution of Castile brine reservoirs:

1) Reported encounters of pressurized brine flow were listed to include information about location, depth, drillhole name, and stratigraphic basis for assigning the encounter to the Castile.

2) Stratigraphic data were derived from geophysical logs for many drillholes around the WIPP site where the geophysical logs were appropriate with respect to depth, location, and log coverage.

3) From the stratigraphic data, subsidiary tables of unit elevations (for structure maps) and thicknesses (for isopach maps) were prepared. These tables were used to prepare maps of structure and thickness for various horizons and intervals, respectively.

4) A general relationship apparently exists between the location of most brine encounters and areas where the Castile evaporites have been significantly deformed from original position. The structure data for the WIPP site are meager for the Castile, though it appears that the area of the waste panel is not significantly deformed.

5) The statistical relationship or association of structure and brine encounters is still being examined, as appropriate data have just been drawn together.

6) This analysis report discusses data sources, techniques, maps, results, and limitations of the geological analysis of the relationship between brine reservoirs and deformation.

3.1 Responsible Staff

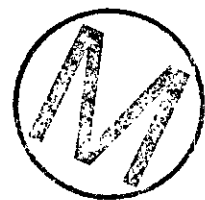The analysis has been conducted by:

Dennis Powers, mainly conducting geological research;

John Sigda, mainly conducting geostatistical analysis; and

Robert Holt, contributing to both geological and geostatistical analyses.

3.2 Schedule and Deliverables

The analysis report includes:

a)   the estimated probabilities that a drillhole will encounter pressurized brine under 1) the waste panel area, 2) shaft and access areas, and 3) experimental area.

b)   a discussion of the apparent relationship between Castile brine and Castile deformation.

The first request for assistance on this issue came in early February, 1996. An initial approach was outlined and followed before developing the broader analysis approach in April. An initial report and supporting data were scheduled for June 18, with a "final" report and data package required by about July 10, 1996.

4.0 DATA TYPES AND SOURCES

4.1 Geostatistical Analysis

The geostatistical methods used in this analysis for estimating probabilities require two related data sets:

a) a set of locations for drillholes, and

b) an indication of whether each drillhole intercepted Castile brine or not.

The location data set needed to be relatively comprehensive for the area in which brine encounters have been reported. Most of the drillholes that penetrate through most or all of the Castile should be represented. In addition, the data set needed to have a consistent coordinate system (e.g., NM State Plane coordinates) for computational purposes. The coordinates for each drillhole needs to be reasonably accurate relative to nearby drillholes, but long-range accuracy (over several miles) is not expected to be important and was not examined.

Two sources of a location data set were found. Petroleum Information Corporation (PI) maintains a large drillhole data set available for lease/purchase; location coordinates were available as an extra service. Through discussions with the Compliance Department, Westinghouse Electric Corporation, it became apparent that a partial set of drillhole data from PI already been purchased and was being used. L. Madl and D. Hughes provided two subsets of this data set. D. Hughes converted the original PI location data for each drillhole into equivalents to the NM State Plane coordinates (see Appendix A). L. Madl provided files that provided common elements with the location (State Plane coordinates) data and the standard locations (Township/Range system) generally available for geophysical data. We added useful WIPP drillholes not in the database using coordinates provided in Gonzales (1989).

The data set for brine occurrences (Table 4.1-1) was compiled from several sources.

Original studies and reports include Griswold (1977), Register (1981), Popielak et al. (1982), and Chaturvedi (1985). More recent summaries have been provided in unpublished documents by Kehrman (1994) and Silva (1996). Silva obtained summary data from a number of petroleum exploration companies active in the area. In addition, Powers examined files at the Oil Conservation Department (NM) in Artesia and Hobbs, NM, to develop additional data and verify some occurrences. Of the total apparent occurrences, several were eliminated as unlikely, usually because of the combination of 1) insufficient evidence of significant volume and/or pressure, and 2) being in the wrong stratigraphic unit. Twenty-seven reports of brine occurrence were accepted as Castile brine intercepts. The analysis is based on this set of encounters, though we demonstrate later (Section 6.3.2) that it is rather insensitive to adding or dropping encounters in areas where they are more common.

The data set for brine occurrences consists of reports of brine intercepts, which is a proxy for actual occurrences, and "non-reports". There is no requirement that all brine intercepts be reported. Some of the earliest known reports of brine came before modern drilling practices and resulted in loss of control of the drillhole and substantial surface flows. We cannot know if some drillholes intercepted a brine reservoir that went undetected because substantial pressure was depleted by other drillholes. Some companies declined to respond to Silva's survey. Other intercepts may have been quickly controlled, and no report was made or required. We accept the reports accumulated as a reasonable representation of the actual history of brine intercepts. In later discussion, we address alternatives.

Tables 4.1-1 and 4.1-2 include basic information about the drillholes included in this analysis as encountering brine within the Castile. Some excluded drillholes are also reported with justification for deciding they should not be in the data set.

The map area was selected to encompass the locations of all 27 Castile brine occurrences. We tried to make the area as small as practical to minimize the number of drillholes for which there is no report of a brine intercept. For the geostatistical analysis, the total number of drillholes, including appropriate WIPP drillholes, is 354.
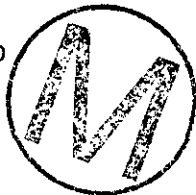
4.2 Geological Analysis

The geological methods used in this analysis for understanding the relationship between brine reservoirs and geological features or processes (mainly evaporite deformation) require two related data sets:

> a) stratigraphic and reference elevation data from drillholes (Appendix B), and

> b) a locations (including State Plane coordinates) for those drillholes.

For most petroleum exploration drillholes in the area around WIPP, one or more geophysical logs have been made that can be purchased or examined. They vary in

Table 4.1-1

Location Data for Drillholes
Considered to have Castile Brine

IDnum	T.	R.	Section	from section line (e.g.,n=north)		Drillhole Name
1104	21	31	35	2152s	910e	ERDA 6
1159	22	31	17	148s	84e	WIPP 12
5014	22	31	2	2310s	330e	Pogo State "2" No. 3
5128	23	30	1	1830n	1980w	Belco Hudson Federal No. 1
5275	21	32	31	1980n	660w	Phillips Luke Federal No. 1
5305	21	31	26	1980n	1980w	Pogo Federal No. 1
5306	21	31	35	660n	660w	Union Federal FI No. 1
5307	21	31	36	1980s	660e	Yates Lost Tank "AIS" State No. 1
5308	21	31	36	1980s	1980w	Yates Lost Tank "AIS" State No. 4
5326	22	31	1	660n	1980w	Phillips Molly State No. 1
5327	22	31	1	660n	660w	Phillips Molly State No. 3
5328	22	31	1	660n	1980e	Yates Unocal "AHU" Federal No. 1
5337	22	31	11	660s	1650e	Yates Martha "AIK" Federal No. 3
5338	22	31	11	1980s	1650e	Yates Martha "AIK" Federal No. 4
5339	22	31	12	330n	1650w	Pogo Federal 12 No. 8
5340	22	31	13	1980n	1980w	Texaco Federal Neff 13 No. 5
5348	22	32	5	660n	1580e	Getty Bilbrey Federal No. 1
5365	22	32	15	660s	1650w	Strata Lechuza Federal No. 4
5366	22	32	16	330s	330e	Yates Kiwi "AKX" State No. 1
5382	22	32	25	660n	1980w	Pogo Covington "A" Federal No. 1
5392	22	32	34	660n	1650e	Pogo Red Tank "34" Federal No. 1
5394	22	32	36	330n	1980w	Shell Bootleg Ridge Unit No. 1
5404	22	32	36	660n	660e	Richardson & Bass Tidewater No. 1
5405	22	32	36	1980n	1980e	Culbertson & Irwin Culbertson No. 1
5406	22	29	9	660s	660e	H & W Danford No. 1
5407	22	33	20	660s	1980e	Yates Mascho Cloyd No. 2
5408	22	33	20	660s	660e	Yates Mascho Cloyd No. 1

Data sources for this table include Popielak et al (1983), Register (1981), Kehrman (1994), Silva (1996), and information developed by Powers through visits to OCD offices in Artesia and Hobbs, NM.

Table 4.2-2
Brine Occurrence Depths
and Unit Assignments
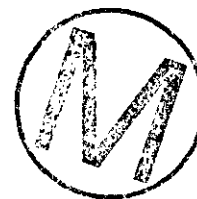
IDnum	Drillhole Name	Brine Depth (ft)	Depth* Data Source	Unit at Brine depth	Notes
1104	ERDA 6	2711	1,6,8,9	A2?	Uppermost anhydrite; may be A3
1159	WIPP 12	3017	1,7	A3	
5014	Pogo State "2" No. 3	3083	5	A3	May only be gas
5128	Belco Hudson Fed No. 1	2802	1	A3	
5275	Phillips Luke Fed No. 1	3050-57	3,4,5	A3	Lost Tank SWD#1-E
5305	Pogo Fed No. 1	3322	1	A2-A3?	A units coalesce?
5306	Union Fed Fl No. 1	2810	1	A3	
5307	Yates Lost Tank "AIS" State No. 1	2970	4	H2-A3	A3-H2 contact 2932
5308	Yates Lost Tank "AIS" State No. 4	3280	4	A2	Uppermost anhydrite? No A3?
5326	Phillips Molly State No. 1	3080	4	A3	
5327	Phillips Molly State No. 3	3023	4	A3	
5328	Yates Unocal "AHU" Fed No. 1	3068	3	A3	
5337	Yates Martha "AIK" Fed No. 3	3311	3,4	H2	A3-H2 contact 3267
5338	Yates Martha "AIK" Fed No. 4	3750, 3745	3,4	H1	H1 from 4170 to 3688
5339	Pogo Fed 12 No. 8	3050	3	A3	
5340	Texaco Fed Neff 13 No. 5	3340	4	A3	
5348	Getty Bilbrey Fed No. 1	3090; 2965-3066	1,5; 4	A3	
5365	Strata Lechuza Fed No. 4	3500	4	H2	H2 from 3700 to 3371
5366	Yates Kiwi "AKX" State No 1	TD(4535) ; 3400; 3360	3;5;4	A3	A3-H2 contact 3430
5382	Pogo Covington "A" Fed No. 1	3600	1,5	A3?	A3 in #5208 from 3385 to ?3650

IDnum	Drillhole Name	Brine Depth (ft)	Depth* Data Source	Unit at Brine depth	Notes
5392	Pogo Red Tank "34" Fed No. 1	3590-4489; 3000	3,5	A3-A1; Salado (3000)	
5394	Shell Bootleg Ridge No. 1	3671	1	A3 probably	A3-H2 not interpreted top A3 at 3466
5404	Tichardson & Bass Tidewater No. 1	3730	1	A3?	Compared to #5397
5405	Culbertson & Irwin Culbertson No. 1	3515	1,5	A3	Compared to #5210
5406	H & W Danford No. 1	1930; 2208	1;5	Cowden? @ 1952; A3 2150-2380	Scout report & NMBMMR well log report interpreted for Castile anhydrites/salt
5407	Yates Mascho Cloyd No. 2	3298; 3362	1;5	A3?	Unit inferred from maps, nearby wells
5408	Yates Mascho Cloyd No. 1	3322; 3362	1;5	A3?	Unit inferred from maps, nearby wells
	BOREHOLES NOT INCLUDED				
5315	Collins & Ware Lincoln Fed. No. 1	2000	3	Upper Salado	MB109 base 1926; top Vaca Triste 2106
5094	Phillips James A No. 9	7529	4	nd	Castile-BC contact at 3658 ft
5276	AEC 7	3918?	2,10	nd	gas blowout after well reached TD 3918

*References for Data Sources of Depths (see Reference list for complete citation):

1. Popielak et al, 1983
2. Register, 1981
3. Kehrman, 1994
4. Silva, 1996
5. Powers notes from OCD offices in Artesia and Hobbs, NM
6. Sandia National Laboratories and US Geological Survey, 1983
7. D'Applonia Consulting Engineers, Inc., 1982
8. Anderson and Powers, 1978
9. Jones, 1981
10. Sandia National Laboratories and D'Appalonia Consulting Engineers, Inc., 1983

Note: All stratigraphic unit assignments were reviewed by Powers based on reexamination of geophysical logs or by inferring units from nearby drillholes and contour maps of relevant units.

type (e.g., acoustic or neutron), drillhole conditions (open/cased), logged interval, and quality, which can be affected by unknowns such as hole diameter behind casing or by equipment development and improvement over the years. Where the geophysical log covers the appropriate interval and is at least partially interpretable, the principal data for geological analysis includes the elevation of the log reference or beginning point (commonly KB or kelly bushing) and the depth from the reference point to various stratigraphic markers.

With these basic data, two additional kinds of useful information are calculated:

> structure data - the elevation of any identifiable stratigraphic marker (Appendix C), obtained by subtracting the depth from the reference point elevation, and

> isopach (thickness) data - the thickness between any two identifiable stratigraphic markers (Appendix D), obtained by subtracting the depth to the uppermost marker from the depth to the deeper marker.

Both kinds of data are generally plotted on maps and then the elevations of the horizon for structure or the interval thickness values are contoured. The evaporite beds are expected to have been deposited essentially horizontal, and the upper surface of each unit was probably about horizontal when the overlying unit began to be deposited. Many of the units are expected to be reasonably uniform in thickness across significant areas, but there can also be differences if there was differential subsidence during deposition across the area.

The stratigraphic information is interpretive. Geophysical logs obtain data about rock characteristics indirectly. An example is natural gamma, a measurement of the natural radiation of the rocks the drillhole penetrates. The instrument is calibrated to a standard for the industry, and the display is scaled such that 100 API units (one full log cycle) would be the response from a hypothetical average mid-continent North American black shale. In a drillhole through unknown rocks, the natural gamma indicates the total gamma radiation from all sources, and it would be tentatively interpreted in terms of general expectations of the natural gamma of different rock types. Cuttings, other geophysical logs, or cores might be used to supplement the interpretation. In the area of WIPP, the evaporite units are well known in general from many thousands of drillholes and previous studies (e.g. Bachman, 1985), and their geophysical log characteristics are also well known (e.g., Jones et al., 1960; Holt and Powers, 1988; Powers and Holt, 1990). There is little difference in interpretation of the geophysical logs for many studies (see analysis in Appendix C of Powers and Holt, 1995). For this work, the main problem is that most geophysical logs for the Castile were taken in open holes. (See Limitations discussion below - section 5.5.)

The location data in standard township/range form were used to plot drillhole locations on preliminary maps and post values for structure and isopach maps. Such data are available from the geophysical logs and from Midland Map Company ownership maps
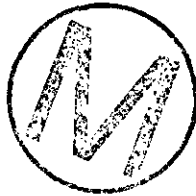
used as convenient base map. State Plane coordinates were also assigned to each drillhole with stratigraphic data to examine statistical relationships between structural properties at drillhole locations and reports/nonreports of Castile brine. The statistical studies of this relationship are incomplete at this time.

5.0 CASTILE DEFORMATION

Early in the history of the WIPP project, pressurized Castile brines were considered to be related to deformation of the Castile (e.g., Griswold, 1977; Anderson and Powers, 1978; Register, 1981; Popielak et al., 1983). Popielak et al. (1983) proposed that brine resides in fractures created within anhydrite by deformation and that fewer large fractures provide vigorous initial flow when hit with a drillhole. Borns et al. (1983) reviewed basic information on evaporite deformation in the northern Delaware Basin, considered five hypotheses on the origin of deformation, and concluded that gravity foundering (due to denser anhydrite overlying halite) and gravity sliding were the most likely explanations. Nonetheless, the physical conditions for either mechanism exist over broad areas while deformation is apparently not widespread. Borns et al. (1983) suggest intergranular water may have varied areally, changing rock strength somewhat locally and leading to deformation in these areas. Petrofabrics in the deformed Castile are also consistent with pressure solution and intergranular fluids (e.g., Borns, 1987). It is possible that intergranular fluids contribute directly to deformation and are also the source of the pressurized brines, but this has not been established.

The analysis by Register (1981) reported 10 brine encounters from the 62 drillholes (existing at that time) into the Castile near the WIPP and inferred that nine of the 10 were associated with known anticlinal structures. There has been considerable drilling since 1981; in this section we report structural information from a much larger data base and examine whether we can still conclude that brine reservoirs are associated with Castile deformation.

Our data around Danford well (T.22S., R.29E., sec. 9) are so limited that we draw no conclusions about structure. Our maps for this analysis do not extend to the Danford well.

We use two main forms of structure information: structure contours on selected stratigraphic contacts and maps of thickness (isopachs) of selected intervals. We assume that the evaporites were deposited on generally planar, horizontal surfaces, though we also recognize that there may have been differential subsidence or tilting during some of the deposition. We also begin with a working assumption that most of the units were deposited with a reasonably uniform thickness; regional and local trends can be depositional, compensating for synsedimentary subsidence or tilting.

While the focus is on Castile deformation, we have examined some of the effects on higher units as background. There are two reasons for this. The structure and thickness of higher units help delineate or bound the extent and age range for deformation. In addition, there are many more data points on mid-Salado to Rustler stratigraphic units across the WIPP site. If brine is associated with Castile structure, but the effects of that structure can also be seen in higher units, it may be possible to

better judge the possibilities that brine underlies parts of the WIPP. This possibility had not been adequately tested statistically at this time.

5.1 Methods

Data for structure and isopach maps were managed and computed using Rbase 5.5. Data were posted manually to maps and were contoured by Powers. All data were honored by contouring except some isolated points at the contour value (e.g., 1500) and some values at map edges, particularly along the northeast side of the map area where the Capitan reef underlies the area. Interpolation of values between data points is subjective but is generally roughly scaled. Dashes and dots for contour lines reflect decreasing confidence, generally in areas of fewer data points and at greater distance from data points.

Single hole anomalies that remain generally have not been reconfirmed or resolved with available data. They should be treated with caution at this time.

5.2 Structure Contours

Drillhole locations are identified on Figure 5.1-1 with identification numbers tied to data tables (e.g. ~~Table 4.2-2~~) *Appendix B but*

5.2.1 General

Over the area south of the study area, the top of the Delaware Mountain Group (DMG) displays relatively uniform strike slightly east of north and dips east about 75-100 ft/mile (about 1 degree) (Borns and Shaffer, 1985, fig. 16). This unit is the "basement" rock for our discussion.

For much of the study area, the DMG (Figure 5.2-1) continues the trends mapped by Borns and Shaffer (1985) for areas south of WIPP. Data for this contact are almost non-existent for the site area. We assume the NNE-SSW strike and modest east dip continues under the site.

In T.22S., R.32E., the contours indicate the DMG dips less than regional dip. Near the eastern edge of the map, some contours may be showing basin margin effects, though we include too few data to be certain.

While there are some differences from areas to the south, these are relatively minor. The structure of the DMG contrasts significantly with upper Castile horizons, as shown below.

Structure contours have been drawn for the top of the middle (A2) and upper A3) anhydrites of the Castile to demonstrate the main Castile features.

5.2.2 Anhydrite 2 (A2) (Figure 5.2-2)

Over the area south of the study area, A2 has strike and dip similar to the DMG (see figure 13 of Borns and Shaffer, 1985). The southern margin of our map study area appears to be the transition area to more complex structure to the north in the study area.

The few data points at the site area show deformation in the northern area and approximately "normal" structure in the southeastern site area (the vicinity of DOE 1). Near the southwest corner of the site, this unit in the Hudson Belco well appears also to be structurally high, though no nearby wells exist west of the Belco well to confirm closure. Near the northwest corner of the WIPP, it appears that the attitude of A2 is changing to more east-west strike. Three holes, each somewhat isolated, indicate structure lows. There are no known brine encounters in the cluster of drillholes near the northwest corner of WIPP

East and northeast of WIPP, A2 has been deformed into a major anticline trending about NW-SE. At least half of the known brine encounters closely relate to this major anticline, and several others are located along subsidiary structures. A structural low in east-central T22S., R.32E., interrupts part of this trend. Along the southeast corner of the map area, structure contours run approximately east-west, normal to the strike further south and west. Three brine encounters are in this area, 200 - 300 ft above projected contours from the south. The Mascho 1 and 2 brine encounters in T.22S., R.33E., are near deformed areas, but data near these wells are few.

Nearly all the brine encounters on the map appear to be related to areas deformed at the A2 level. More than half appear in areas where structural closure is demonstrable or very likely. Most of the rest are in areas where A2 differs considerably from contours projected from the south into the area.

5.2.3 Anhydrite 3 (A3) (Figure 5.2-3)

In this area, the top of A3 is also the top of Castile. Most of the brine encounters are interpreted to flow from the lower part of this bed.

The major structures of A3 and associations with brine encounters are very similar to those described for A2. The top of A3 was uncertain in the Belco well, though other nearby wells indicate some local structure.

5.2.4 Comparison with Culebra Dolomite Member (Rustler Formation)

A recent structure contour map of the Culebra (Powers and Holt, 1995) shows that the main anticlinal structure north and east of WIPP persists to the level of the Culebra. Over the WIPP site, there are limited changes from regional trends that may be difficult to attribute to any process (Powers and Holt, 1995).

5.3 Isopach Information

5.3.1 General

Three intervals were chosen to represent the main value of thickness maps: 1) Castile thickness, 2) the combined thickness of both halite numbers (H1, H2) and anhydrite (A2) between these halites, and 3) the thickness from base of Castile to base of the Cowden Anhydrite (of the Salado Formation). For simplicity, we call the third interval the IsoCowden.

5.3.2 Castile Thickness (Figure 5.3-1)

In areas near the southern margin of the site, the undeformed Castile is generally 1300-1400 ft thick. South and west of the site, isopach data are not very helpful. There may be local relative thickening and thinning near Hudson Belco, but the data are few. Over the site, DOE 2 shows thinning of the Castile; Borns (1987) described deformation features from Castile cores. While other WIPP drillholes at the site show structure, they do not go as deep as the DMG, and we have not inferred thickness in such drillholes for this analysis.

As expected, this map shows a strong thickening trend along the anticline north and east of WIPP. Just northeast of WIPP, there is an apparent minor thickening trend of about NNE-SSW. A localized thin area in east-central T.22S., R.32E. is consistent in location with a structural low along the anticline trend.

The apparent thickening of Castile northeast and east of WIPP is associated with many of the brine encounters. Nonetheless data are not available at several holes with brine, mainly because the DMG was not drilled or we cannot determine the stratigraphic contacts for the relevant beds. Some encounters east of WIPP are around areas of thickening or thinning, but thickness at the brine locations is not greatly different from undeformed areas.

5.3.3 Middle Castile (H1-A2-H2) Interval (Figure 5.3-2)

The main thickening and thinning trends and locations shown by the total Castile isopach are present in this map. There are more site details because more wells penetrated the relevant interval. Some local features show finer detail in this map compared to "smoother" contours for the thicker total Castile map. In "undeformed" areas south of the site, the thickness of the interval is about 600-700 ft.

In the northern part of the WIPP site a few drillholes are available that show the effects of deformation in the "disturbed zone" (see Powers et al., 1978). WIPP 12 and WIPP 11 show thickening, while WIPP 13 is much thinner. In the southeast part of WIPP, drillhole DOE 1 shows a "normal" thickness. The contours in these area are very approximate, and the thickness north of WIPP 12 is expected to be quite variable. While DOE 2 is difficult to interpret, there is almost no halite in the Castile at that location. If A2 was correctly identified, the thickness could be less than 150 ft.

Off the southwest corner of WIPP, there are some limited indications of thickening, but the interval was not definable at Hudson Belco. Off the northwest corner of WIPP, there is northward thickening.

Northeast and east of the site, a thick area trends along the anticlinal structure and zone of thickening for the entire Castile. The thinner area in east-central T.22S., R.32E., displays some apparent "fabric" of local thin zones approximately normal to the trend of the thick zone.

Most of the known brine occurrences can be associated with areas of thickening/thinning of this interval. There are several occurrences where data are inadequate and few where isopach changes are smaller or can be questioned.

5.3.4 IsoCowden (Figure 5.3-3)

This interval is very similar to the total Castile isopach, and it should be because it is the Castile plus the salt (commonly called the InfraCowden) between Castile and Cowden Anhydrite. The main structures are present, though there is some broadening across the main structure of the ERDA 6 anticline.

This map includes some estimated values noted by [ ]. The basis for the estimated values included on the map is provided in Appendix E. [Additional values for the thickness were generated from this map for later analysis in Section 8.0; only values that could be estimated independently from this map were included in this map.] The map was contoured in more detail than some others because this map has the most values, including estimates, of the thickness interval compared to other intervals.

While many of the brine intercepts occur in areas that are near the maximum thickness for the interval, some intercepts are not. While we think that most of the brine intercepts are in areas differing in thickness from regional trends, some are located in the mid-range of thickness for this map area.

5.3.5 Comparison of "Normal" and Thickened Zones

All three isopach maps show similar thickness differences between areas that are undeformed and deformed. This means that the thickening can principally be attributed to the halite members or the combined H1-A2-H2 interval. The basal (A1) and upper (A3) anhydrites included in the total Castile isopach differ much less from normal to deformed areas than does the interval with halite.

In order to examine further the relationship between various thickness intervals and the occurrence of brine, we plotted (Figure 5.3-4) the basic statistics (minimum, maximum, range of ± 1 standard deviation around the mean) for a number of intervals for comparison. Those intervals are:

IsoA1   top of Bell Canyon to top of A1
IsoH1   top of Bell Canyon to top of H1
IsoA2   top of Bell Canyon to top of A2
IsoH2   top of Bell Canyon to top of H2
H1A2H2   base of H1 to top of H2
IsoCas   top of Bell Canyon to top of Castile (A3)
IsoCow   top of Bell Canyon to base of Cowden Anhydrite
Iso124   top of Bell Canyon to base of MB 124
IsoRus   top of Bell Canyon to base of Rustler Formation
Cashal   sum to H1 and H2 thickness
IsoVT   top of Bell Canyon to base of Vaca Triste Sandstone Mbr
A1-Cow   top of A1 to base of Cowden Anhydrite
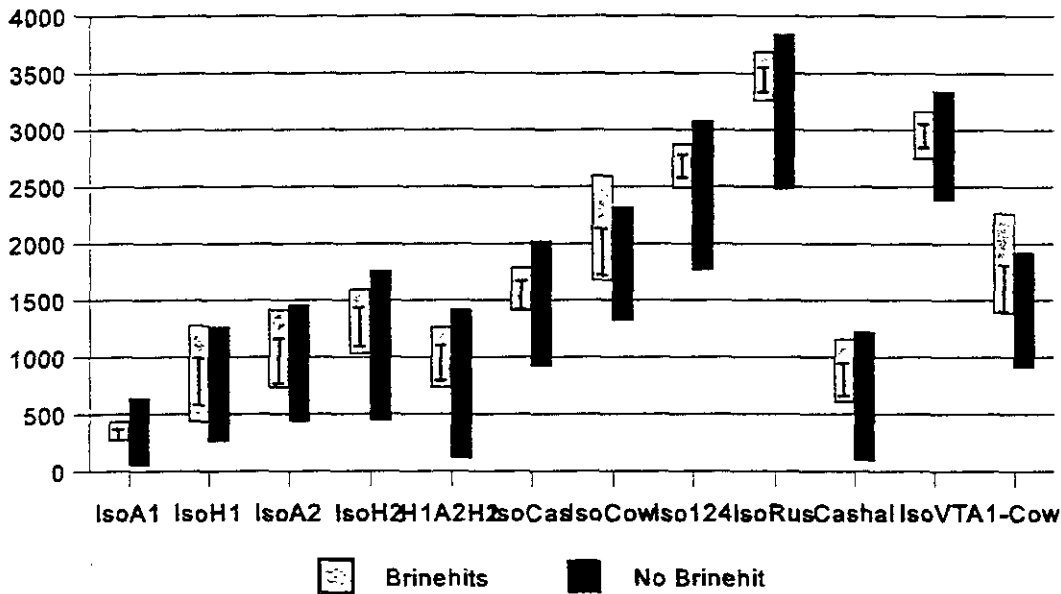
Figure 5.3-4 Color bars show range of thickness for each interval. Bars
represent ± 1 standard devation around the mean.

We see that the thickness associated with brinehits tends to be greater than for
the other drillholes. Each Cowden interval shows greater thickness for brine
hits. The minimum thickness of IsoCow associated with a brine reservoir is 1677
ft; at ERDA 9, near the waste panels, the estimated thickness of the IsoCow is
1532 (± 25) ft. This interval is the most reliable of all listed above with respect to
largest number of data points with direct thickness information at any drillhole

This is because the Bell Canyon structure is reasonably well understood and
considered to be best for interpolation and because the Cowden could be

interpreted reliably in more wells than the top of Castile. This interval is considered as a possible exclusionary indicator for brine reservoirs under the waste panel. The statistical data are further examined in Section 7.0.

5.4 Summary of Geological Relationship to Brine Encounters

The majority of reported occurrences of Castile brine are clearly associated with areas of deformed evaporites in the Castile. Geological information is too limited for one drillhole (Danford) to determine if the evaporites are deformed at that location. Several drillholes are located in the general area of deformation, but they are not on extreme features. Brine appears to be strongly related to structure in Castile.

Very limited data on the top of the Castile near the WIPP site indicate that there is little, if any, deformation under the waste panel area. From this, we would infer that there is low likelihood of intercepting a brine reservoir in a drillhole through the waste panel area. The thickness of some of the intervals, especially the IsoCowden (base Castile to base Cowden), at the waste panel is estimated to be about 145 ft less than the minimum thickness for this interval at any known brine encounter, suggesting there may be a threshold excluding the panel area as an area to expect brine encounters.

Though the association of brine to structure appears to be strong, we note that most drillholes in areas of structure do not report brine in the Castile. A drillhole that does not intercept brine is not a demonstration that brine does not exist within an area.

5.5 Limitations

Some of the limitations for the geological data are due to the nature of the data. The geophysical logs for this study are dominated by neutron and gamma logs taken through casing in the evaporite section. While many of the stratigraphic "picks" are relatively straightforward, some are not, requiring more subjective decisions based on experience. The posted values for the structure contour and isopach maps do not differentiate between such kinds of data. The contoured maps are themselves a means of checking the likelihood of any individual value by the surrounding values. Single hole anomalies should be reexamined regardless of the apparent quality of the original data.

Another limitation to the geological study is that several of the holes with brine encounters were drilled before modern geophysical logging and have such limited geological data available that we are unable to confidently interpret the stratigraphic horizons and structural features at the drillhole location. Because more reliable data from other drillholes demonstrates that the structure and isopachs can vary over short distances, we have limited our inferences/extrapolations about the structure at these hole locations.

Work has not been completed to examine possible statistical relationships between structure or isopachs and brine encounters. If there is found a relationship strong enough to be helpful, we expect to incorporate this later into a re-evaluation of the
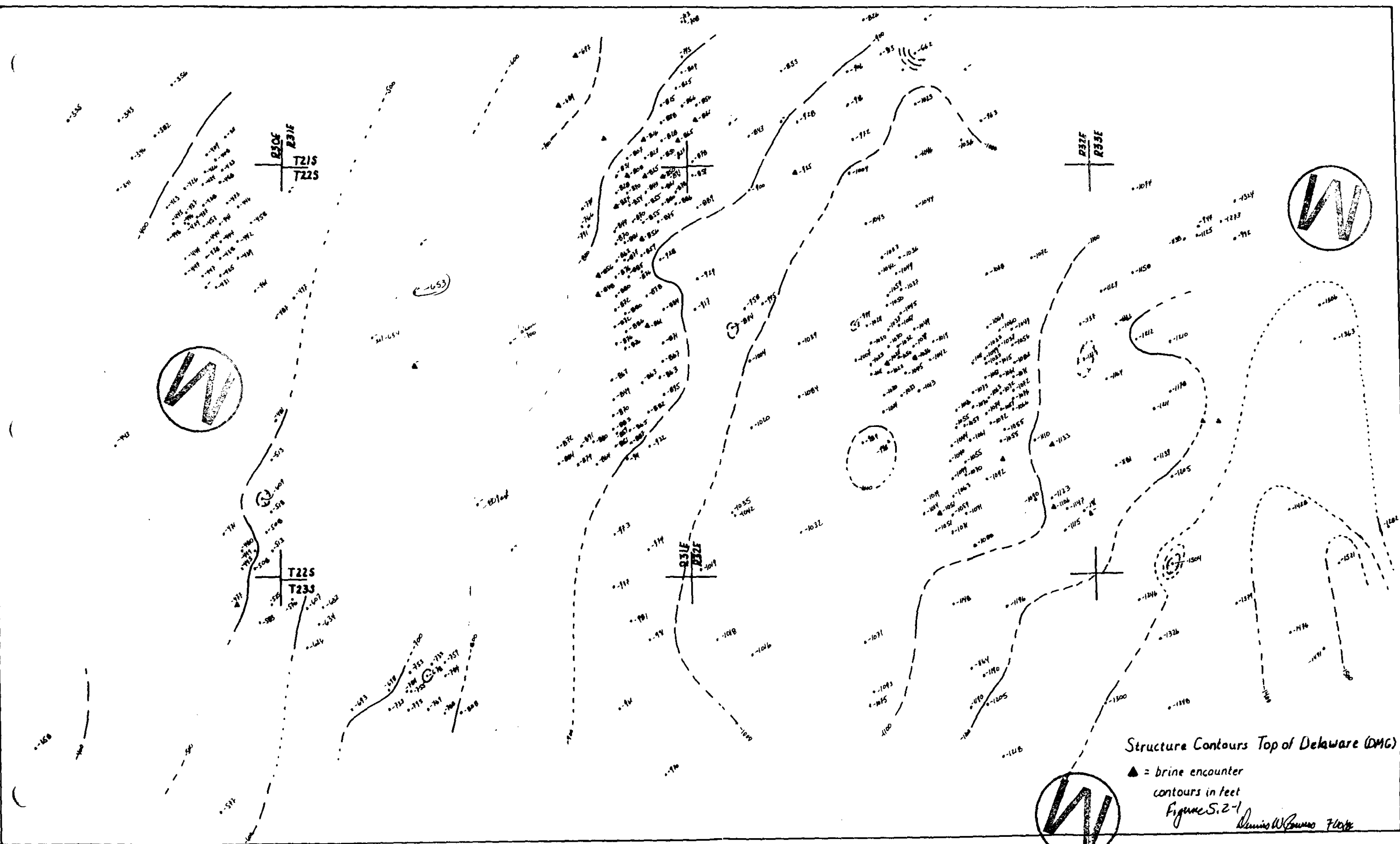
16
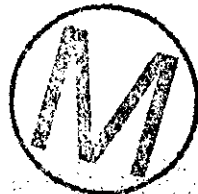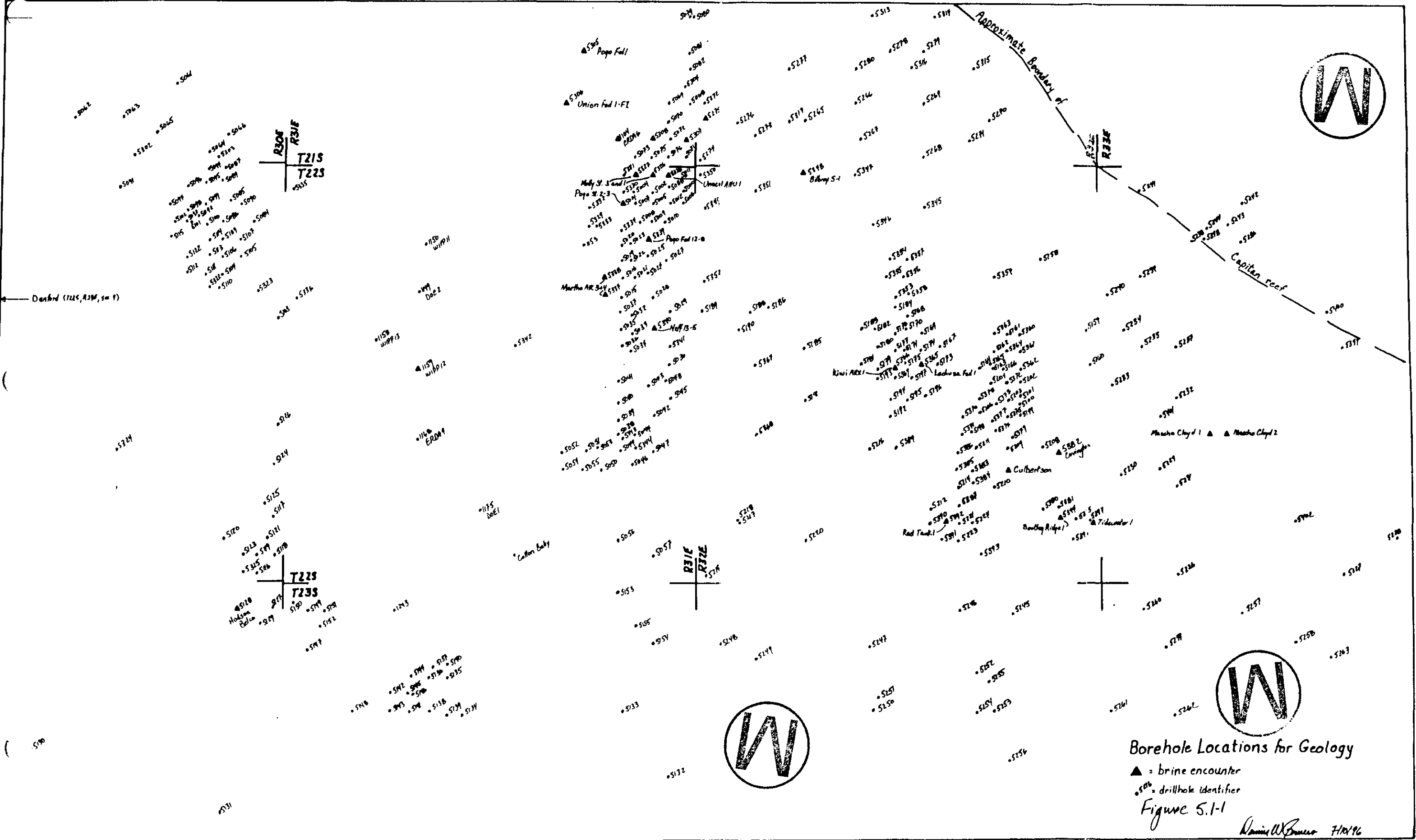
Borehole Locations for Geology

▲ = brine encounter

•506 = drillhole identifier

Figure 5.1-1

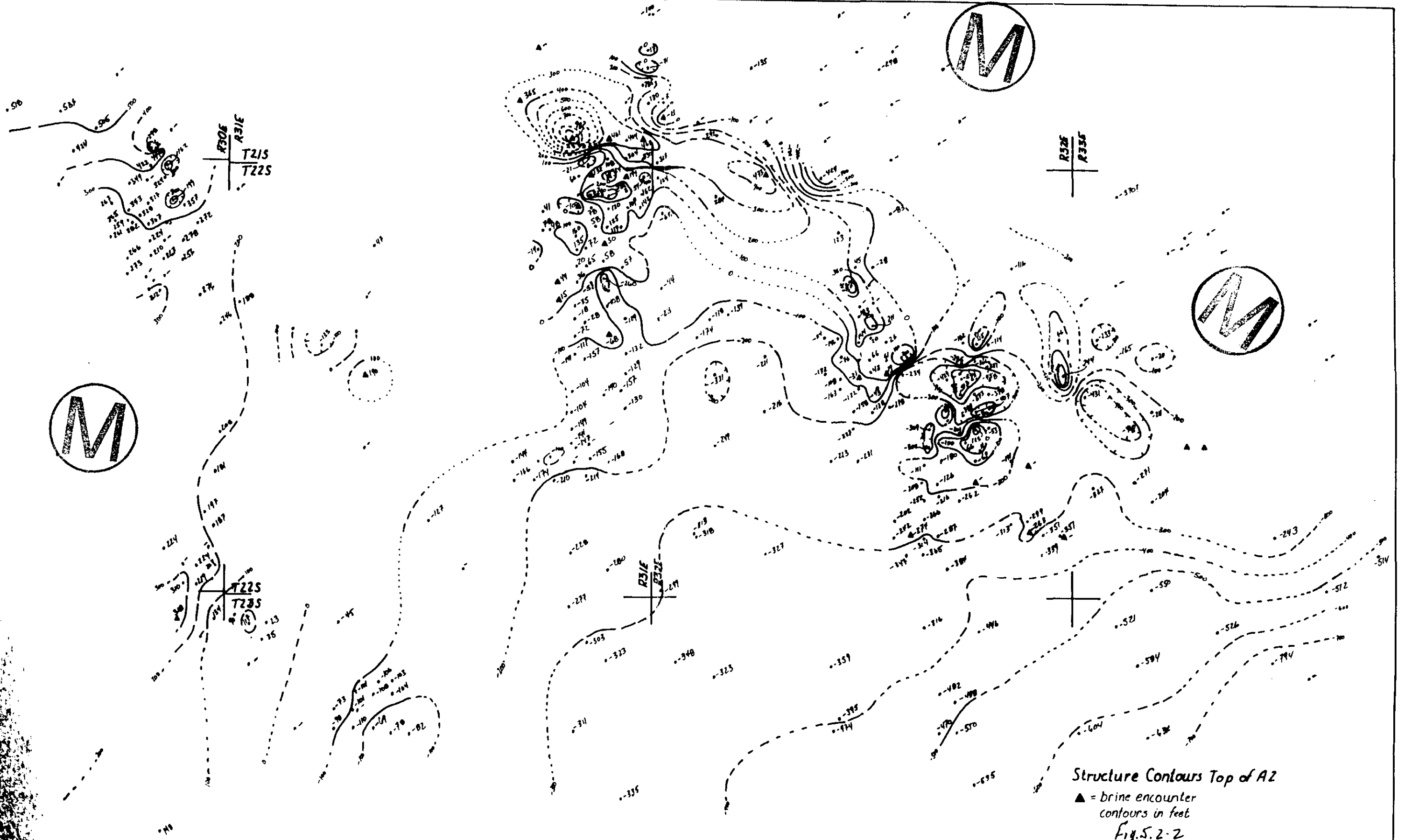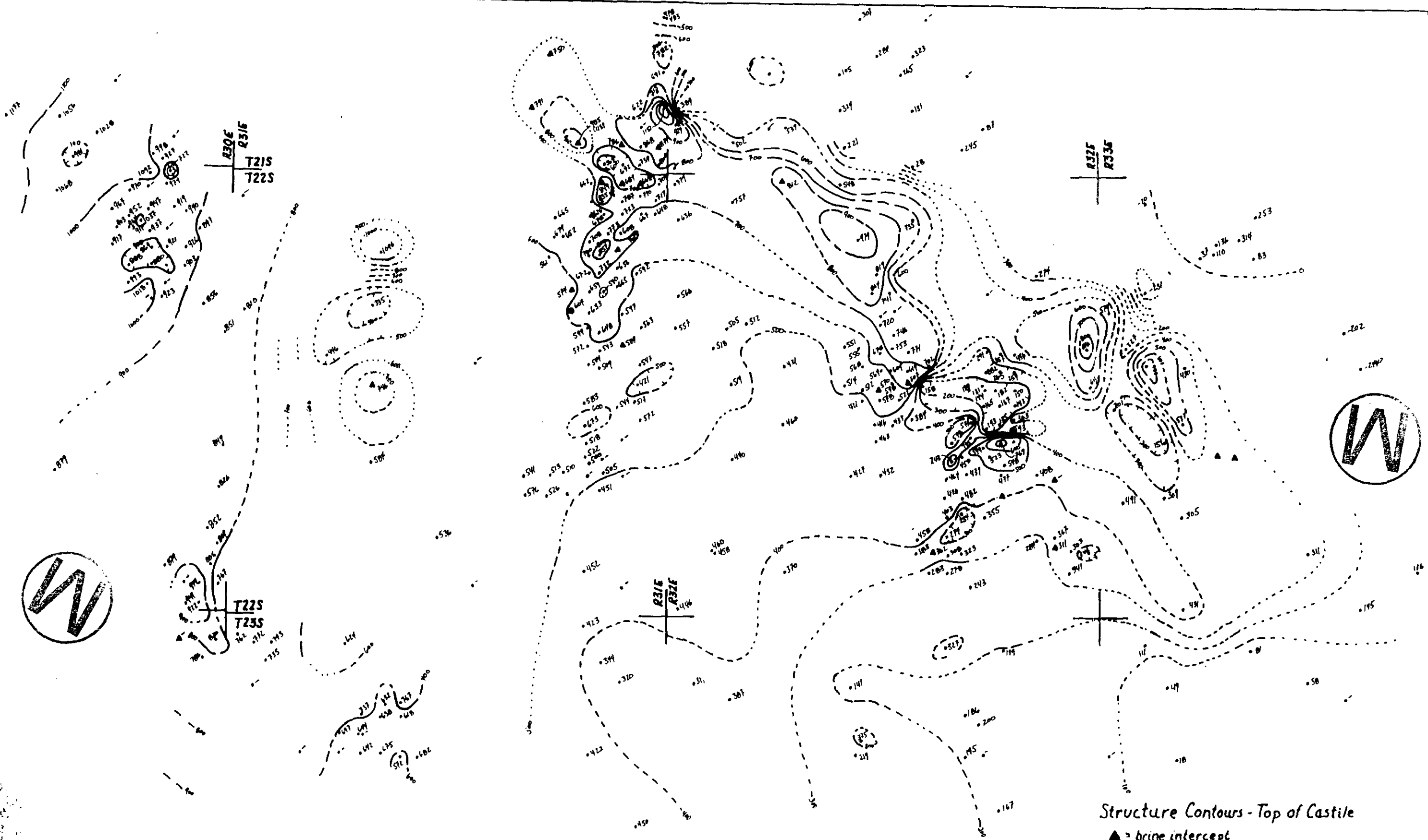Structure Contours Top of Delaware (DMG)

▲ = brine encounter

contours in feet

Figure S.2-1

Structure Contours Top of A2

▲ = brine encounter
contours in feet

Fig. 5.2-2

Structure Contours - Top of Castile

▲ = brine intercept

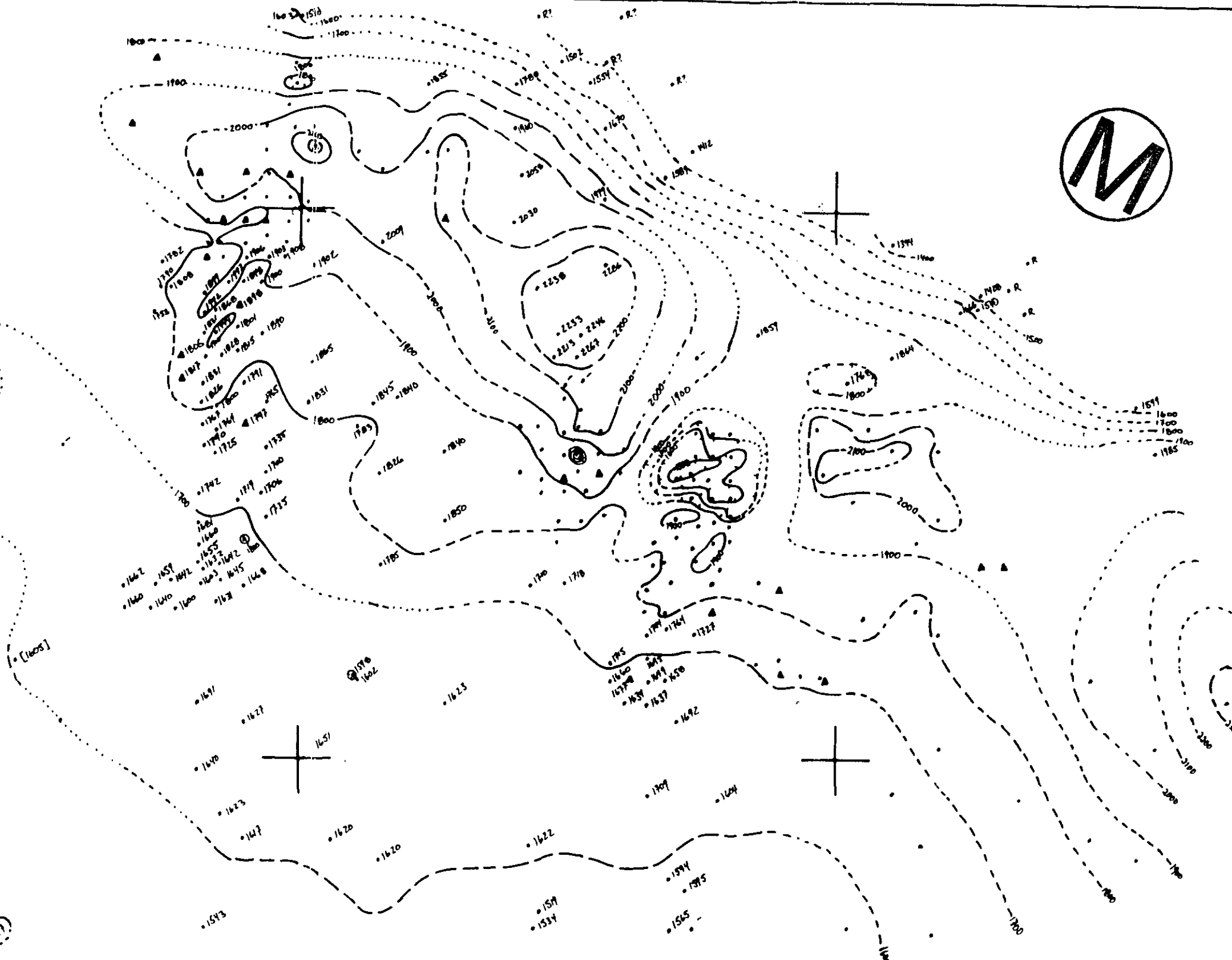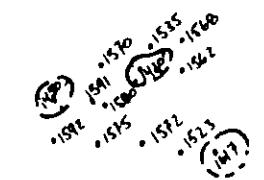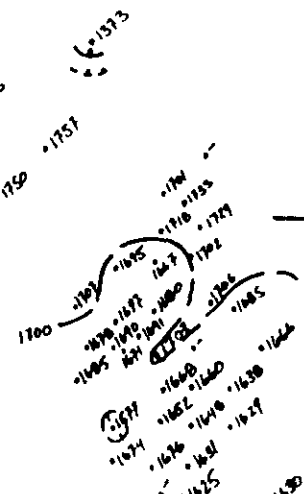contours in feet

Figure 5.2-3
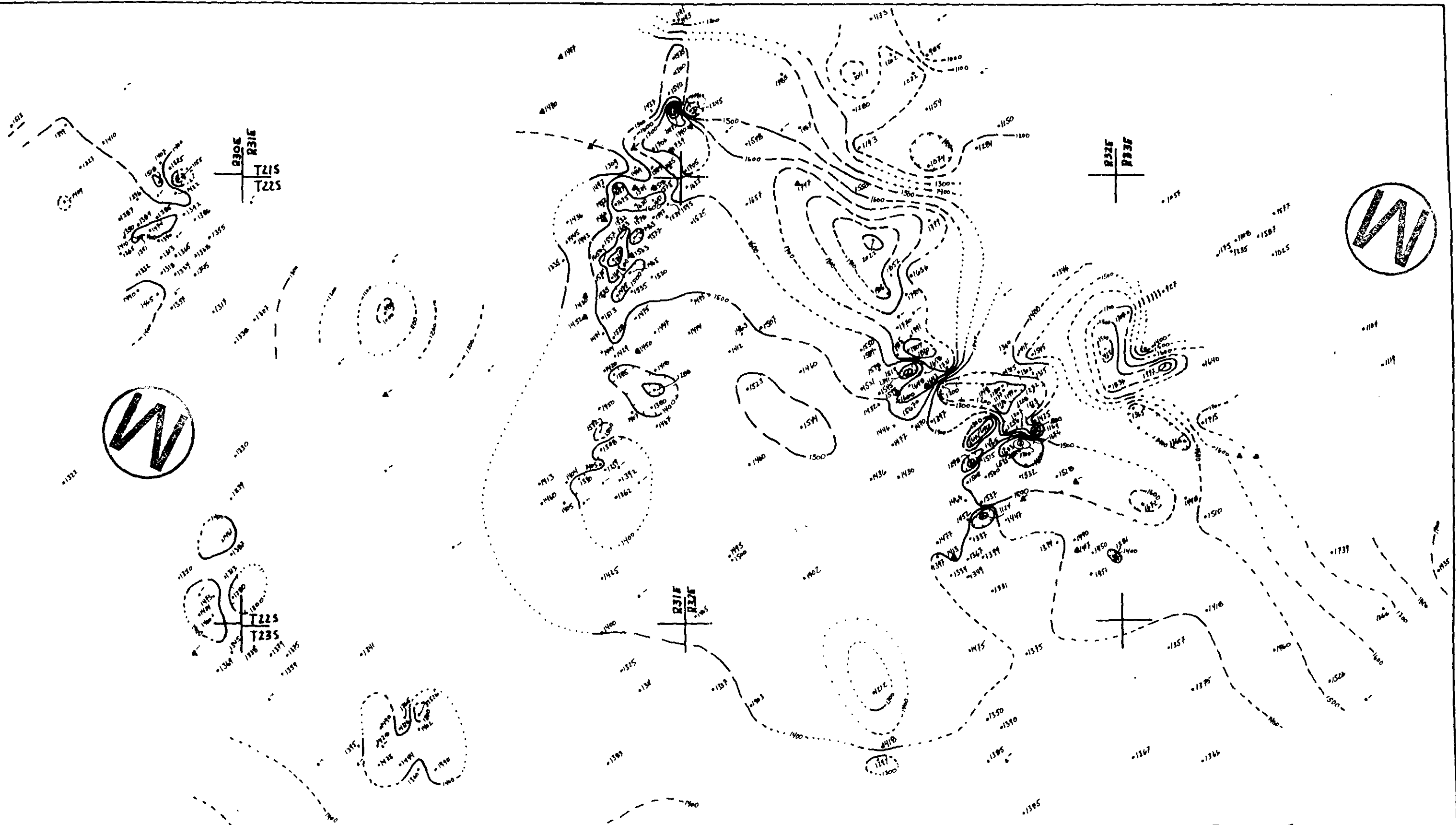
Isopach Castile Fm.   Figure S.3-1

▲ - brine intercept
contours in feet
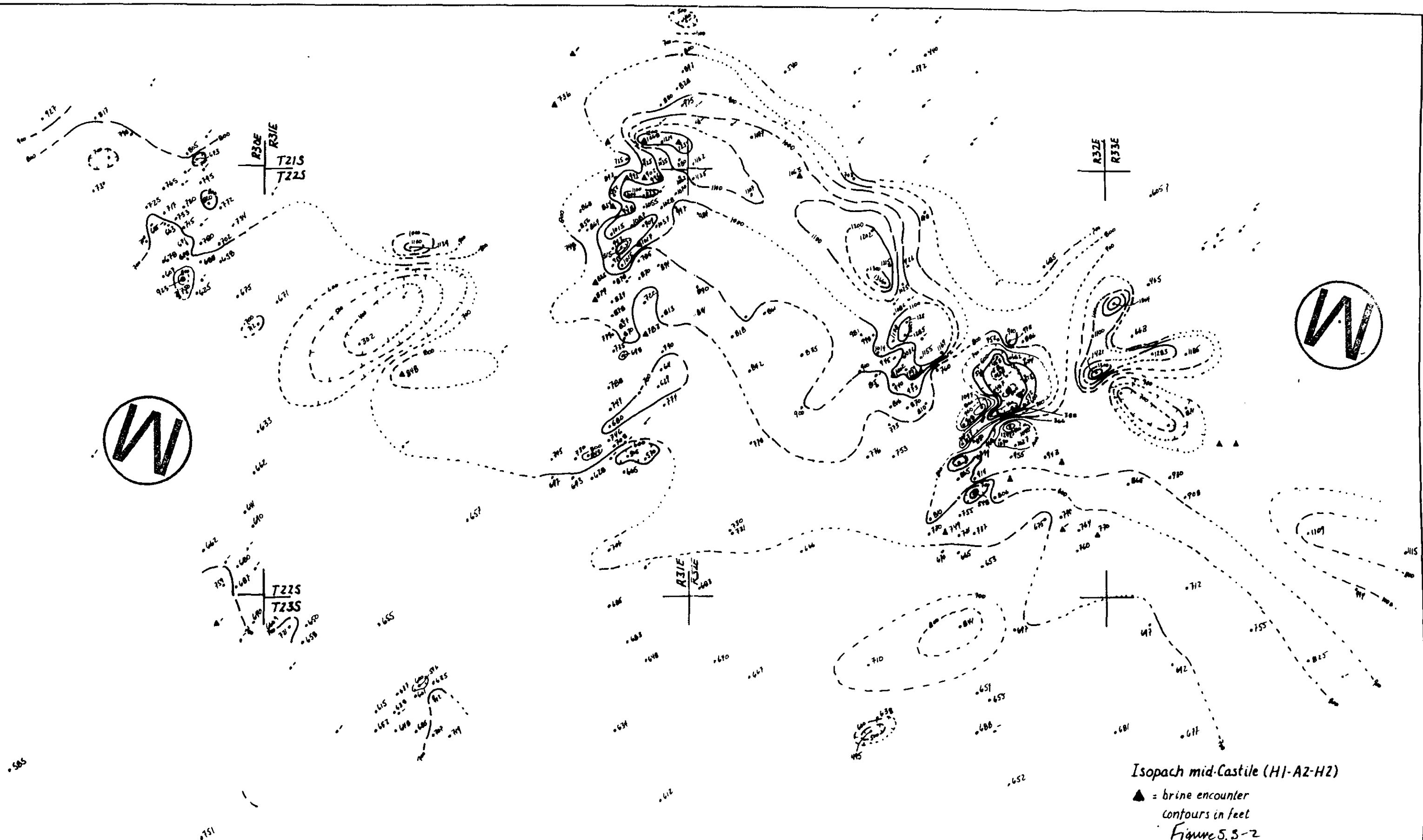
Isopach mid-Castile (H1-A2-H2)

▲ = brine encounter

contours in feet

Figure 5.3-2

Dennis W Powers 7/13/96
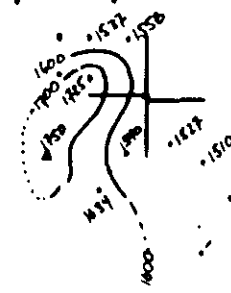
Isopach Bell Canyon - Cowden

▲ = brine intercept
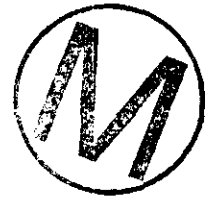contours in feet
[ ] = estimated value
R = reef location

Figure 5.3-3

Dennis V Powers 7/10/80

kriging estimates of intercepting brine under the WIPP site (see section 7.0).

6.0 GEOSTATISTICAL ANALYSIS

6.1 INTRODUCTION

We utilize a geostatistical approach to estimate the conditional probability of a brine reservoir intercept within the Castile Formation because geostatistics permits quantification of a phenomenon's spatial correlation and it provides robust estimation algorithms in kriging. The data are first examined with a suite of geostatistical tools to estimate the phenomenon's covariance function and then test the covariance estimate's robustness. This function quantifies how the phenomenon's observed values are correlated in space, in time, or in both. We can gain a better understanding of the scale of the phenomenon from the correlation scale, the distance over which the observed values appear to be correlated, of most estimated covariance functions. The data and the estimated covariance function are then input into a kriging algorithm to give a "best" unbiased, minimized least-squares error estimate of the phenomenon's value at unsampled locations while honoring the data exactly. For a binary phenomenon, such as the presence or absence of a brine reservoir intercept, kriging provides a direct estimate of the probability of the phenomenon at an unsampled location conditioned on the data locations and on the estimated covariance function (Deutsch and Journel, 1992). We can test the validity or appropriateness of the probability estimates by comparing the estimated covariance with covariance functions estimated from related phenomena, particularly those which may have created or influenced the spatial distribution of interest.

Our phenomenon of interest is whether a borehole will intercept a brine reservoir in the Castile Formation. We have observations of intercept/no-intercept from 354 wells distributed across roughly 645 km² (252 mi²) of Delaware Basin. The WIPP site is roughly centered within this area. Taking on a value of either 1 or 0, binary variable observations are a type of categorical variable, which can represent phenomena such as rock types, counts of numbers of species, or whether a contaminant concentration exceeds a given threshold value. In contrast, continuous variables describe phenomena whose values vary more continuously than discretely; e.g., hydraulic conductivity, chemical concentration, temperature, etc. We seek the probability of a brine reservoir intercept at specific unsampled locations. Assuming the data set is representative and that classification errors are negligible, we can calculate a probability estimate for the unsampled locations which depends on the observed values: divide the 27 intercepts by 354, the total number of observations, to get a mean probability of 0.076. Although legitimate, this approach does not include information contributed by locations of the observed values relative to the

unsampled locations of interest. It is equivalent to deciding that there is no spatial relationship between occurrences; the mean probability can be reduced by simply enlarging the study area, which will include more drillholes without evidence of brine occurrences.

We can treat the observed values as having originated from a random function (RF), a name which is applied to a collection of random variables distributed across a domain of interest. The spatial correlation of a RF Z is described by the (auto)covariance, $C_{Z(x), Z(x+h)}$, where E is the expectation operator, **x** is the location vector for an observation, and **h** is the distance between it and another observation.

$$C_{Z(x), Z(x=h)} = E\{[Z(x) - E\{Z(x)\}][Z(x+h) - E\{Z(x+h)\}]\} \qquad (Eqn.6-1)$$

If we assume that the mean is constant and that the covariance is simply a function of the distance **h** separating the two values within the domain of interest, we can then simplify the covariance function:

$$C_z(h) = E\{[Z(x) Z(x+h)]\} - E\{Z(x)\}^2 \qquad (eqn.\ 6-2)$$

These assumptions are the result of deciding to treat the random function Z as a stationary RF. It is useful to decide an RF is stationary because we seldom can take repeated measurements of the phenomenon of interest at the same location, making it impossible to estimate the cumulative distribution function (cdf) at that point. Instead, by deciding to use a stationary random function model, we can use samples from other locations to estimate the cdf. It cannot be determined from the data whether the stationarity decision is valid . See Deutsch and Journel, 1992, p 12-13; Isaaks and Srivastava, 1989, p. 220-221; and Journel, 1986 for further discussion. This decision, however, permits us the use of a range of geostatistical tools, such as the semi-variogram, to estimate the covariance and thereby quantify the spatial variability.

The semi-variogram, g(h), is the variance of the difference between observations separated by a distance (or lag) **h**:

$$\gamma(h) = \frac{Var\{Z(x-h) - Z(x)\}}{2} = C_z(0) - C_z(h) \qquad (Eqn.\ 6-3)$$

The covariance at separation distance **0** is simply the variance of Z. Equation 3 demonstrates the relationship between the variogram and the covariance function for a stationary RF. Their interrelationship is depicted in Figure 1. The

FIGURE 6-1
Interrelationship Between the Covariance
and Semi-Variogram Functions
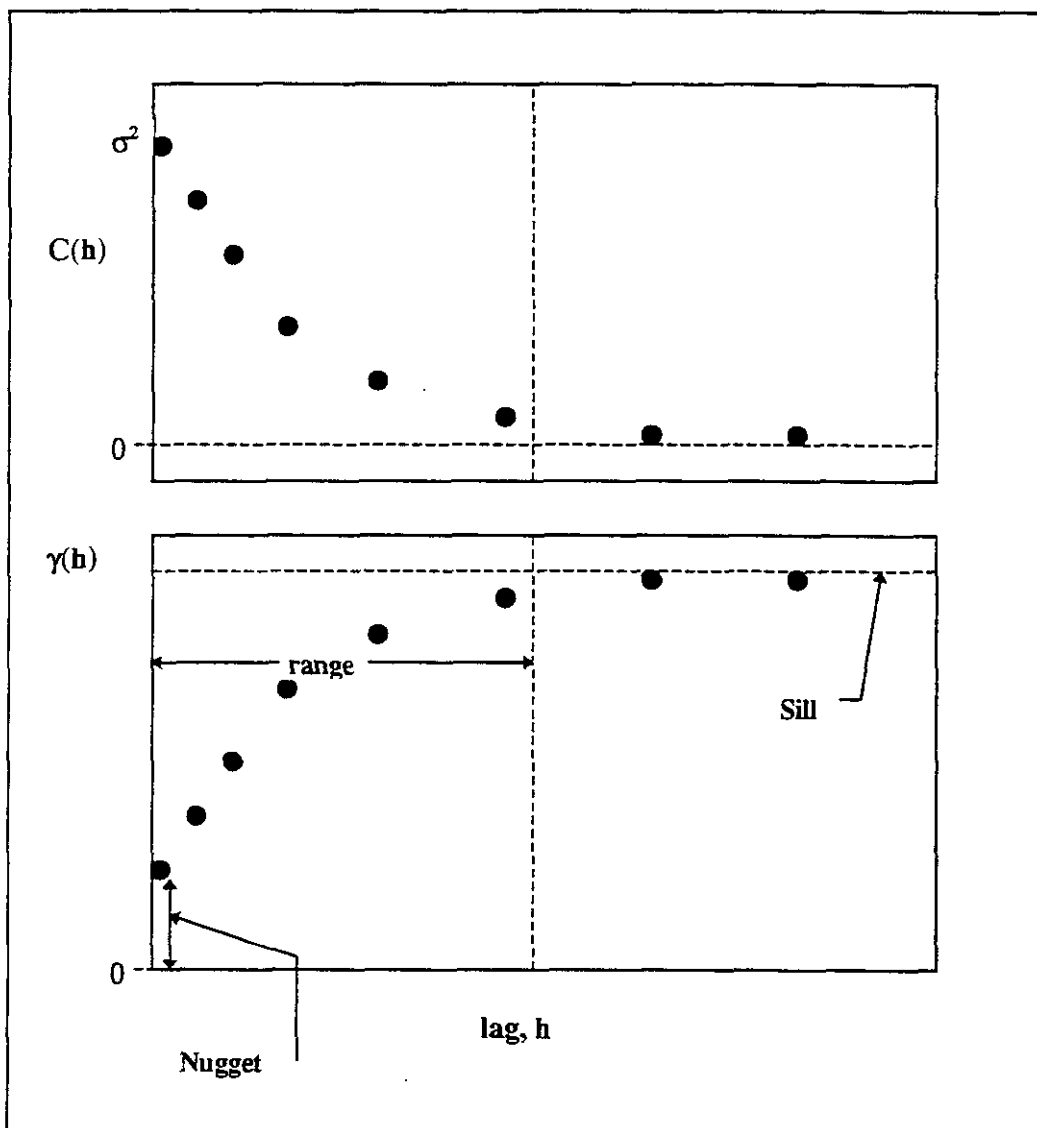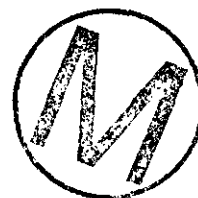
following discussion assumes a random function defined over a two-dimensional domain; generalization to a three-dimensional domain is straightforward. Most semi-variograms consist of three parameters: the range, defined as the lag at, which the semi-variogram value levels out, i.e., the correlation between two observations decreases to zero; the sill, defined as the $\gamma(h)$ value at which the semi-variogram levels out; and the nugget, which refers to a discontinuity between the estimated semi-variogram's first point (nearest to a zero lag) and the origin. The range represents the length (or time) scale over which correlation between any two observations is still observed. The sill represents the population or sample variance of all the observations, and the nugget represents the sum of measurement errors and small-scale spatial variability not yet resolved. Each of these is depicted in Figure 6-1.

If, when calculated along a number of different directions, the sample semi-variograms show no significant changes in range, nugget, or sill values then the phenomenon is said to be isotropic; otherwise, it is anisotropic. Anisotropy in the directional semi-variograms is analogous to the major and minor axes of an ellipse (or ellipsoid in 3-D space). The directions corresponding to the major and minor axes can be thought of as the phenomenon's preferred or principal directions. Figure 6-2 demonstrates the relevant parameters for calculating a directional semi-variogram. To calculate an isotropic semi-variogram, which is also called an omni-directional semi-variogram, the search and bandwidth distances and half-angle should be set to their maxima, e.g., the length of the domain and 90 degrees, respectively.

A host of related geostatistical tools for describing spatial variability have been developed to complement the strengths and weaknesses of the semi-variogram (see Deutsch and Journel, 1992, p. 56). The correlogram and non-ergodic covariance functions can filter out trends in the variances and means for each lag group respectively. The relative semi-variograms and semi-rodogram are less susceptible to data clustering and outlier values than the semi-variogram. The semi-madogram is more robust to outliers than the semi-variogram. Prudent practice requires that one or more of these alternative measures of spatial variability be examined in addition to the traditional semi-variogram.

Estimation of the values at unsampled locations can begin once the spatial variability has been adequately characterized by a semi-variogram (or covariance) function with an estimated sill, nugget, and range. A very wide range of methods have been developed to solve the general interpolation problem (see Cressie, 1991), but only the kriging algorithms provide an unbiased, minimum error variance estimate, which exactly honors observed values, for an explicit covariance model. The kriged or predicted value is a function of the estimated covariance and of the locations, not the values, of the initial observations of the phenomenon. However, the value predicted for an unsampled location is conditional on the observed values, since they are

FIGURE 6-2
Parameters for Calculating Sample Semi-Variograms
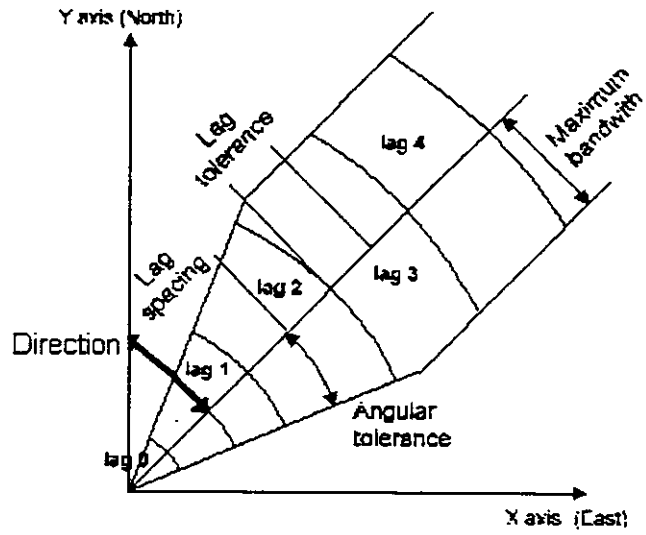
Adapted from Y. Pannatier, VARIOWIN HELP.
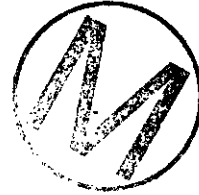
reproduced exactly by the algorithms. When applied to a binary variable, such as the presence or absence of a rock type or a brine reservoir intercept, the most commonly used kriging algorithm, ordinary kriging, provides a direct estimate of the conditional probability of that variable (Journel, 1984; Deutsch and Journel, 1992, p. 73). As above, this probability estimate is a function of the covariance model adopted and of the data locations and is conditioned on the observations.

6.2 METHODS

6.2.1 Variography

Variography is the process of extricating a phenomenon's spatial correlation from a set of observed values. Also known as structural analysis, the process focuses on estimating a sample semi-variogram or related functions, which are proxies for the covariance function, and then critically examining the estimate for sensitivity to individual data points, data clustering, and extreme values (outliers). Values for the range, sill, and nugget are determined from a theoretical semi-variogram model which is fitted to the sample semi-variogram.

6.2.1.1 Sample Semi-Variogram Calculation

Semi-variograms are calculated according to

$$\gamma(h) = \frac{1}{2N(h)} \sum_{i=1}^{N(h)} (x_i - y_i)^2 \qquad (Eqn. \quad 6\text{-}4)$$

where **h** is the approximate or average lag distance for each lag class, N(h) is the number of pairs for each lag class, x_i is the initial or tail value, and y_i is the final or head value for the pair. All variographic calculations were carried out using the VARIO module of the public domain software package UNCERT (Wingle et al, 1994), available from the Colorado School of Mines in Golden, CO. Calculations for the final semi-variograms were compared with those from two other geostatistical software packages: GSLIB (Deutsch and Journel, 1992) and VARIOWIN (Pannatier, 1994).

Since the geological structure data were not available to help constrain the choice of geometric directions prior to this study's start, we calculated sample semi-variograms for the isotropic (omni-directional) case and for a full range of anisotropic geometric directions. This ensured there was no bias in the selection of sample semi-variogram directions. We did not consider zonal anisotropy in this analysis because we have assumed the Castile Formation, from which all of the observations were collected, has a homogeneous variance

about the probability of a brine intercept. That is, the brine intercept probability variance is constant across the study area. Our results indicate the sill does not vary significantly compared to the ranges for the directional sample semi-variograms and therefore the anisotropy is better described by the geometric rather than the zonal approach.

The directional semi-variograms were estimated for azimuths 0, 20, 45, 70, 90, 110, 135, and 160 degrees measured clockwise from a 0 degree north. Lag spacings between 1000 ft and 2000 ft were examined because they bracketed the most common borehole spacings observed in the data. The maximum search distance, directional bandwidth, and horizontal half-angle were set to their maximum values of 150000 ft, 150000 ft and 90 degrees for the isotropic sample semi-variogram. The data were sufficient in number to restrict the horizontal half-angle to 15 degrees, maximum search distance to 50000 ft, and the directional bandwidth to 10000 ft and still have adequate numbers of observation pairs (>30) within each of the first 20 or more lags for all of the anisotropic sample semi-variograms.

Sample semi-variograms were judged significant if they exhibited a reasonably monotonic increasing structure within the first 25% of the lag classes with adequate numbers of pairs within each lag class. All significant sample semi-variograms were retained for fitting of theoretical semi-variogram model parameters (range, sill, and nugget variance). When an anisotropic sample semi-variogram was found significant, we calculated the sample semi-variogram along its orthogonal direction.

6.2.1.2 Sample Semi-Variogram Robustness

Clustering of the data locations can create apparent structure in sample semi-variograms (Deutsch and Journel, 1992; Isaaks and Srivastava, 1989, p. 162). Given the obvious clustering of borehole locations (see Figure 6-3), we tested the sample semi-variogram robustness to clustering using two different approaches. The first compares sample semi-variograms from the entire data set with those computed for two non-overlapping data subsets which have relatively uniform spatial distributions of boreholes and possess adequate numbers of brine reservoir intercepts. Subset 1 contains 81 boreholes, 15 of which had brine intercepts. Subset 2 holds 93 boreholes, 9 of which had evidence of brine intercepts. Figures 6-4 and 6-5 show the locations of the two data subsets. These two subsets were the only areas to possess both a relatively uniform distribution of boreholes and sufficient numbers of brine intercepts. Most of the boreholes in these two subsets were drilled to explore sand channels which underlie the Castile Formation. Correlation structures which appeared significant in each of the data subsets and in the complete data set were judged to be independent of the large scale data clustering evident in Figure 6-3.

21

Figure 6--

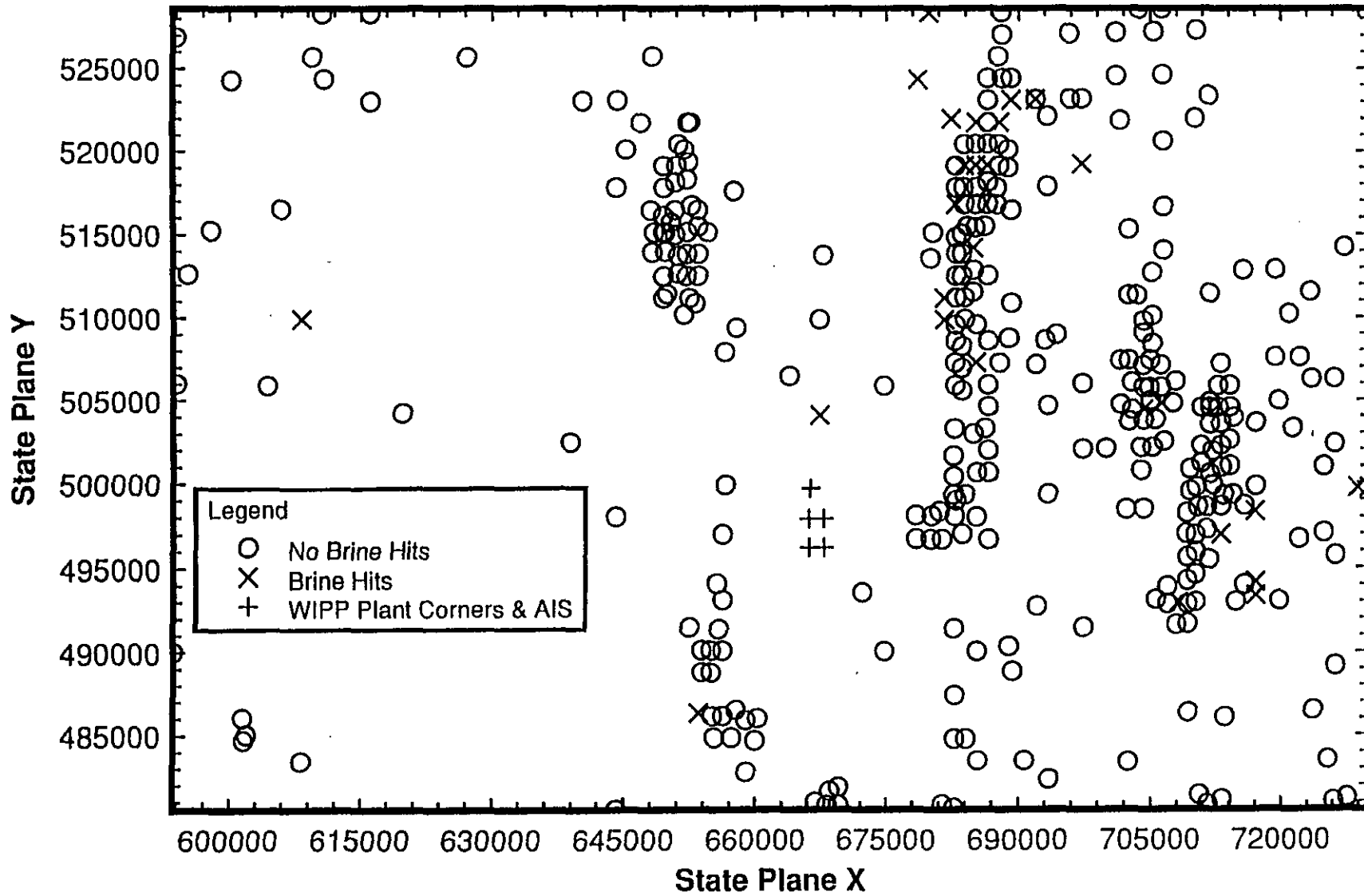# All Borehole Locations

Legend
- O No Brine Hits
- X Brine Hits
- + WIPP Plant Corners & AIS

State Plane Y

State Plane X

Borehole Locations
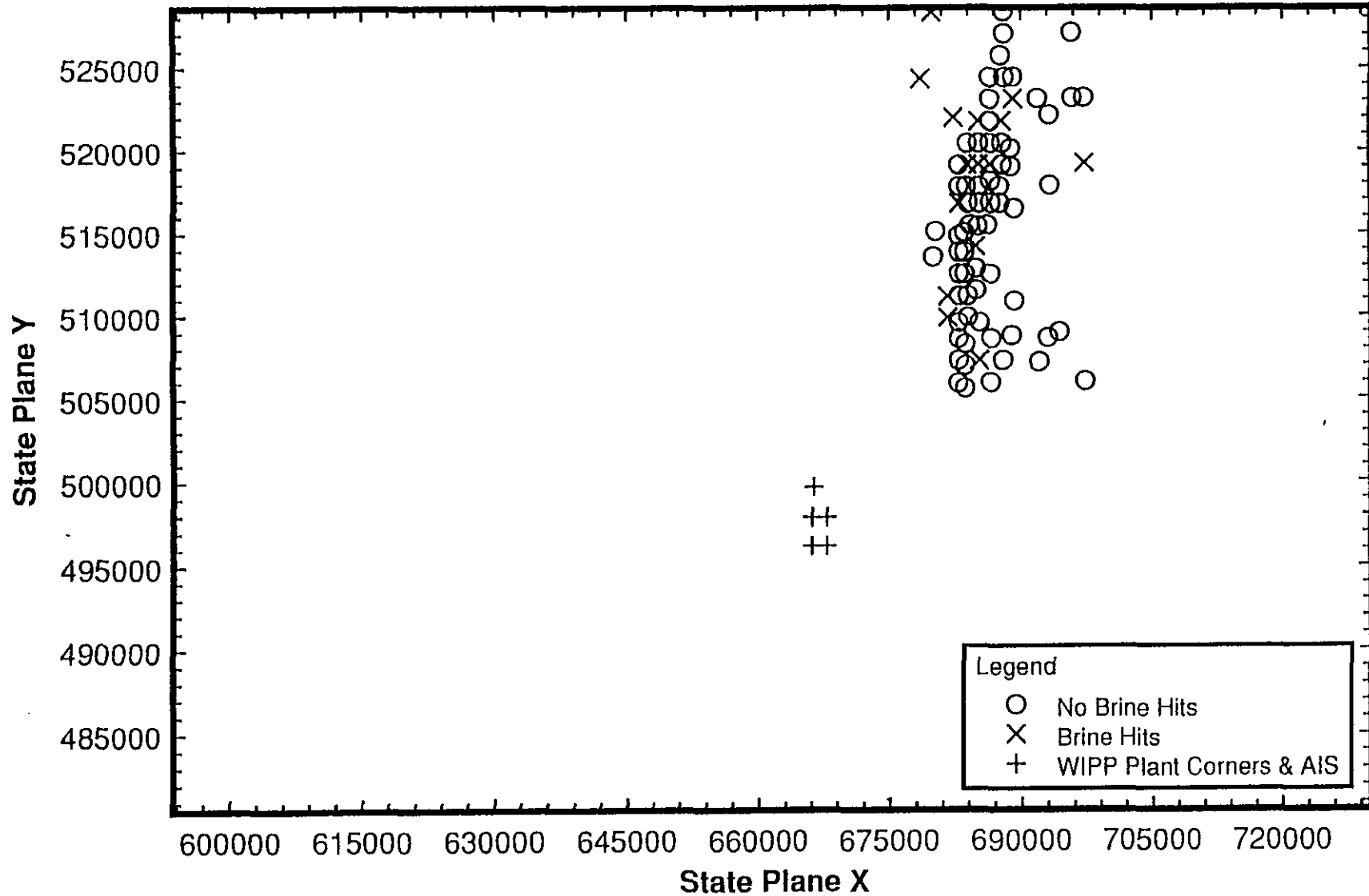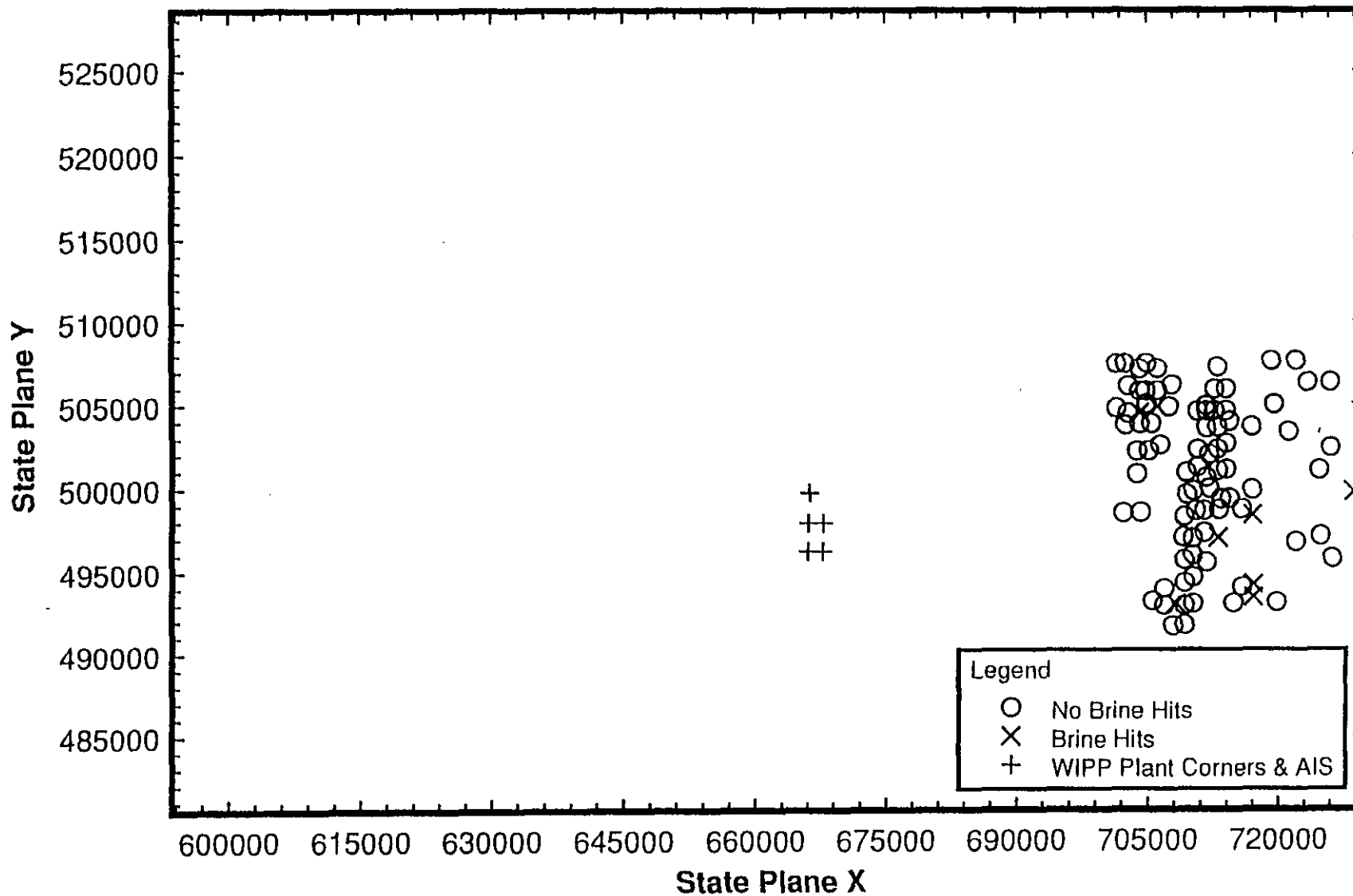First Data Cluster: BRSM1.DAT

Figure 6-

Figure 6-5

Borehole Locations
Second Data Cluster: BRSM2.DAT

The second approach utilizes alternative measures of spatial continuity which are less sensitive to data clustering. The general and pairwise relative semi-variograms are typically less vulnerable to clustering because they normalize the semi-variogram value for each lag class by the squared mean of the data and the squared average of the paired values; however, they can only be computed for strictly positive data (Deutsch and Journel, 1992). Since our data were mainly zeros and a few ones, we added a value of one to each data point, shifting the data range from [0,1] to [1,2] and then calculated the relative semi-variograms. This shift preserves the maximum and minimum differences between any two data points, which are all that is required for calculation.

The semi-rodogram, defined as

$$Y_R(h) = \frac{1}{2N(h)}\sum_{i=1}^{N(h)} \sqrt{|x_i - y_i|} \qquad (Eqn.6-5)$$
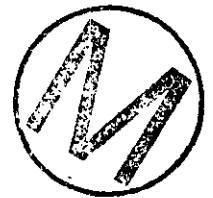
is also more resistant to clustering than the semi-variogram (Deutsch and Journel, 1992, p. 56). However, this measure (and the related semi-madogram) is numerically identical to the semi-variogram when computed for a binary variable limited to differences of 1 and 0. While this may suggest the semi-variogram for a binary variable with the same maximum and minimum differences should be relatively indifferent to data clustering, it may simply be a numerical artifact. Accordingly, the semi-rodograms were not used in the analysis.

We examined the impact of classification error on the sample semi-variogram calculations. Initial variographic calculations had been made prior to reclassifying well AEC7 from a brine intercept to a non-intercept. We recalculated sample semi-variograms for each of the data subsets and for the entire data set and then compared them to the previous results.

Undue influence of outlier data values was not considered to be significant because the range of allowable values was strictly limited to 0 and 1.

6.2.1.3 Theoretical Variogram Model Fitting

The range, sill, and nugget variance were estimated for each of the final sample semi-variograms using UNCERT's VARIOFIT module. Fits of each of the most common theoretical semi-variogram models: spherical, exponential, and Gaussian, were made both with and without non-zero nugget variances. Model fit was evaluated subjectively with the objective of preserving the apparent smaller scale range and nugget as much as possible. Automated, non-linear curve fits of theoretical models to the sample semi-variograms were also examined to check for subjective bias in the initial manual fit.

22

6.2.2 Kriging of a Binary Categorical Variable

We estimated the conditional probabilities of a brine intercept at regularly-spaced grid nodes using ordinary point kriging for each of the selected theoretical semi-variogram models. An areally-averaged probability was then computed from the kriged point probabilities for the waste panel area.

Ordinary point kriging was carried out using UNCERT's GRID module for each theoretical semi-variogram model. Inputs include the estimated semi-variogram parameters, the intercept/no-intercept observations, grid definition parameters, and search parameters. We selected a 1000 ft grid node spacing along both the N-S and E-W axes. The kriged domain range included all of the data points and had an E-W range of [590000, 731000] and a N-S range of [480000, 530000] in NM state plane coordinates. We compared results from the normal search mode, with minimum and maximum number of data points set to 4 and 16, to those from the octant search mode, which had minimum and maximum number of data points set to 2 and 16 and a maximum per octant of 8 points.

The CONTOUR module from UNCERT was used to create color-coded maps of the conditional brine intercept probabilities for each of the semi-variogram models. Point-kriged probabilities for each node within the waste panel, the shaft pillar, and the experimental areas were pulled from the output files and noted. We estimated an average conditional probability for the entire waste panel area through weighting each nodal conditional probability by the percentage of the total waste panel area it influenced. These calculations were made using the EXCEL spreadsheet package.

We checked the point-kriged probabilities from UNCERT's GRID module against results from GSLIB's KTB3D algorithm using the same grid, search, and variogram model parameters.

6.3 RESULTS AND DISCUSSION

6.3.1 Variography

6.3.1.1 Sample Semi-Variogram Calculations
Figures 6-6ab and 6-7ab show all the sample semi-variograms for the first and second data subsets. Figure 6-6a depicts the most significant sample semi-variograms found in Subset 1: the isotropic case and azimuths 20 and 160 degrees together with their orthogonals (110 and 70 degrees, respectively). The remaining directional sample semi-variograms, shown in Figure 6-6b, demonstrate a pure nugget effect, i.e., there is no spatial correlation. Figure 6-7a shows that only the azimuth 160 directional semi-variogram clearly demonstrates any correlation structure. The isotropic case semi-variogram also
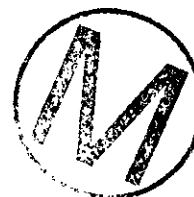
Castile Brine Reservoirs: BRSM1.DAT
Semi-Variogram: Lag = 1500 ft; BW = 10000; HA = 15

Fig 6-6a

Legend
- ‑ ‑ ‑ Variance
- ● Isotropic
- Az = 0 deg
- Az = 20 deg
- ■ Az = 45 deg
- Az = 70 deg
- ⊖ Az = 90 deg
- Az = 110 deg
- Az = 135 deg
- ⊟ Az = 160 deg

Figure 6-66

Castile Brine Reservoirs: BRSM1.DAT

Semi-Variogram: Lag = 1500 ft; BW = 10000; HA = 15

Legend
- Variance
- Isotropic
- Az = 0 deg
- Az = 20 deg
- Az = 45 deg
- Az = 70 deg
- Az = 90 deg
- Az = 110 deg
- Az = 135 deg
- Az = 160 deg
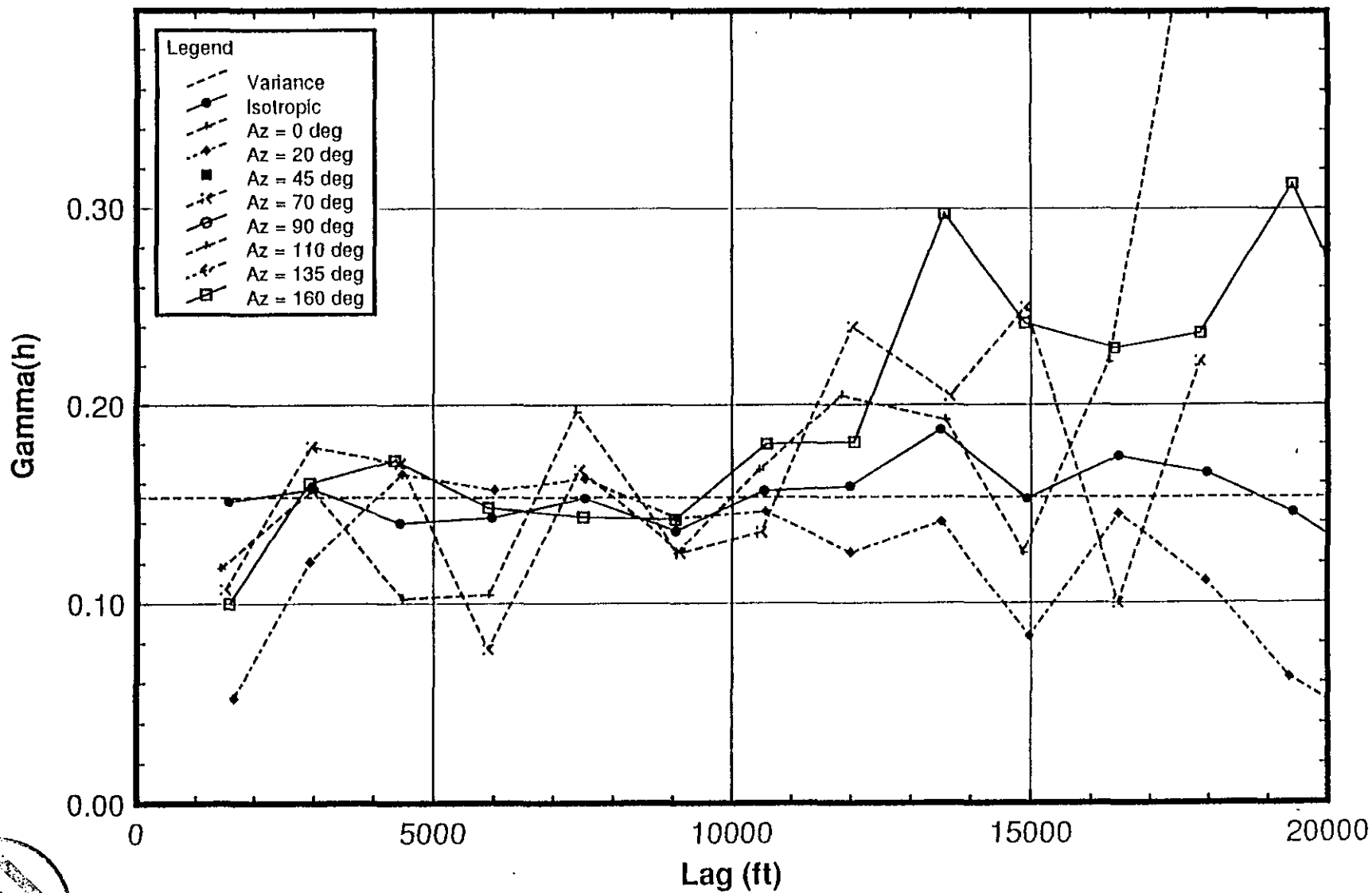
Castile Brine Reservoirs: BRSM2.DAT

Figure 6-7a

Semi-Variogram: Lag = 1500 ft; BW = 10000; HA = 15

Legend
- Variance
- Isotropic
- Az = 0 deg
- Az = 20 deg
- Az = 45 deg
- Az = 70 deg
- Az = 90 deg
- Az = 110 deg
- Az = 135 deg
- Az = 160 deg

Gamma(h)

Lag (ft)

Castile Brine Reservoirs: BRSM2.DAT
Semi-Variogram: Lag = 1500 ft; BW = 10000; HA = 15

Figure 6-7b

Legend
- Variance
- Isotropic
- Az = 0 deg
- Az = 20 deg
- Az = 45 deg
- Az = 70 deg
- Az = 90 deg
- Az = 110 deg
- Az = 135 deg
- Az = 160 deg

Gamma(h)

Lag (ft)
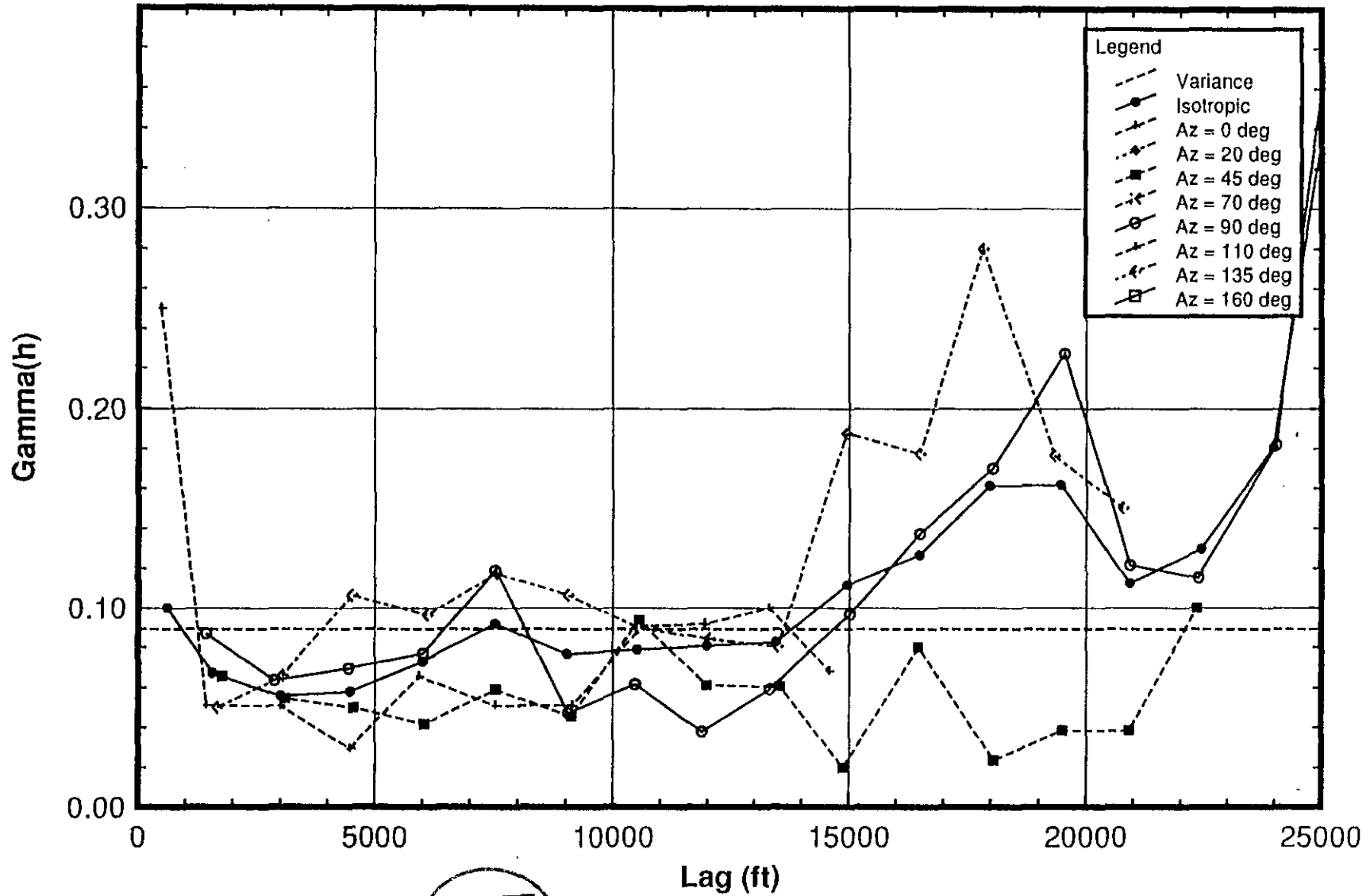
demonstrates correlation structure because its first lag spacing point has too few pairs to be considered a valid estimate. The 20 degree azimuth does not exhibit significant correlation structure. The same holds for all the remaining directions depicted in Figure 6-7b.

Figure 6-8a indicates that significant correlation structure can be found in the isotropic and 20, 70, and 160 degrees azimuth sample semi-variograms for the complete data set. Figure 6-8b shows that the remaining directions have no correlation structure and are best described by a pure nugget effect. The relatively large number of data points within the complete data set ensured that large numbers of pairs were found in all of the early lag classes, e.g., from 0 to 20000 ft lags. The semi-variogram values are typically less dependable for the later lag classes because the semi-variogram estimates become increasingly unstable as lag spacing increases beyond 25 to 40% of the maximum separation distance within the data set.

The only spatial correlation structures which appear consistently across the three data sets are the isotropic (omni-directional) and the anisotropic 160 degrees azimuth sample semi-variograms. The latter sample semi-variogram persisted across a fairly narrow range of azimuth angles: from 157 to 162 degrees azimuth. Although it exhibits some noise (or, potentially, cyclicity) at the fourth lag, the 70 degree azimuth sample semi-variogram was consistent across the three data sets. The correlation structures observed for the 160 and 70 degree azimuth and isotropic semi-variograms persisted when lag spacings were varied from the initial value of 1500 ft to 1000 and 2000 ft. This was not the case for the 20 degree azimuth semi-variogram, which was observed at 1500 and 2000 ft lags but not at the 1000 ft lag. Furthermore, its orthogonal semi-variogram (azimuth of 110 degrees) did not show any significant correlation structure in any of the data sets for any lag spacing. Consequently, the 20 degree azimuth model was not considered to be a significant sample semi-variogram.

The relative semi-variograms for the complete data set shifted from [0,1] to [1,2] (see Figures 6-9ab and 6-10ab) confirm the isotropic and 160 and 70 degree azimuth semi-variograms demonstrate significant correlation structure. Changing borehole AEC7 from an intercept to a no-intercept had a negligible impact on the estimated sample semi-variograms. We found an exact equivalence to four or more decimal places between the calculations made with UNCERT's VARIO and those made using the GSLIB and VARIOWIN variography routines. The calculation results for each package are presented in Appendix I.

6.3.1.2 Theoretical Semi-Variogram Model Fitting

Table 6-1 presents the range, sill, and nugget variance parameters fitted for the

Castile Brine Reservoirs: BRSM5.DAT Figure 6-89

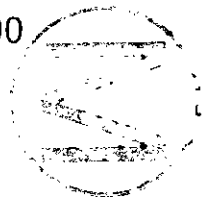Semi-Variogram: Range = 1500 ft; BW = 10000; HA = 15

Legend
- Variance
- Isotropic
- Az = 0 deg
- Az = 20 deg
- Az = 45 deg
- Az = 70 deg
- Az = 90 deg
- Az = 110 deg
- Az = 135 deg
- Az = 160 deg

Gamma (y-axis)

Lag (ft) (x-axis)

Castile Brine Reservoirs: BRSM5.DAT

Semi-Variogram: Lag = 1500 ft; BW = 10000; HA = 15

Figure 6-86

Legend
- Variance
- Isotropic
- Az = 0 deg
- Az = 20 deg
- Az = 45 deg
- Az = 70 deg
- Az = 90 deg
- Az = 110 deg
- Az = 135 deg
- Az = 160 deg

Gamma

Lag (ft)
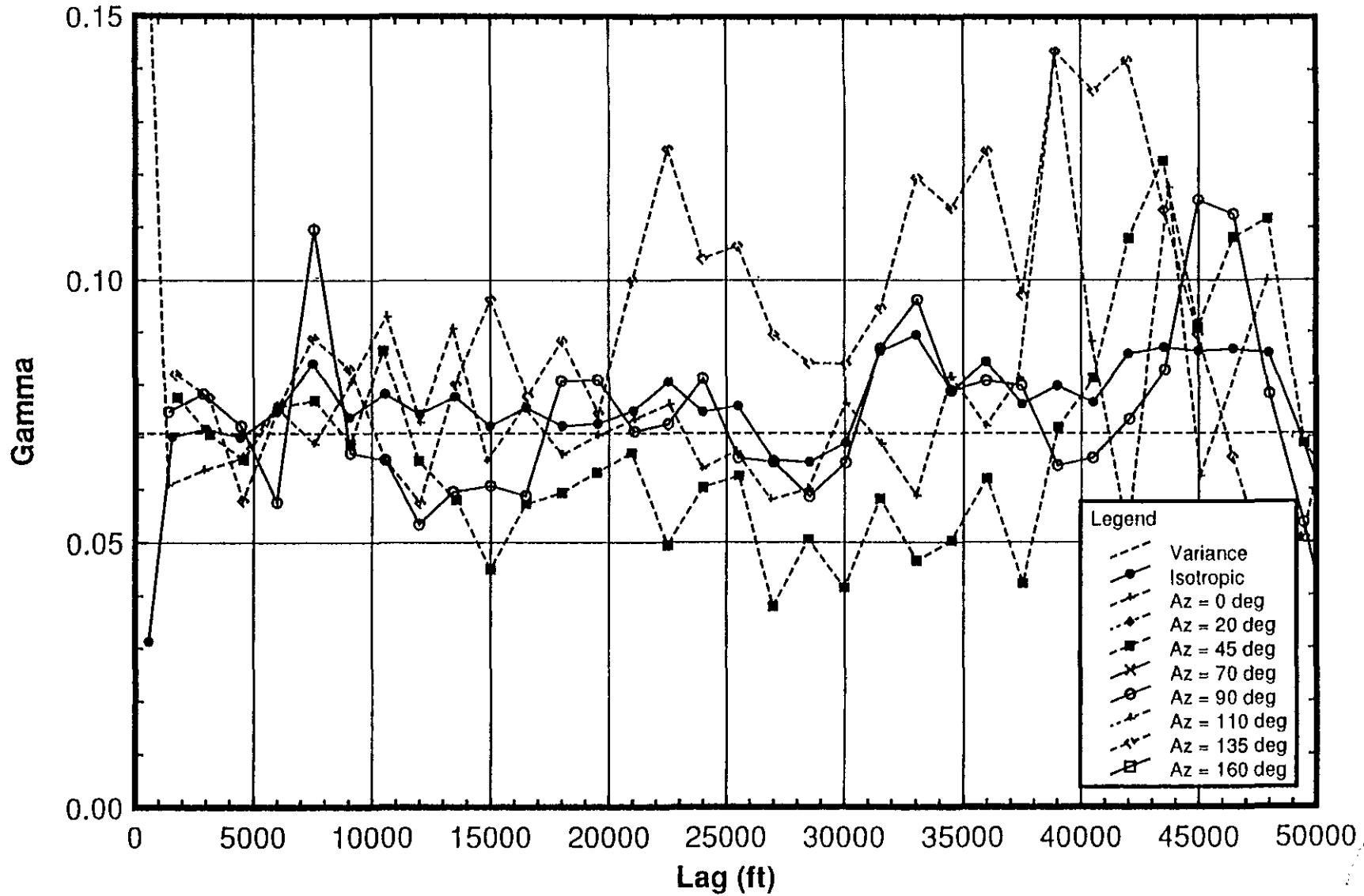
Castile Brine Reservoirs: BRSM512.DAT

General Relative Semi-Variogram: Lag = 1500 ft; BW = 10000; HA = 15

Figure 6-9

Legend

- - -	Variance
–•–	Isotropic
–+–	Az = 0 deg
⋯◆⋯	Az = 20 deg
–■–	Az = 45 deg
–✕–	Az = 70 deg
–⊕–	Az = 90 deg
⋯◣⋯	Az = 110 deg
–▾–	Az = 135 deg
–⊟–	Az = 160 deg

Gamma (y-axis)

Lag (ft) (x-axis)

Castile Brine Reservoirs: BRSM512.DAT

General Relative Semi-Variogram: Lag = 1500 ft; BW = 10000; HA = 15

Figure 6-96

Legend
- - - - Variance
—•— Isotropic
—+— Az = 0 deg
—▲— Az = 20 deg
—■— Az = 45 deg
—✕— Az = 70 deg
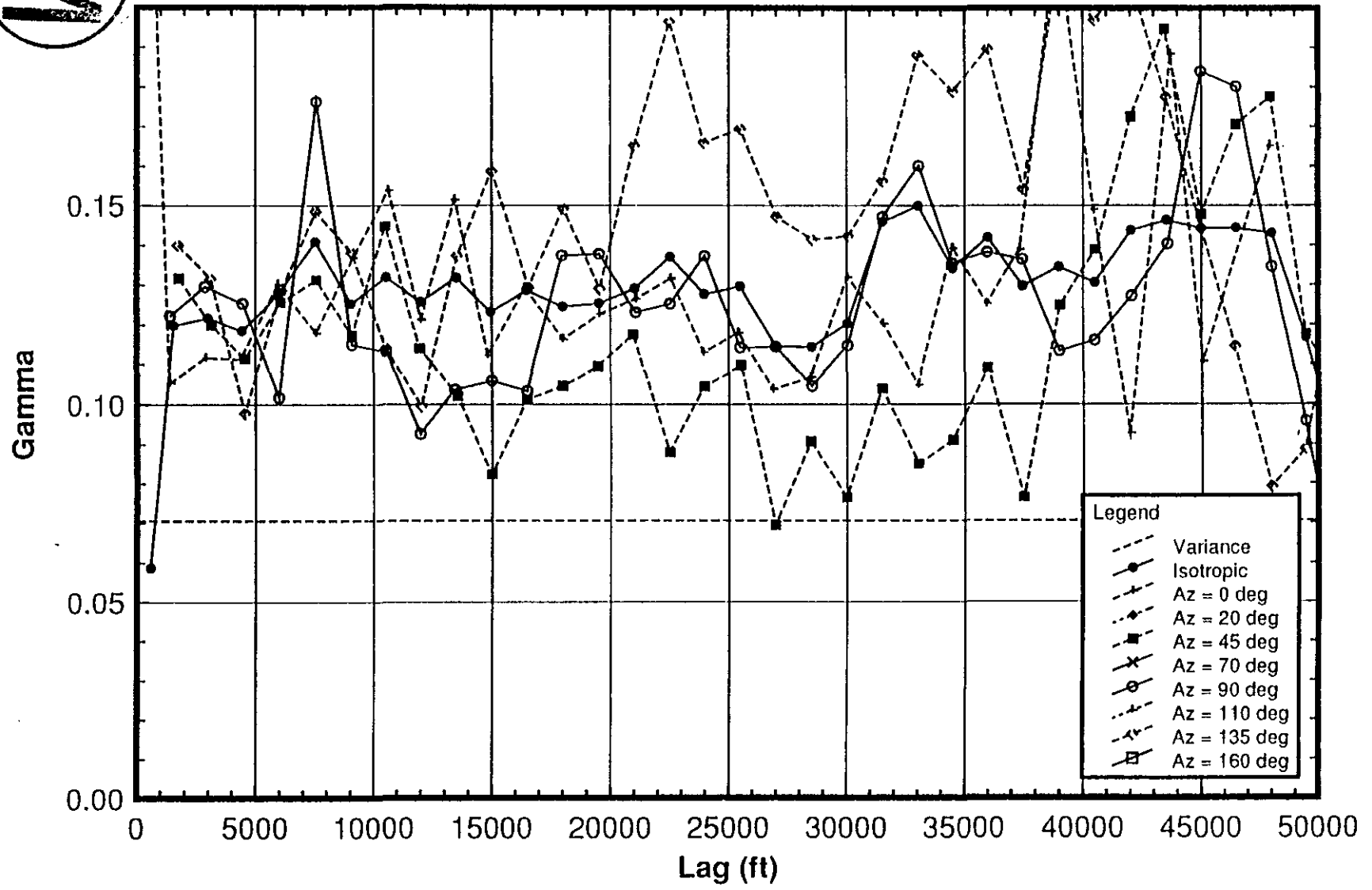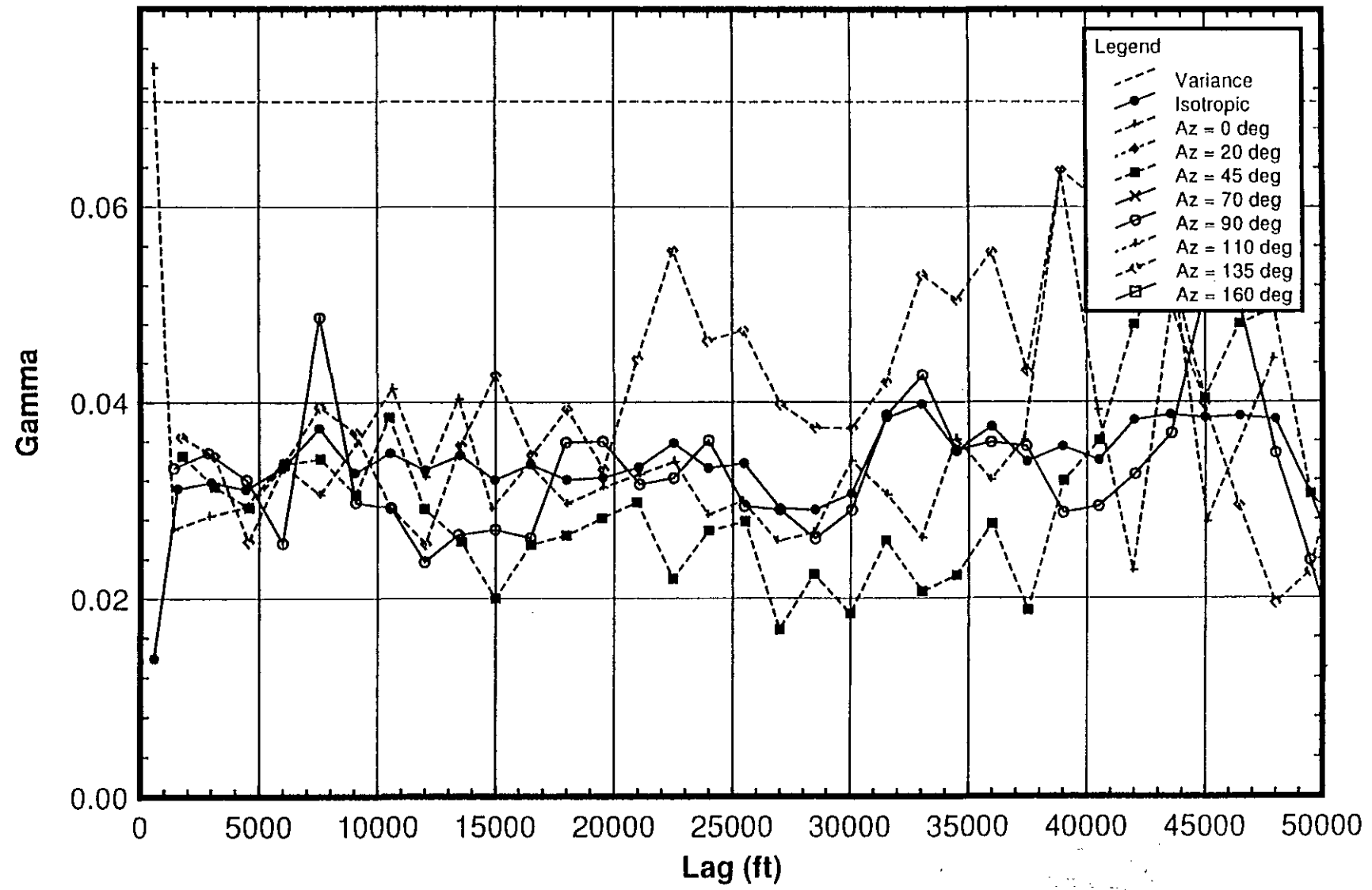—⊖— Az = 90 deg
—⊀— Az = 110 deg
—✕— Az = 135 deg
—⊟— Az = 160 deg

Gamma

Lag (ft)

Figure 6-10a

Castile Brine Reservoirs: BRSM512.DAT

Pairwise Relative Semi-Variogram: Lag = 1500 ft; BW = 10000; HA = 15

Legend
- - - - Variance
—•— Isotropic
—+— Az = 0 deg
··▲·· Az = 20 deg
—■— Az = 45 deg
—✕— Az = 70 deg
—⊕— Az = 90 deg
··+·· Az = 110 deg
—▽— Az = 135 deg
—□— Az = 160 deg

Castile Brine Reservoirs: BRSM512.DAT

Pairwise Relative Semi-Variogram: Lag = 1500 ft; BW = 10000; HA = 15

Figure 6-106

Legend
- Variance
- Isotropic
- Az = 0 deg
- Az = 20 deg
- Az = 45 deg
- Az = 70 deg
- Az = 90 deg
- Az = 110 deg
- Az = 135 deg
- Az = 160 deg

isotropic and two anisotropic sample semi-variograms. The "best" fits were made using the spherical theoretical variogram model, typically with zero nugget variance. The Gaussian theoretical variogram model allowed a non-zero nugget for the 160 degree azimuth sample semi-variogram. Figures 6-11abc show how the fitted spherical theoretical variograms match the sample semi-variograms.

It is important to note that the effective ranges of the various theoretical model types differ substantially. While the spherical model's range and effective range are equal, the effective range for the Gaussian model is √3 times its range. Similarly, multiply the exponential model's range by 3 to get its effective range. Only the effective ranges can be compared across model types.

Table 6-1
Fitted Model Variogram Parameters

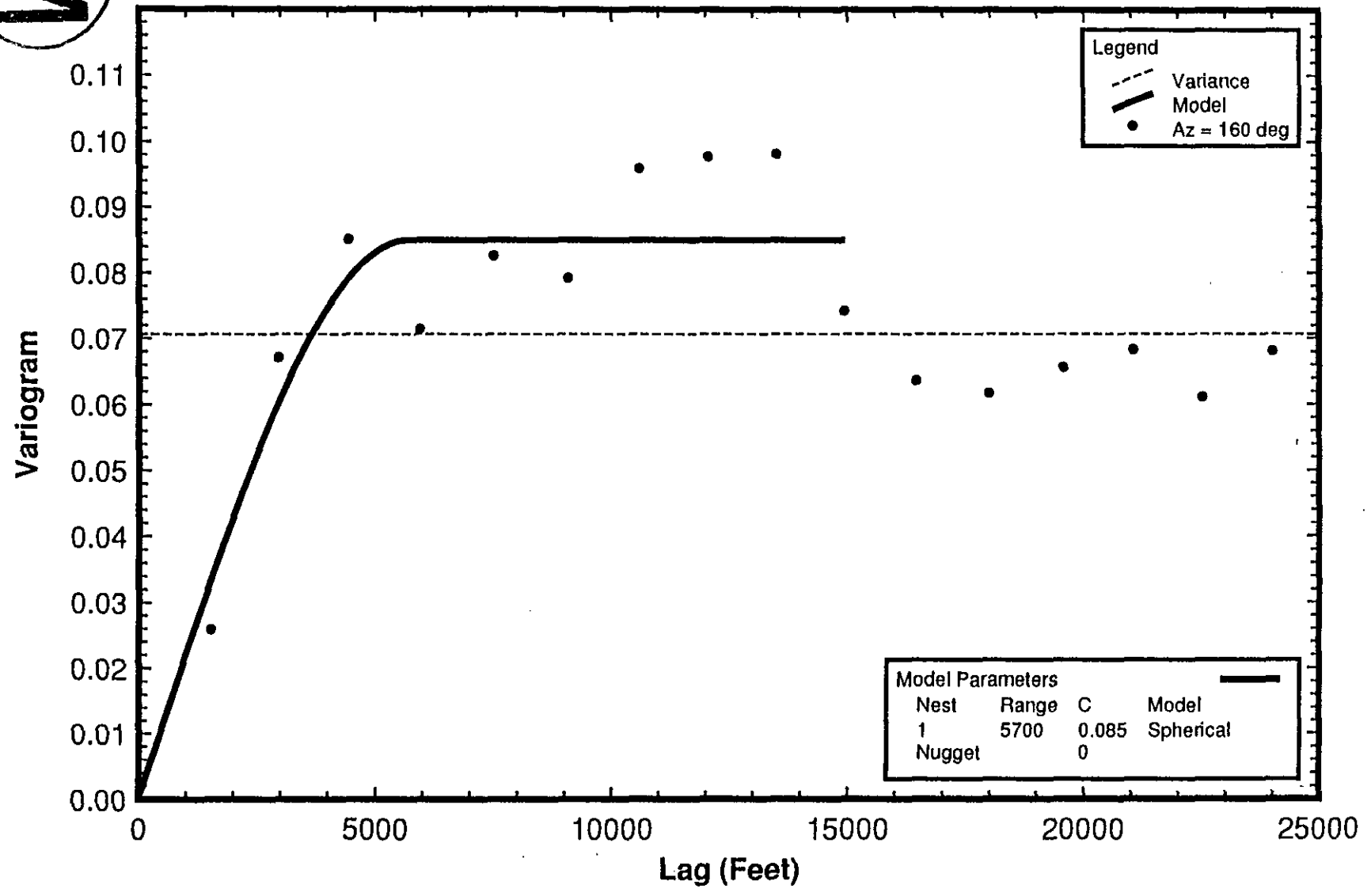| Sample Semi-Variogram	Theoretical Model Type	Nugget	Range (ft)	C (= Sill - Nugget)
Azimuth 160 degrees	Spherical	0.00	5700	0.085
	Gaussian	0.01	2500	0.074
Azimuth 70 degrees	Spherical	0.00	2880	0.080
	Gaussian	0.01	1400	0.068
Isotropic	Spherical	0.01	2500	0.065
	Exponential	0.00	800	0.076

6.3.2 Kriging

Figure 6-12 shows the point-kriged conditional probability of a brine reservoir intercept for the WIPP site and the surrounding vicinity using the 160 - 70 degree azimuth model semi-variograms. The waste panel centers are indicated by four crosses located in the center left of the map at roughly state plane coordinates [667000, 499000]. It is immediately south of the isolated brine reservoir hit shown as a high probability zone in yellow and orange. Note the anisotropic orientation of the probability contours: they are aligned along an azimuth corresponding to the 160 degree sample semi-variogram orientation. The contours form an ellipse because the 70 degree azimuth range is roughly half the range for the 160 degree orientation. The were no differences observed, to three or more decimal places, in point-kriged intercept probabilities within the site area footprints when results from the normal and octant search methods were compared. Figure 6-13 shows the individual nodal kriged probabilities within the site's three areas of interest: waste panel, shafts and access, and the experimental area. The kriged probabilities show an increasing trend moving from south to north as you approach the observed brine intercept at the WIPP-12 borehole.

Within the waste panel area, however, the kriged probabilities range between

Figure 6-11a

Castile Fm. Brine Reservoir: BRSM5.DAT

Legend

- - - Variance
—— Model
• Az = 160 deg

Model Parameters				
Nest	Range	C	Model	
1	5700	0.085	Spherical	
Nugget		0		

Variogram

Lag (Feet)
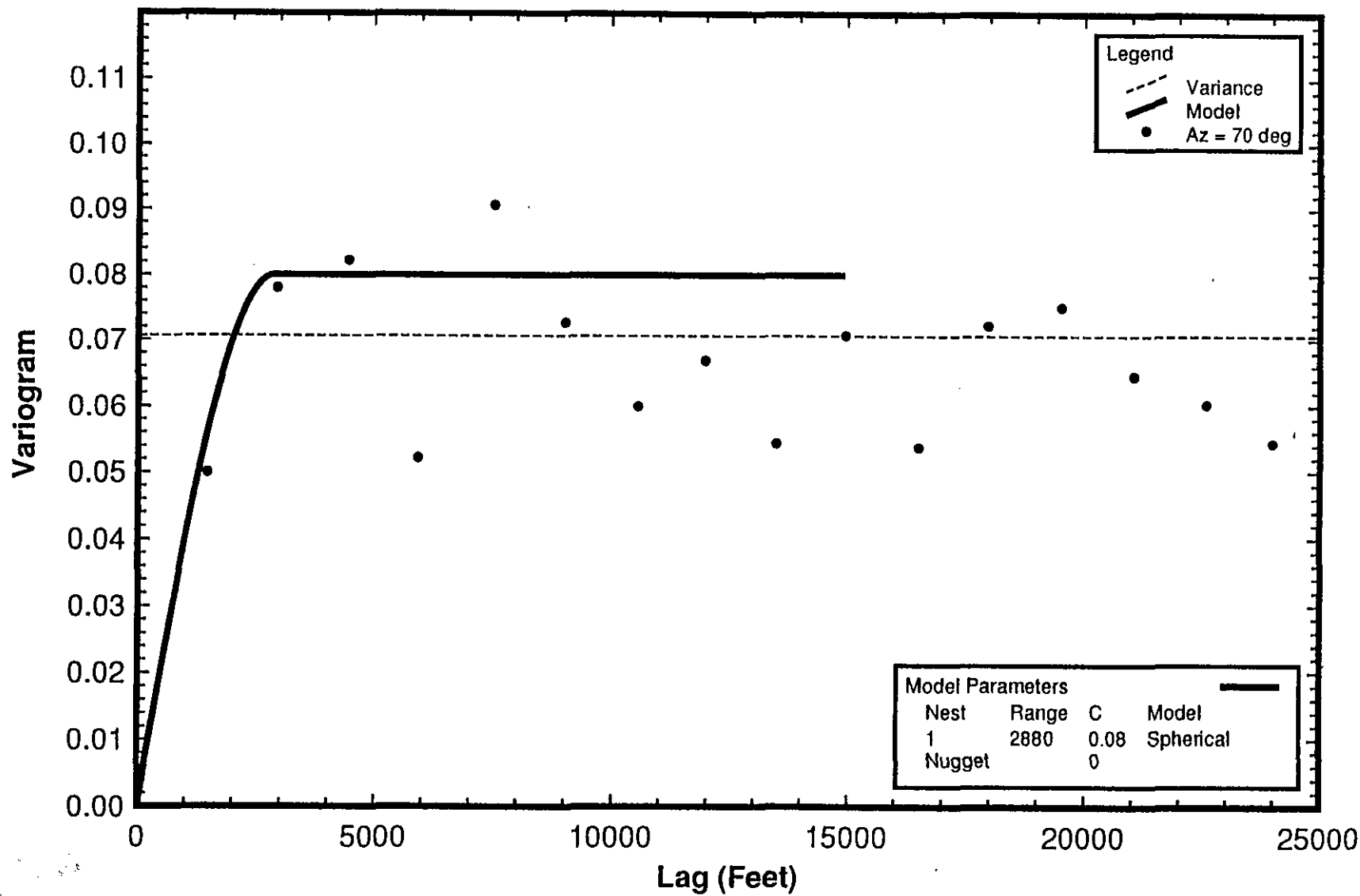
Figure 6-11b

Castile Fm. Brine Reservoir: BRSM5.DAT

Figure 6-11c

Castile Fm. Brine Reservoir: BRSM5.DAT
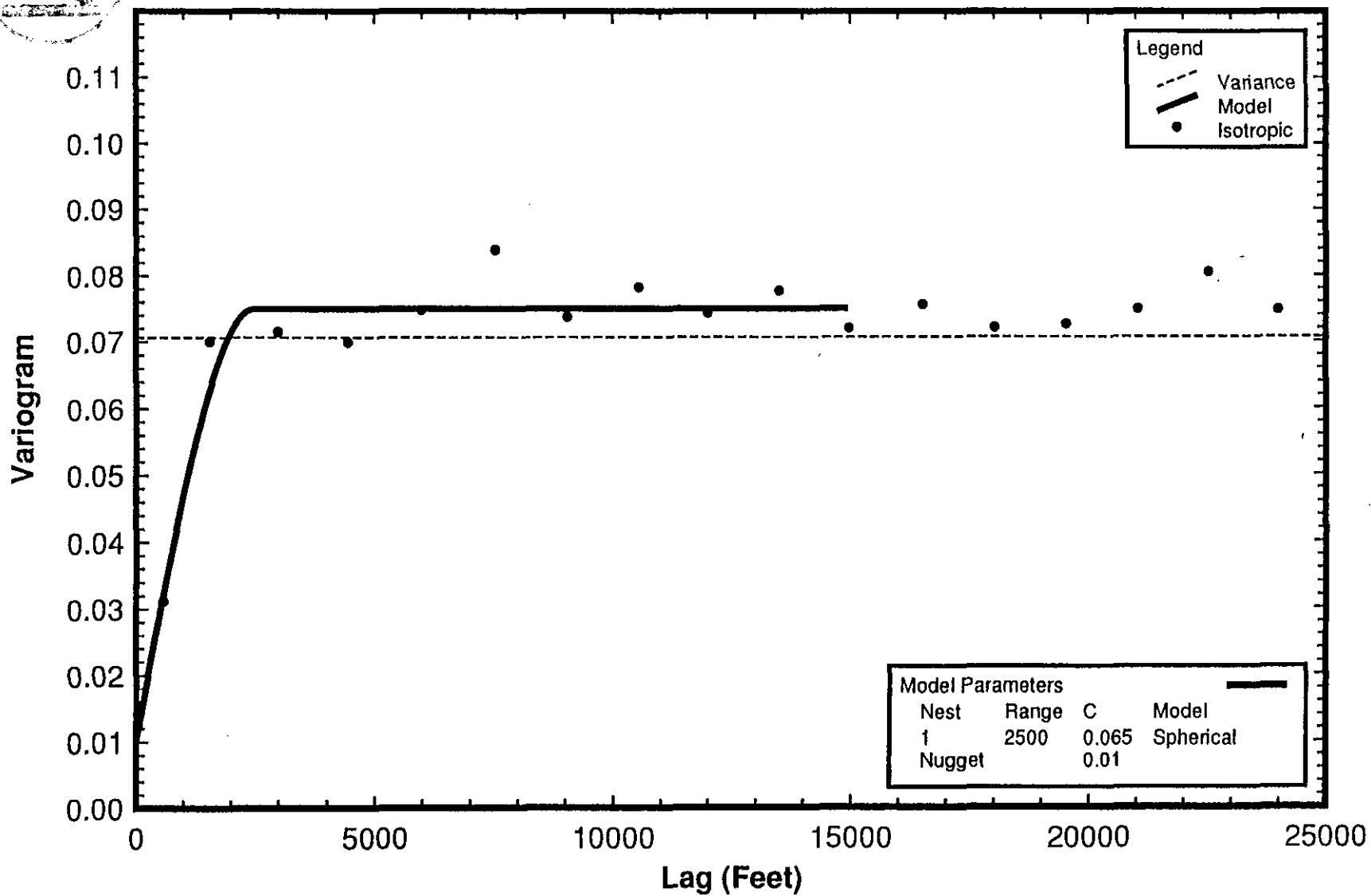
Figure 6-12

Probability of Encountering a Castile Brine Reservoir
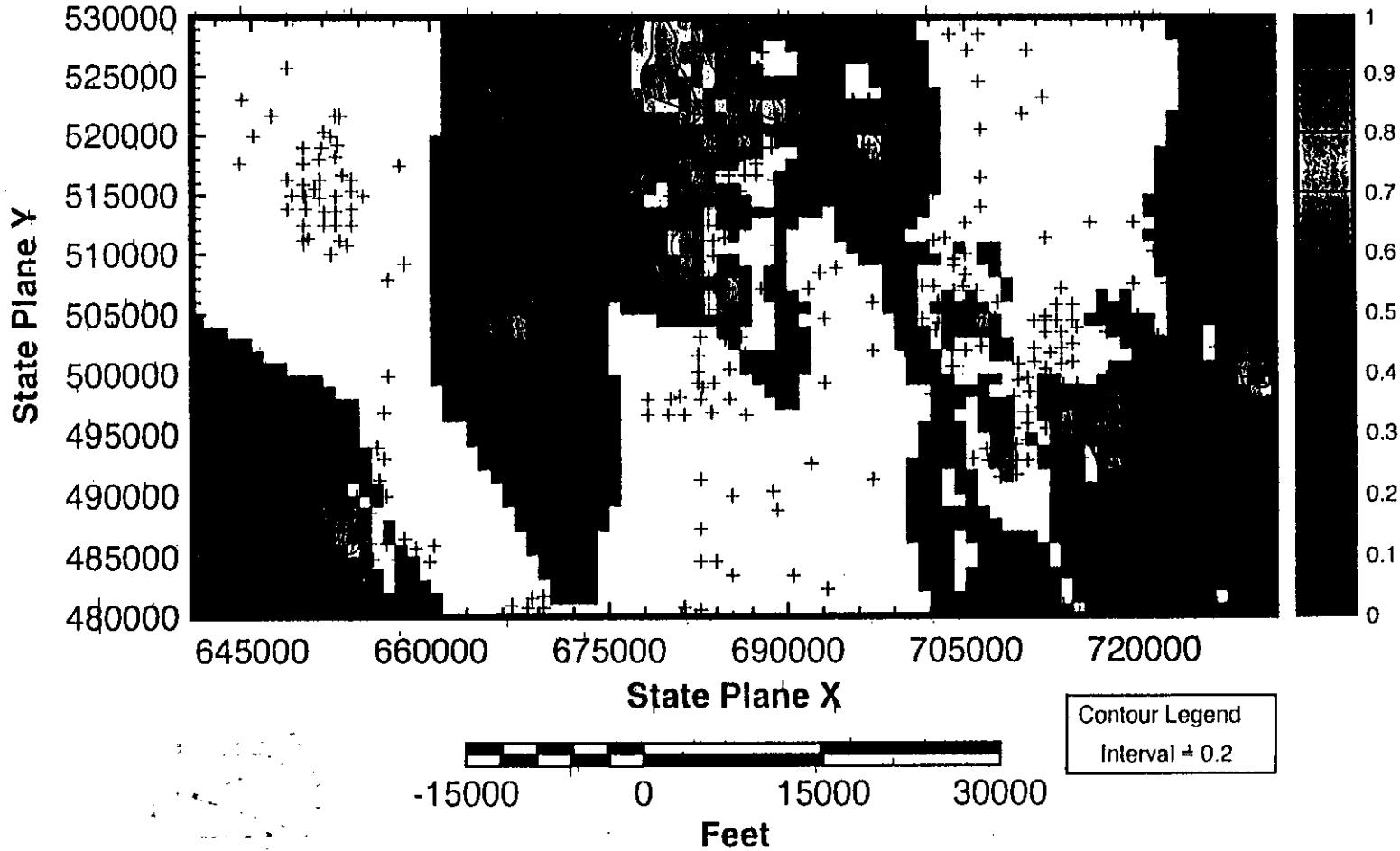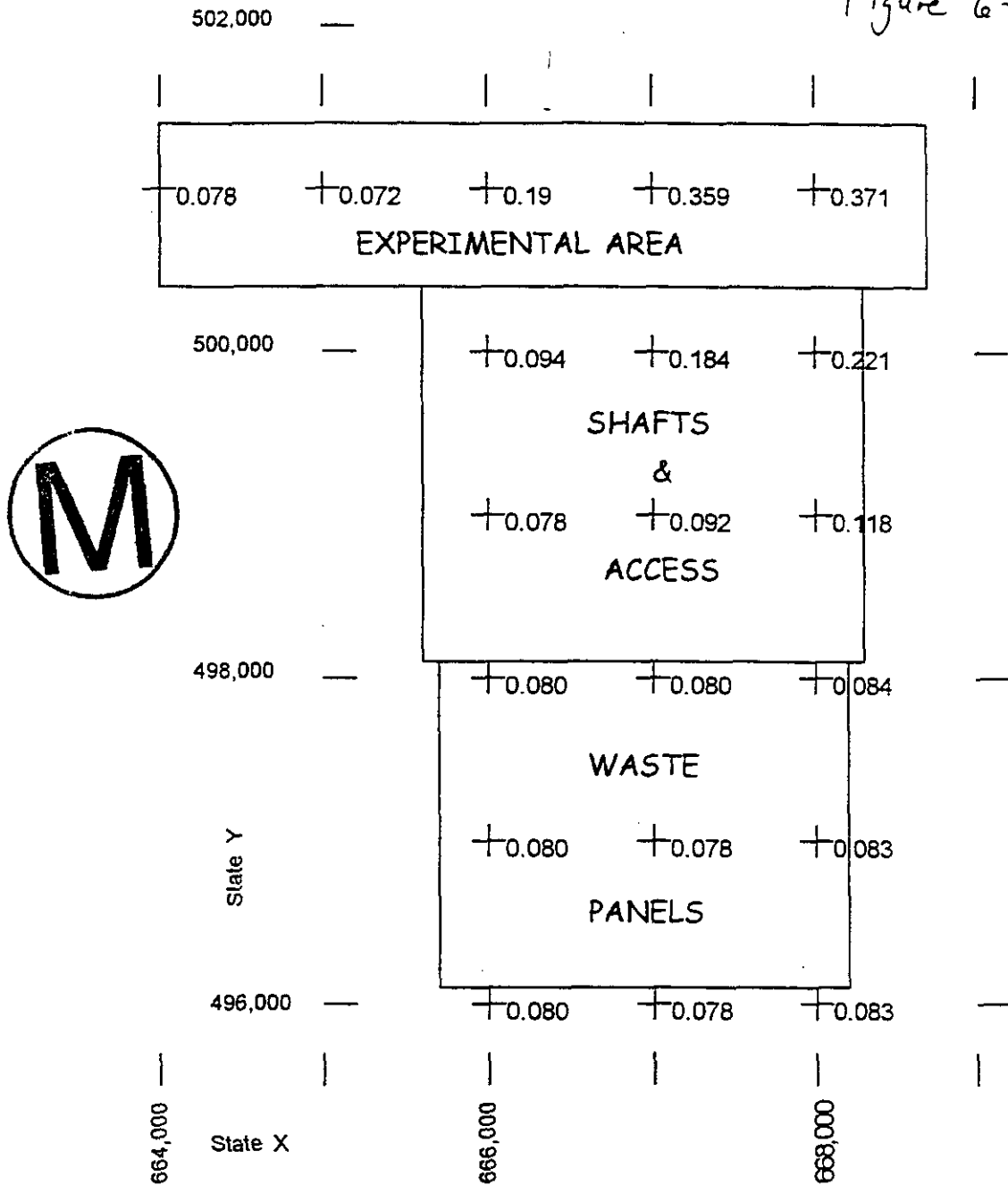## Anisotropic Spherical Semi-Variogram: Azimuth = 160 deg; Range = 5700 ft; Nugget = 0

Figure 6-13

502,000

0.078 +0.072 +0.19 +0.359 +0.371

EXPERIMENTAL AREA

500,000 +0.094 +0.184 +0.221

SHAFTS
&

+0.078 +0.092 +0.118

ACCESS

498,000 +0.080 +0.080 +0.084

WASTE

+0.080 +0.078 +0.083

PANELS

496,000 +0.080 +0.078 +0.083

State Y

664,000   State X   666,000   668,000

Nodal Probabilities of Intercepting Brine in Castile
(Anisotropic: az = 160; range 5700 ft, nugget = 0)

0.078 and 0.084. Each node is centered in a grid block which has dimensions of 1000 ft on each face. We calculated an areally-averaged probability of 0.080 for the entire waste panel site by weighting each point-kriged probability by the proportion of the waste panel area its grid block occupies. This weighted probability average is roughly equivalent to a 3x3 block-kriged probability if the block overlaid the waste panel area exactly.

The waste panel point-kriged probabilities calculated using the isotropic theoretical semi-variogram model were all less than 0.07. The lower probabilities were caused by the substantially shorter range (2500 vs 5700 ft). Figure 6-14 shows the point-kriged conditional probability map assuming the isotropic theoretical model semi-variogram.

6.3.3 Variations in Kriging Results

We examined partially the effects of "errors" in classification equivalent to either missing a brine intercept in a drillhole or believing pressurized brine is present when it is not. Drillholes AEC 7 was included in our first analyses because it was included in some lists as a potential brine reservoir. After further review of the basic data report (Sandia National Laboratories and D'Appolonia Consulting Engineers, 1982), we have excluded it from the list (Table 4.1-2).

The kriging results were unchanged by the change in classification of borehole AEC 7 from an intercept to a no-intercept. The negligible impact of the classification error is attributable to the large distance (roughly 10 km), relative to the semi-variogram ranges observed, between the site and AEC 7's location. This suggests that classification errors must be considered with regard to the location of interest before their impact on the estimated probabilities can be understood. Individual misclassification errors will have continue to have a negligible impact on estimated intercept probabilities at the site unless those errors occur within one or two correlation lengths (ranges) of the site footprint and they are Type II errors. Type I errors are also known as false positives; Type II errors are known as false negatives. Thus, to create a significant change in the estimated site probabilities, one of the nearby no-intercept observations would have to reclassified as a brine intercept. It is unlikely such an error has occurred because most of the wells near the WIPP site were drilled by the Department of Energy, and conditions should have been quite favorable for detecting such Castile brine reservoirs. Our approach is robust with regard to individual misclassification errors located beyond several miles from the WIPP site.

Differences in the intercept probabilities estimated using UNCERT's GRID module and those estimated using the KT3B algorithm found in GSLIB (Deutsch and Journel, 1992) were 5% or less within the waste panel footprint. The GSLIB routine estimates for the shaft & access and experimental areas were less than

Figure 6-14

Probability of Encountering a Castile Brine Reservoir

Isotropic Spherical Semi-Variogram: Range = 2500 ft; Nugget = 0.01
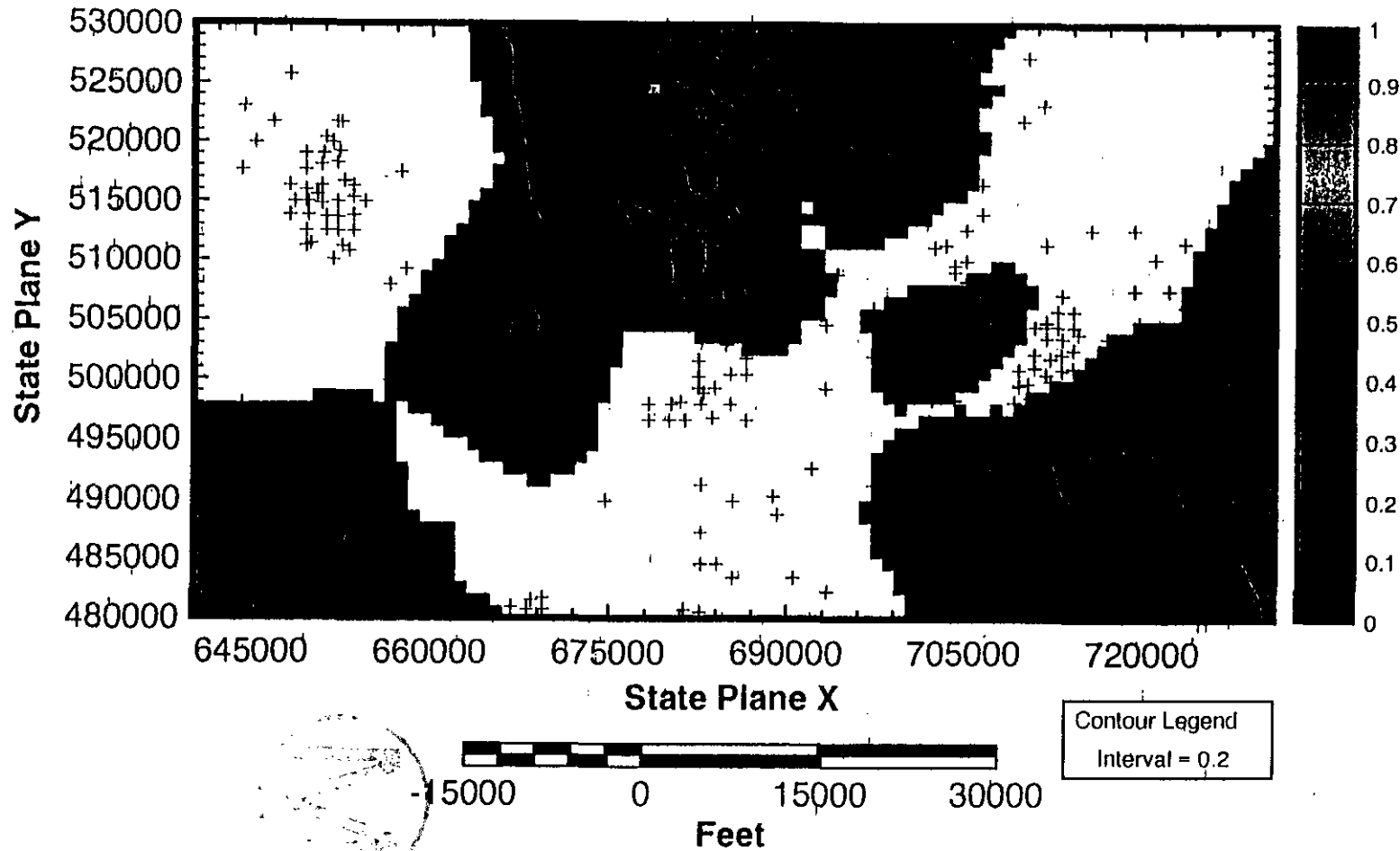
those calculated with GRID, which was based on the KT3B algorithm. This is attributed to the different search strategies utilized by the packages.

6.4 SUMMARY

- There is significant spatial correlation to the presence of brine reservoirs based on the available data. The physical cause of the correlation is, at present, unknown.
- The most significant correlation occurs along an azimuth of 160 degrees counterclockwise from north. It is anisotropic. This correlation structure does not appear to significantly influenced by data clustering. The main drilling trends are north-northeast.
- Another model of spatial correlation, along azimuth of 20 degrees, may be significant. However, it appears to be influenced by data clustering.
- The spatial correlation length scale of a brine reservoir hit, as described by the semi-variogram range, is relatively small: less than 6000 ft.
- The kriged point probability of a borehole encountering a brine reservoir in the Castile Formation within the waste panel footprint does not exceed 0.10, regardless of which spatial correlation model is chosen.
- The point-kriged probability estimates are insensitive to individual data classification errors located more than several miles from the WIPP site areas of concern.

7.0 GEOSTATISTICAL INVESTIGATION OF THE CASTILE FORMATION'S GEOLOGICAL STRUCTURE

7.1 INTRODUCTION

The objective of this investigation is to determine whether there are significant quantitative relationships between the brine reservoir intercepts and structural geologic data, particularly data that may be indicative of processes which created or influenced the observed brine intercept spatial distribution. Ideally, a geostatistical analysis will identify a random field's spatial correlation structure that is consistent with the processes which controlled the distribution of that random field. For example, the spatial variability of soil lead concentrations in fields surrounding a lead smelter should be consistent with the orientation of the prevailing winds and smelter operation patterns.

We believe brine reservoirs were caused by deformation of the uppermost units within the Castile Formation. We hypothesize that structural data, such as the thickness of these units, can provide insight into the amount and location of deformation. We began testing our hypothesis by 1) estimating the spatial variability of the structural data to compare with the brine intercept results from section 6.0 and 2) using statistics to examine potential interrelationships between geological structure and brine intercept data. Given our assumptions that structural data and brine reservoirs are functions of the amount of deformation in the upper Castile, any structural data similarities to the correlation scale and direction observed for brine intercepts adds greater weight to our conclusions about brine reservoir spatial variability. This investigation could potentially provide significant improvements in predicting the conditional probability of a brine reservoir intercept within the WIPP site.
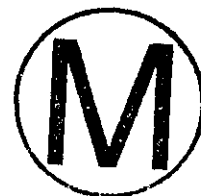
For example, Figure 6-1 shows there are relatively few boreholes within 10000 ft of the WIPP site with information about brine intercepts/no-intercepts. There are, however, numerous boreholes across the site with information about the geologic structure of the Salado and Rustler Formations. If a strong association between brine intercepts/no-intercepts and geological structure data can be determined, then we could use the cokriging approach to get better-constrained estimates of the conditional probability of a Castile brine reservoir intercept within the site than can be estimated using brine hit/miss data alone. Cokriging extends the kriging algorithms by conditioning prediction of a random field at unsampled locations (e.g., brine hit probability) on observations of the original and a second, related, random field (e.g., brine hits/misses and amount of deformation). It also assumes knowledge of the random fields' autocovariance and cross-covariance functions, which are typically estimated from sample semi-variograms and cross-semivariograms. Cokriging can only improve on a standard kriging algorithm when observation locations of the second random field are more numerous within the area of interest than those for the first

28

random field. At the WIPP site, this would require a strong relationship between brine hits and structural information for units above the Castile Formation, such as Marker Bed 124, since there are many more different observation locations for these units than for units within the Castile across the WIPP site.

We have some doubts whether the cokriging approach will work for the specific case of brine intercepts/no-intercepts and structural data since the cross-covariance (or cross-semivariogram) for each lag only receives a positive contribution from pairs which include brine intercepts (see Eqns 7-1 and 7-2 below). This suggests that the estimated cross-covariance is then a function of the ratio of brine intercepts to brine no-intercepts. However, cokriging may still provide significant improvements in the conditional probability estimates from Section 6 because it, like standard kriging and unlike many other interpolation algorithms, honors the data exactly.

We focused on the thickness between the top of the Bell Canyon and the base of the Cowden, which immediately overlies the presumed location of the brine reservoirs within the Castile's uppermost anhydrite (Anhydrite III) and halite (Halite II) zones. Measurements of this thickness, called here the Cowden isopach of IsoCowden, were made using geophysical logs for 352 boreholes. The dataset differs slightly from that used for geostatistical analysis of brine reservoir intercepts (Section 6.0). We estimated the Cowden isopach for five brine intercept boreholes and several drillholes without intercepts using information from nearby boreholes (section 5.0; Appendix E). As before, the 352 wells are distributed across roughly 645 km^2 (252 mi^2) of Delaware Basin. The WIPP site is roughly centered within this area.

In addition to estimating the spatial variability of the Cowden isopach, we examined the spatial cross-correlation between the Cowden isopach and brine intercept/no-intercepts. The cross-covariance between two random fields, Y and Z, is described by $C_{Y(x),Z(x+h)}$, where E is the expectation operator, x is the location vector for an observation, and h is the distance between it and another observation:

$$C_{Y(x),Z(x+h)} = E\{[Y(x) - E\{Y(x)\}][Z(x+h) - E\{Z(x+h)\}]\} \qquad (Eqn.7-1)$$

The cross-semivariogram, $\gamma_c(h)$, is the variance of the difference between observations of two variables separated by a distance (or lag) h:

$$\gamma_c(h) = \frac{Var\{Z(x-h) - Y(x)\}}{2} \qquad (Eqn.\ 7.2)$$

7.2 METHODS

7.2.1 Exploratory Data Analysis

We examined differences in Cowden isopach measurements for two categories: boreholes with brine intercepts and boreholes with brine no-intercepts. Descriptive statistics, such as sample mean, standard deviation, skewness, etc., and sample cumulative frequency distributions for the two categories were compared.

Descriptive statistics and sample cumulative frequency distributions of Cowden isopach measurements were calculated for boreholes with and without brine intercepts. Graphs and calculations were made using the Excel spreadsheet program, version 4, from Microsoft and MathSoft's MathCad 6.0+ mathematical analysis program.

7.2.2 Variography

We quantified Cowden isopach spatial correlation through calculation of sample semi-variograms. We tested our estimates for sensitivity to data clustering and extreme values (outliers) by computing sample semi-variograms for subsets of the data and by examining more robust measures such as the semi-rodogram, general relative semi-variogram, and non-ergodic covariance function (see Section 6.1). Values for the range, sill, and nugget variance are determined by fitting a theoretical semi-variogram model to the sample semi-variogram.

7.2.1.1 Sample Semi-Variogram Calculation

Sample semi-variograms are calculated according to Eqn. 6-4 for the isotropic (omni-directional) case and for a range of anisotropic geometric directions: azimuths 0, 20, 45, 70, 90, 110, 135, and 160 degrees measured clockwise from a 0 degree north. All variographic calculations were carried out using the VARIO module of the public domain software package UNCERT (Wingle et al, 1994), available from the Colorado School of Mines in Golden, CO.

Lag spacing was set at 1500 ft to match the lag spacings from the analysis of brine intercept/no-intercept spatial variability. The maximum search distance, directional bandwidth, and horizontal half-angle were set to their maximum values of 150000 ft, 150000 ft and 90 degrees for the isotropic sample semi-variogram. The data were sufficient in number to restrict the horizontal half-angle to 15 degrees, maximum search distance to 150000 ft, and the directional bandwidth to 10000 ft for all of the anisotropic sample semi-variograms.

Sample semi-variograms were judged significant if they exhibited a reasonably monotonic increasing structure within the first 25% of the lag classes with

adequate numbers of pairs within each lag class. Theoretical semi-variogram model parameters (range, sill, and nugget variance) were estimated for selected sample semi-variograms.

7.2.1.2 Sample Semi-Variogram Robustness

We tested the Cowden isopach sample semi-variogram robustness to clustering using two different approaches. The first compares sample semi-variograms from the entire data set with those computed for two non-overlapping data subsets which have relatively uniform spatial distributions of boreholes and possess adequate numbers of brine reservoir intercepts. Subset 1 contains 80 boreholes, 15 of which had brine intercepts. Subset 2 holds 93 boreholes, 9 of which had evidence of brine intercepts. These two subsets possess both a relatively uniform distribution of boreholes and sufficient numbers of brine intercepts to generate adequate numbers of observation pairs for each lag. Correlation structures which appeared significant in each of the data subsets and in the complete data set were judged to be independent of the large scale data clustering evident in Figure 6-3.

The second approach utilizes alternative measures of spatial continuity which are less sensitive to data clustering. The semi-rodogram and general and pairwise relative semi-variograms are typically less vulnerable to clustering because they normalize the semi-variogram value for each lag class by the squared mean of the data and the squared average of the paired values; Eqn. 6-5 defines the semi-rodogram and Eqn. 7-3 defines the general relative semi-variogram. We calculated sample semi-rodograms, general relative semi-variograms, and non-ergodic covariances for each data subset, their union, and the entire data set.

$$Y_{GR}\ (h) = \frac{Var\{Z(x-h) - Z(x)\}}{[\frac{m_t m_h}{2}]^2} \qquad (Eqn.\ 7-3)$$

where m_t and m_h are the means of the tails and heads of each pair within a lag.

7.2.1.3 Sample Cross-Semivariogram Estimation

We estimated the sample cross-semivariograms for the brine intercept/no-intercept and Cowden isopach using

$$Y_C\ (h) = \frac{1}{2N(h)} \sum_{i=1}^{N(h)} (z_i - y_i)^2 \qquad (Eqn.\ 7-4)$$

Sample cross-semivariograms were determined for the union of Subsets 1 and 2 for the isotropic case and along the same eight sample semi-variogram directions. Calculations were made with the GAM2V routine from the GSLIB library (Deutsch and Journel, 1992) because the Sun OS version of UNCERT's VARIO module does not yet support cross-semivariogram estimation.

7.2.1.3 Theoretical Variogram Model Fitting

We estimated range, sill, and nugget variance using UNCERT's VARIOFIT module for only a few selected sample semi-variograms because of a time limitation and because we did not need to krige Cowden isopach values. We estimated ranges by eye for the remaining sample semi-variograms, assuming a spherical theoretical semi-variogram model, to enable quick comparison with the ranges estimated for the brine intercept/no-intercept variable.
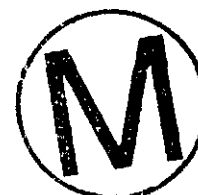
7.3 RESULTS AND DISCUSSION

7.3.1 Exploratory Data Analysis

Table 7-1 summarizes the descriptive statistics for Cowden isopach categorized by whether a brine intercept was observed (or not) in the borehole. Note that the mean, minimum, and maximum for the brine hit group are all larger than those for the brine miss group. Isopach standard deviations relatively close (coefficient of variation is 10% for each group). The brine intercept group is skewed to larger isopach values and is significantly kurtic, i.e., its probability density function (histogram) is more flat than peaked. In contrast, the brine no-intercept group shows relatively little skewness and kurtosis.

Table 7-1
Summary Statistics for Cowden Isopach by Brine Intercept/No-Intercept

Statistic	Brine Intercepts	Brine No-Intercepts
Mean	1905.77	1760.16
Standard Error	37.49	9.99
Median	1891.00	1726.00
Mode	1925.00	1660.00
Standard Deviation	191.16	180.31
Variance	36541.94	32511.90
Kurtosis	5.97	-0.02
Skewness	2.01	0.55
Range	919	944
Minimum	1677	1373
Maximum	2596	2317
Sum	49550	573812
Count	26	326

Figure 7-1 presents the sample cumulative relative frequency distributions for the two groups. Figure 7-2 depicts sample histograms for each group. Comparison of the intercept and no-intercept curves suggests there is a minimum Cowden isopach value of 1650 to 1680 ft below which brine reservoirs are not observed.

We attempted to fit a Poisson distribution to the sample relative frequency distribution for the brine intercepts. Results are shown in Figure 7-3. If we can assume the Cowden isopach for brine intercepts is governed by a Poisson process, then it is highly unlikely that brine intercepts will be observed when the Cowden isopach is less than 1670 ft. We attempted to fit several other distributions but met with no success.

7.3.2 Variography

### 7.3.2.1 Sample Semi-Variogram Calculations

Figures 7-4ab and 7-5ab show the sample semi-variograms for the first and second data subsets, which occupy the same locations used in Section 6.2. Appendix J contains printouts of the calculation log files. The results are less clear-cut than those presented for the brine intercept/no-intercept binary variable in Section 6.3. Locally-varying trends in Cowden isopach values keep both isotropic and anisotropic sample semi-variograms from leveling out near the sill. See, for example, the sample semi-variograms for azimuths 0, 20, 45, and 70 degrees, as well as the isotropic case, for Subset 1 (Figures 7-4ab). These thickening-thinning trends can be seen in Figure 5.3-3, which depicts the top of Bell Canyon to base of Cowden isopach contours. Note the especially strong north-south trend in isopach value across the center of the map. The sample semi-variograms for azimuths 90, 100, and 135 degrees appear to be mostly noise. While some evidence for trends in the sample semi-variograms for Subset 2 can be observed (e.g., azimuths 0 and 45 degrees), it is not as common as in the Subset 1 results. This is most likely attributable to the lack of strong trends within that data set (see Figure 5.3-3).

The sample semi-variogram for azimuth 160 degrees suggests the presence of a nested correlation structure under both data subsets. The small-scale correlation length (range) appears to fall between 4000 and 5000 ft. The azimuth 0, 20, and 135 degree sample semi-variograms for Subset 2 and the 0 degree azimuth sample semi-variogram for Subset 1 also indicate such a small-scale correlation structure. The large-scale correlation length may reach its sill somewhere near 15000 ft; however, this large-scale structure may be an artifact of the small number of pairs found within those largest lags.
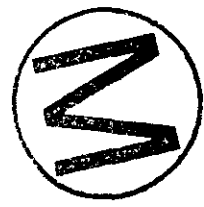
Figures 7-6ab present the sample semi-variograms for the complete data set.

Figure 7-1

Estimated Cumulative Relative Frequency Distributions of Cowden Isopach Values
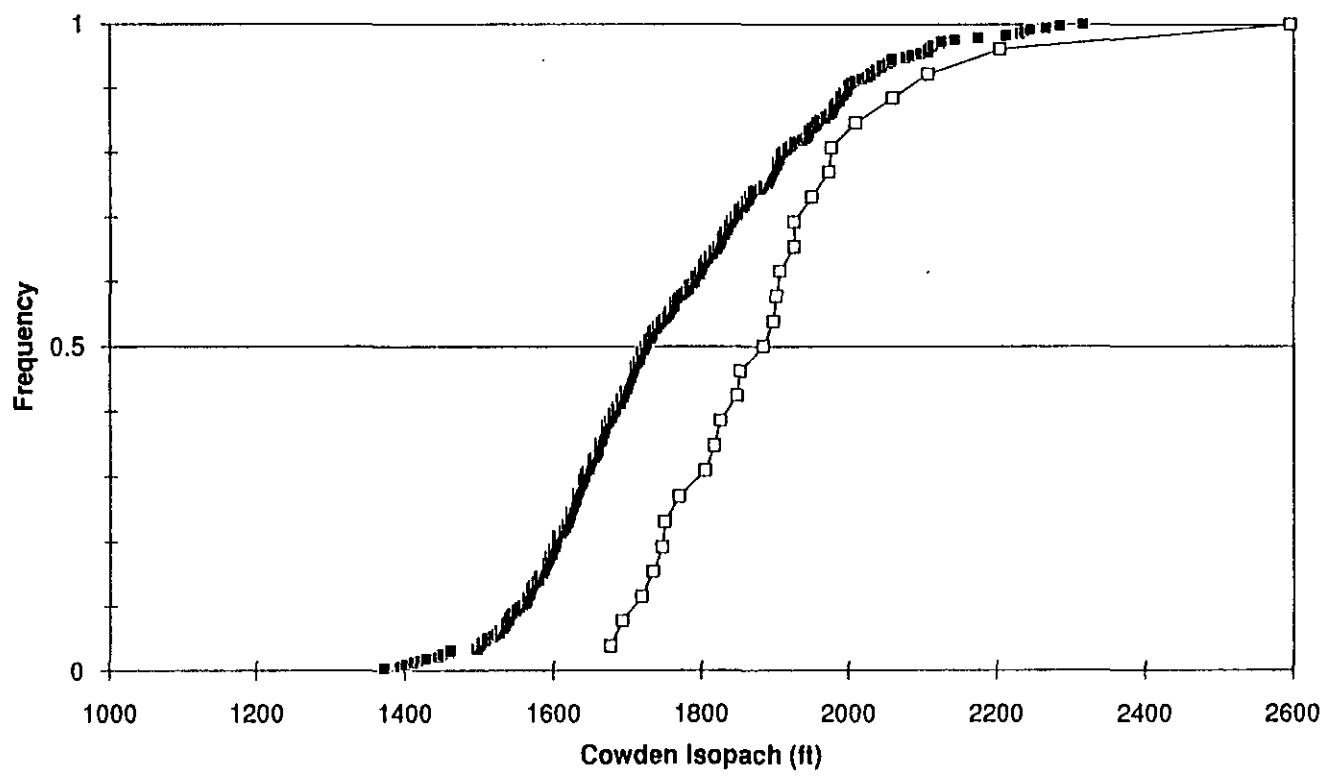
Sample Relative Frequency Distributions

FIGURE 7-3

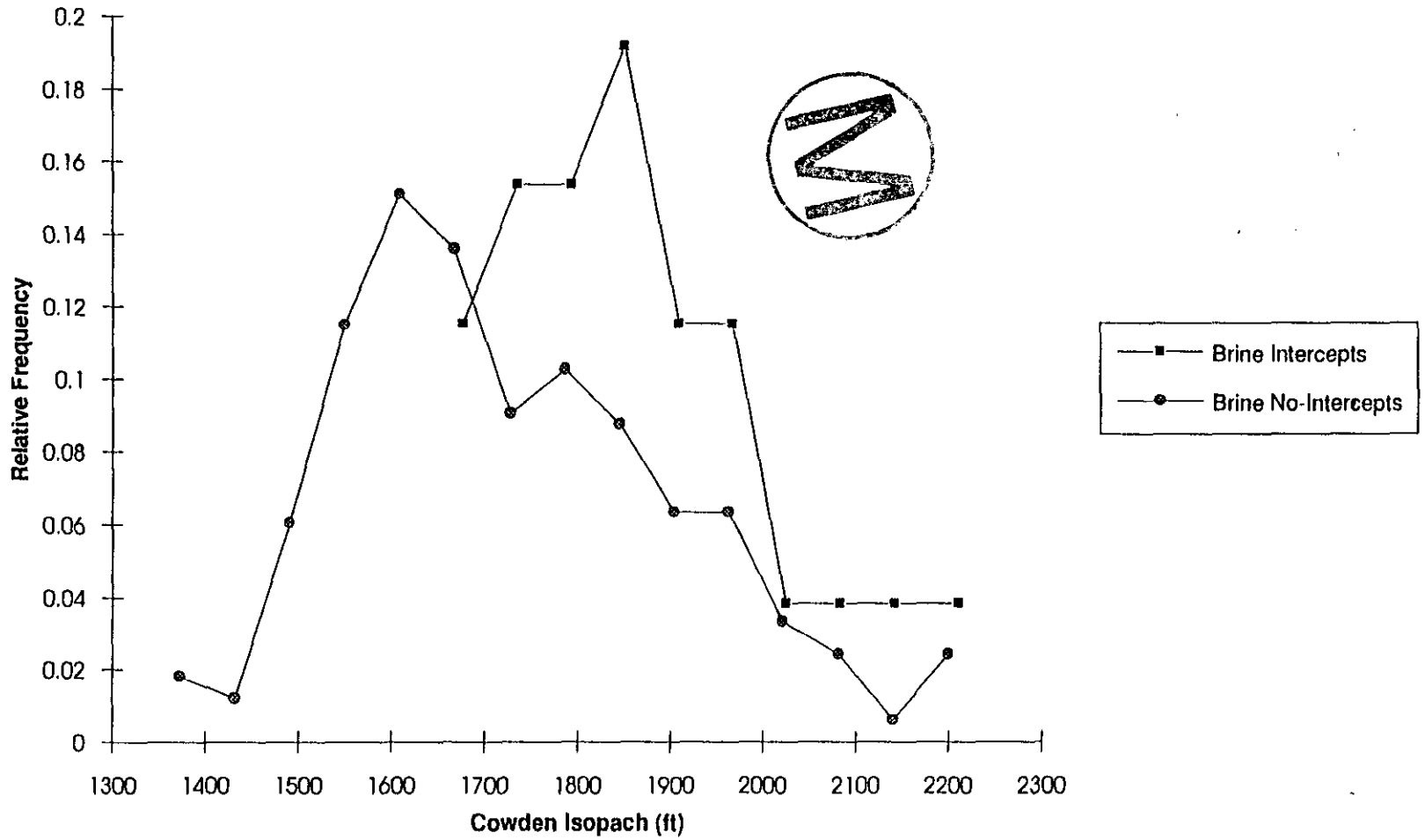Estimated Cowden Isopach Probability Density Function (PDF) vs. Poisson PDF

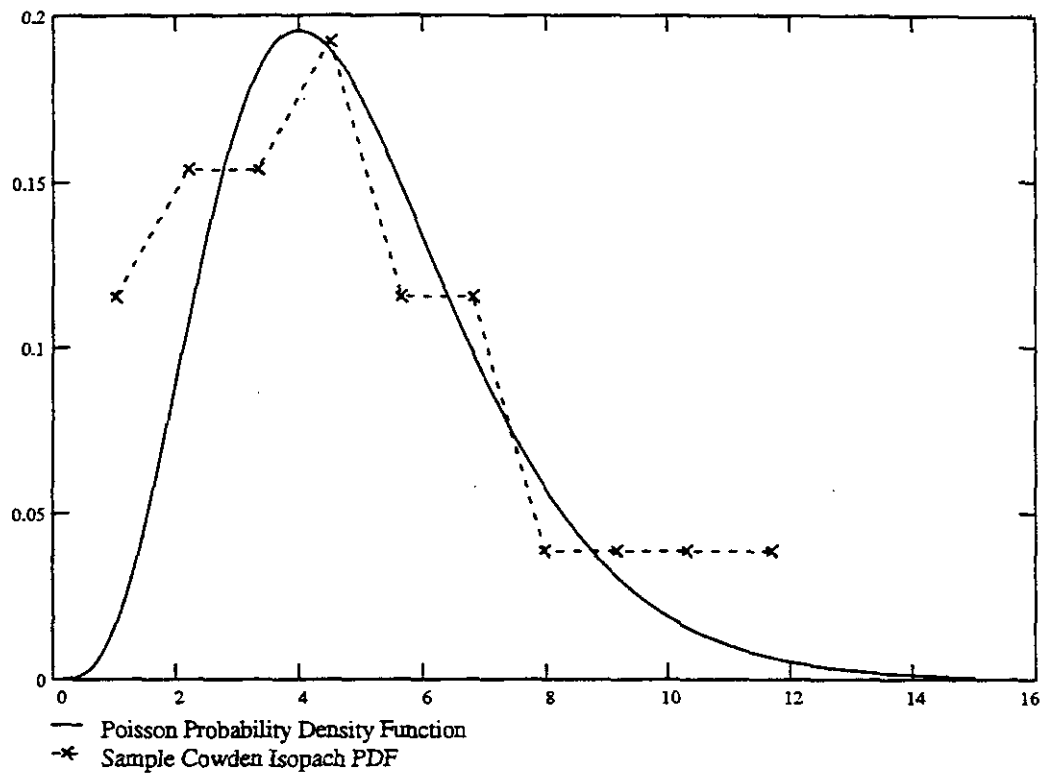— Poisson Probability Density Function
-✻ Sample Cowden Isopach PDF

Figure 7-4a

Castile Fm. Isopach Data for Subset 1: isocow

Semi-Variogram: Lag = 1500 ft; BW = 10000; HA = 15

Legend
- Variance
- Isotropic
- Az = 0 deg
- Az = 20 deg
- Az = 45 deg
- Az = 70 deg
- Az = 90 deg
- Az = 110 deg
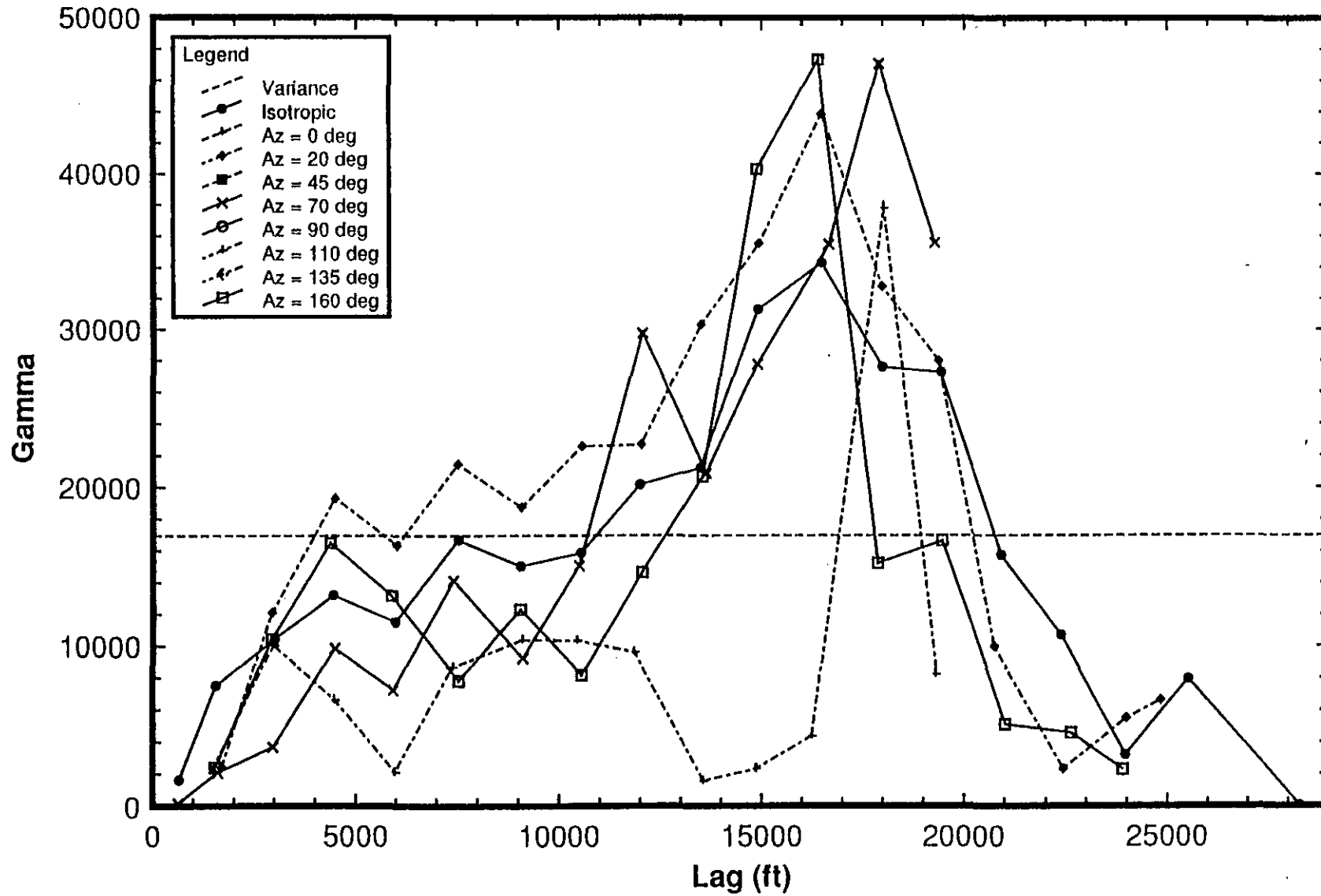- Az = 135 deg
- Az = 160 deg

Figure 7- .5

Castile Fm. Isopach Data for Subset 1: isocow

Semi-Variogram: Lag = 1500 ft; BW = 10000; HA = 15

Legend
- Variance
- Isotropic
- Az = 0 deg
- Az = 20 deg
- Az = 45 deg
- Az = 70 deg
- Az = 90 deg
- Az = 110 deg
- Az = 135 deg
- Az = 160 deg

Gamma

Lag (ft)

Castile Fm. Isopach Data for Subset 2: isocow

Semi-Variogram: Lag = 1500 ft; BW = 10000; HA = 15

Figure 7-09

Castile Fm. Isopach Data for Subset 2: isocow
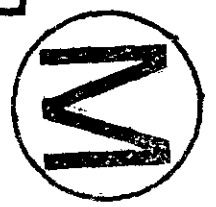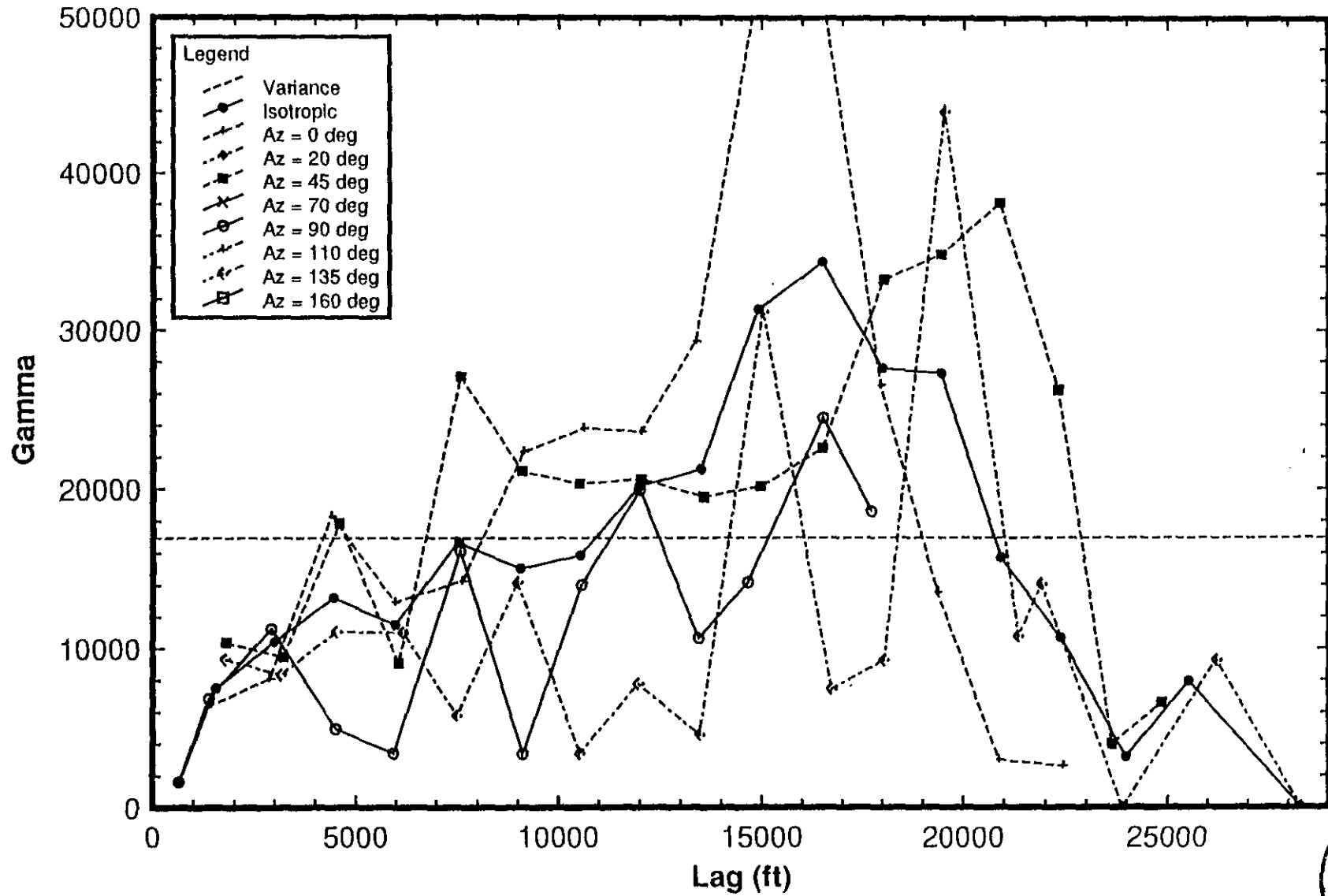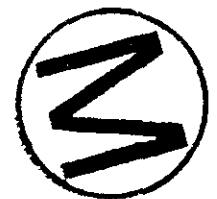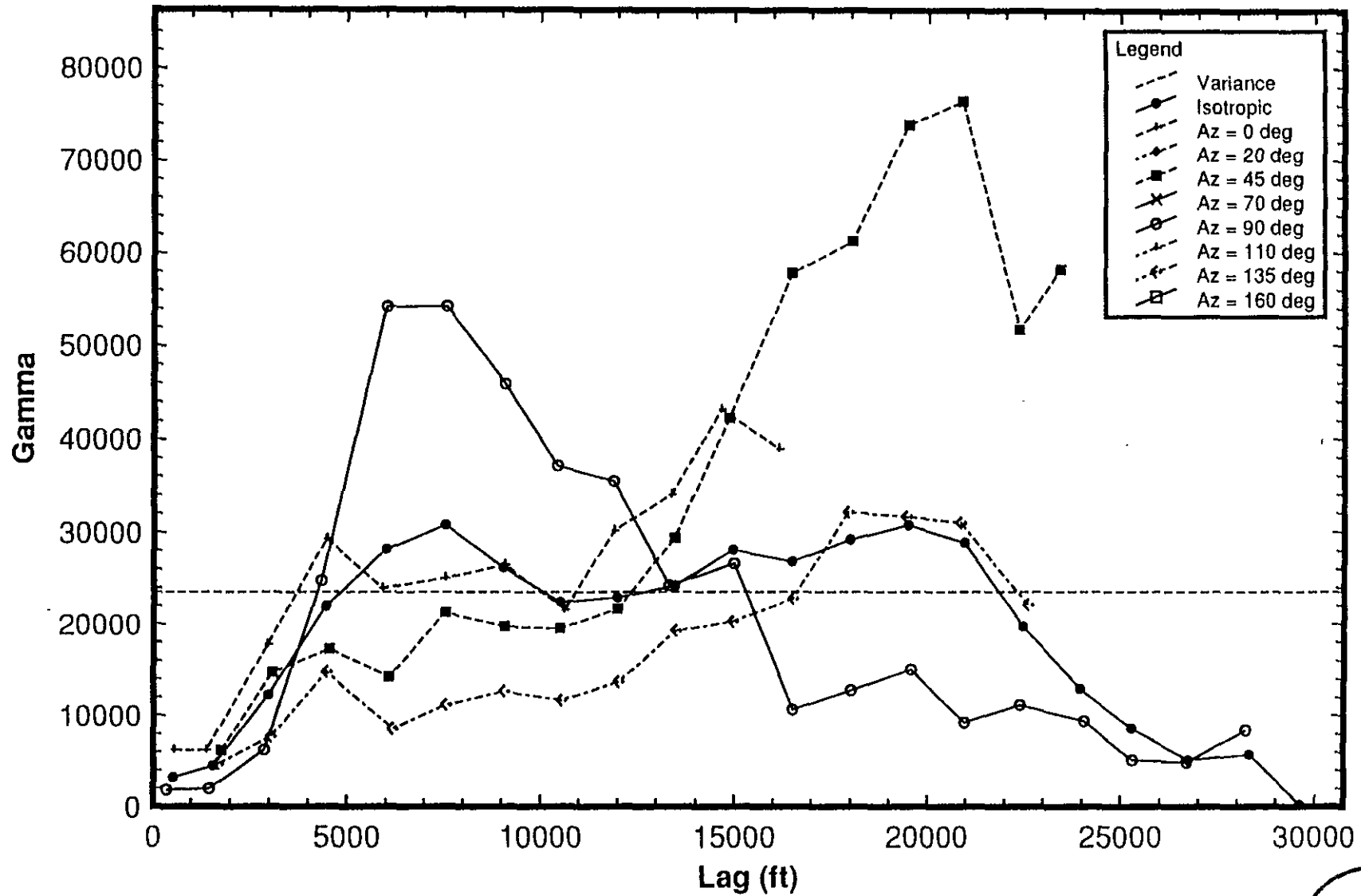Semi-Variogram: Lag = 1500 ft; BW = 10000; HA = 15

Figure 7-61

Castile Fm. Isopach Data: icowr3

Semi-Variogram: Lag =1500 ft; BW = 10000; HA = 15

Legend
- - - - Variance
——•—— Isotropic
——▲—— Az = 0 deg
·· ▲·· Az = 20 deg
——■—— Az = 45 deg
——✕—— Az = 70 deg
——⊘—— Az = 90 deg
·· + ·· Az = 110 deg
·· ◄ ·· Az = 135 deg
——☐—— Az = 160 deg

Castile Fm. Isopach Data: icowr3

Semi-Variogram: Lag = 1500 ft; BW = 10000; HA = 15

Figure 7-66

Legend
- Variance
- Isotropic
- Az = 0 deg
- Az = 20 deg
- Az = 45 deg
- Az = 70 deg
- Az = 90 deg
- Az = 110 deg
- Az = 135 deg
- Az = 160 deg

Gamma

Lag (ft)

Trends in isopach values are evident in the isotropic and azimuth 0, 20, 45, and 70 degree anisotropic sample semi-variograms. Small-scale correlation structures with effective ranges varying between 5000 and 6000 ft are shown most clearly in the azimuth 160, 135, and 70 degree sample semi-variograms. The 0, 20, and 45 degree directional semi-variograms also appear to possess this small-scale structure. Additional analyses indicated that the small-scale correlation features similar to that found in the azimuth 135 and 160 degree directions were observable along azimuths 140, 145, 150, and 155 degrees for the complete data set. This observation is by the orientation of the Cowden isopach maximum shown in Figure 5.3-3, which varies between azimuths 135 and 160 degrees.

Figures 7-6ab also demonstrate a significant large-scale correlation structure which has an effective range between roughly 10000 ft (for azimuth 135 deg.) and 18000 to 20000 ft (azimuths 70 and 160 deg.). The distance separating Subset 1 from Subset 2 closely corresponds to the upper end of the range estimate, possibly indicating the sample semi-variogram values are controlled by data clustering. However, the large-scale correlation structure is observable in the sample general relative semi-variograms for the same directions (see Figures 7-7ab), suggesting that data clustering is not the cause. Plots of the non-ergodic covariance and the semi-rodograms add support to this conclusion. The remaining directional sample semi-variograms demonstrate more trend effects than large-scale spatial correlation at larger lags.

7.3.2.2 Sample Cross-Semivariogram Calculation

Figures 7-8ab show the estimated cross-semivariograms for a combination of data Subsets 1 and 2. As above, there is consistent evidence for a small-scale correlation structure with an effective range of 5000 to 9000 ft (azimuths 0, 20, 70, 135, and 160 deg.). Several of the directional sample cross-semivariograms indicate the possibility of a large-scale correlation structure with an effective range of roughly 20000 ft. Although we have doubts about the impact of computing a cross-semivariogram using a binary variable, these results are consistent with the correlation structures observed along the azimuth 160 degree sample semi-variograms.

If there is a minimum Cowden isopach thickness for brine reservoirs and if the observed minimum is close to the actual threshold, it may be possible to define an indicator variable for the threshold Cowden isopach and then cokrige the brine intercept/no-intercept binary variable with the indicator variable.

7.3.2.3 Theoretical Semi-Variogram Model Fitting

Figures 7-9ab show the fitted theoretical variograms for the small-scale correlation structures observed in the azimuth 160 deg. sample semi-variograms

Castile Fm. Isopach Data: icowr3

Gen. Relative Semi-Variogram: Lag = 1500 ft; BW = 10000; HA = 15

Figure 7-19
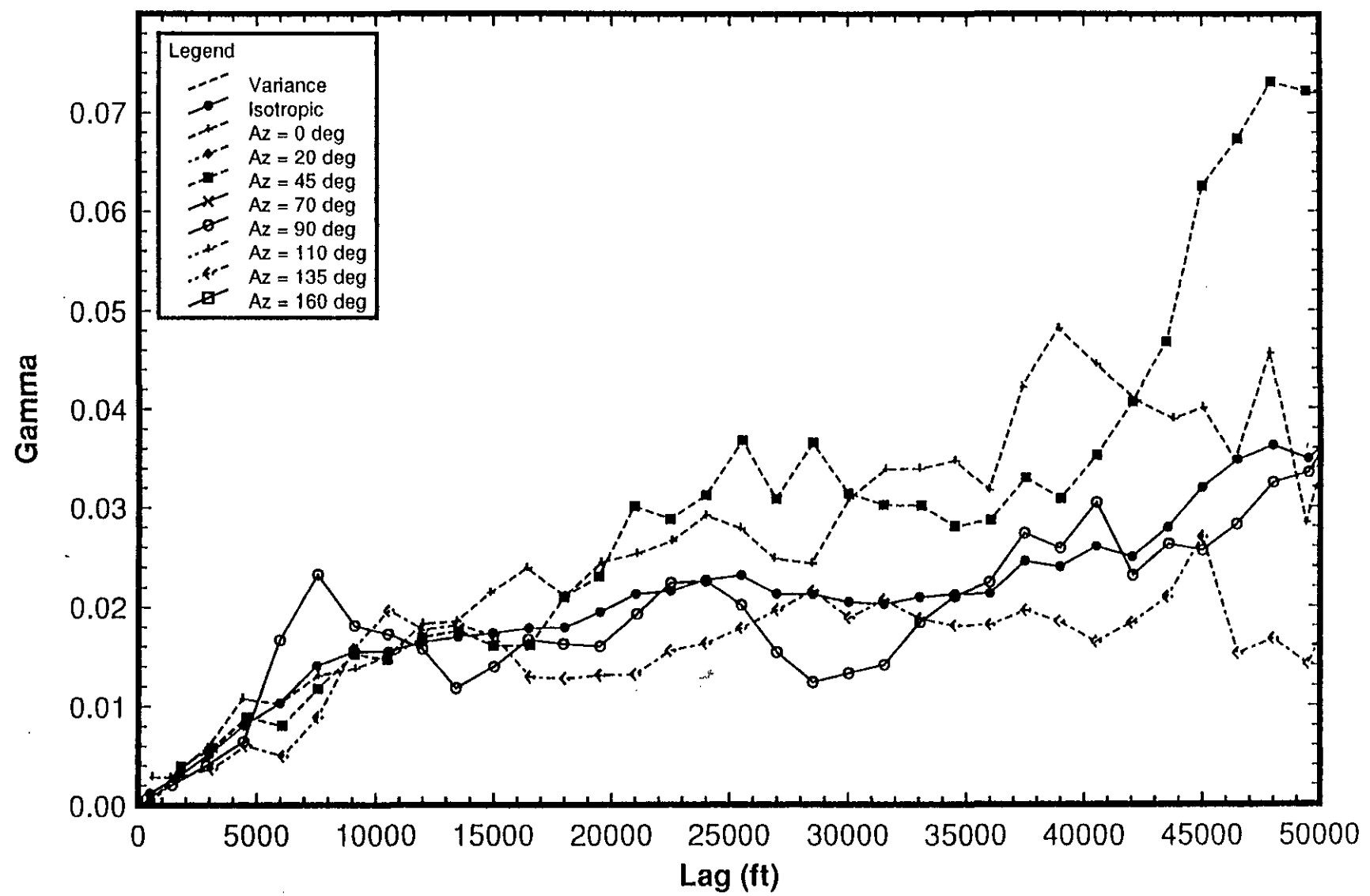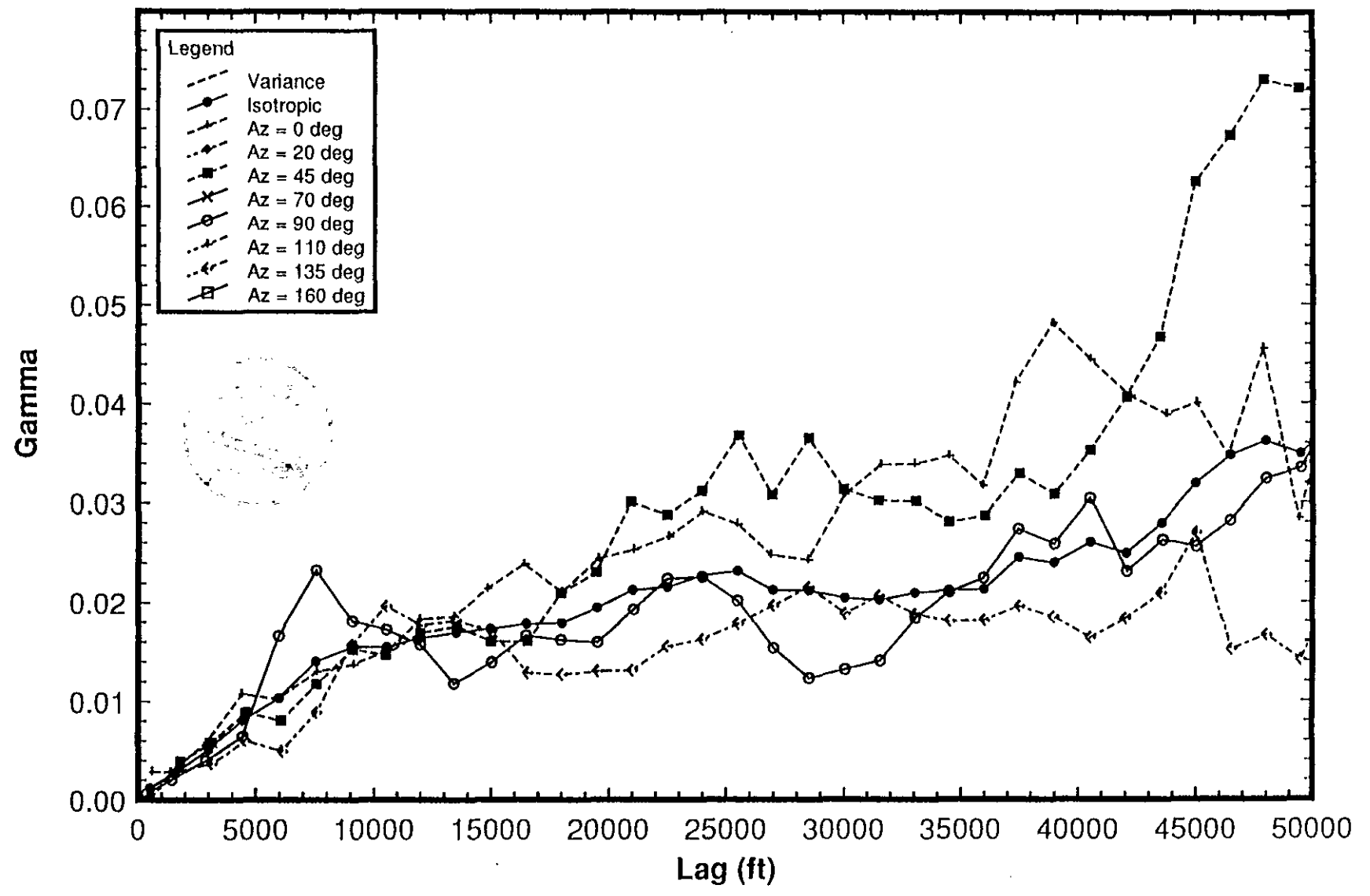
Legend
- - - - Variance
—●— Isotropic
—+— Az = 0 deg
·· ♦ ·· Az = 20 deg
—■— Az = 45 deg
—✕— Az = 70 deg
—○— Az = 90 deg
··+·· Az = 110 deg
··◄·· Az = 135 deg
—□— Az = 160 deg

Gamma (y-axis): 0.00, 0.01, 0.02, 0.03, 0.04, 0.05, 0.06, 0.07

Lag (ft) (x-axis): 0, 5000, 10000, 15000, 20000, 25000, 30000, 35000, 40000, 45000, 50000

Castile Fm. Isopach Data: icowr3
Gen. Relative Semi-Variogram: Lag = 1500 ft; BW = 10000; HA = 15

Figure 7-76

Legend
- Variance
- Isotropic
- Az = 0 deg
- Az = 20 deg
- Az = 45 deg
- Az = 70 deg
- Az = 90 deg
- Az = 110 deg
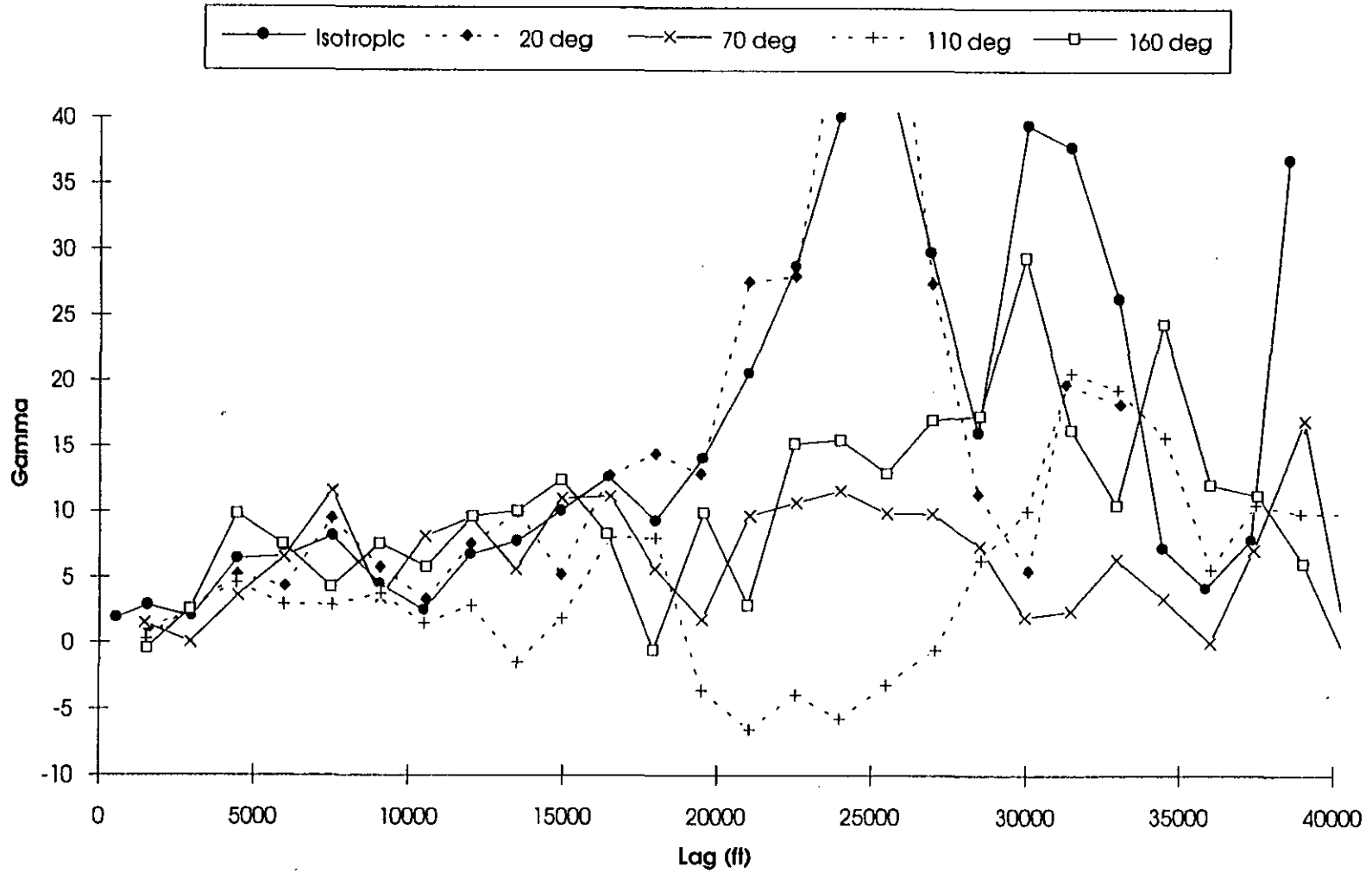- Az = 135 deg
- Az = 160 deg

Castile Fm. Isopach Data: icowr3

Gen. Relative Semi-Variogram: Lag = 1500 ft; BW = 10000; HA = 15

Figure 7-76

Figure 7-89

Cross-Semivariogram for Subset 3: isocow & brinehits

Legend: Isotropic · ◆ · 20 deg —×— 70 deg · + · 110 deg —□— 160 deg

Figure 7-8b

Cross-Semivariogram for Subset 3: isocow & brinehits

Legend: Isotropic | 0 deg | 45 deg | 90 deg | 135 deg
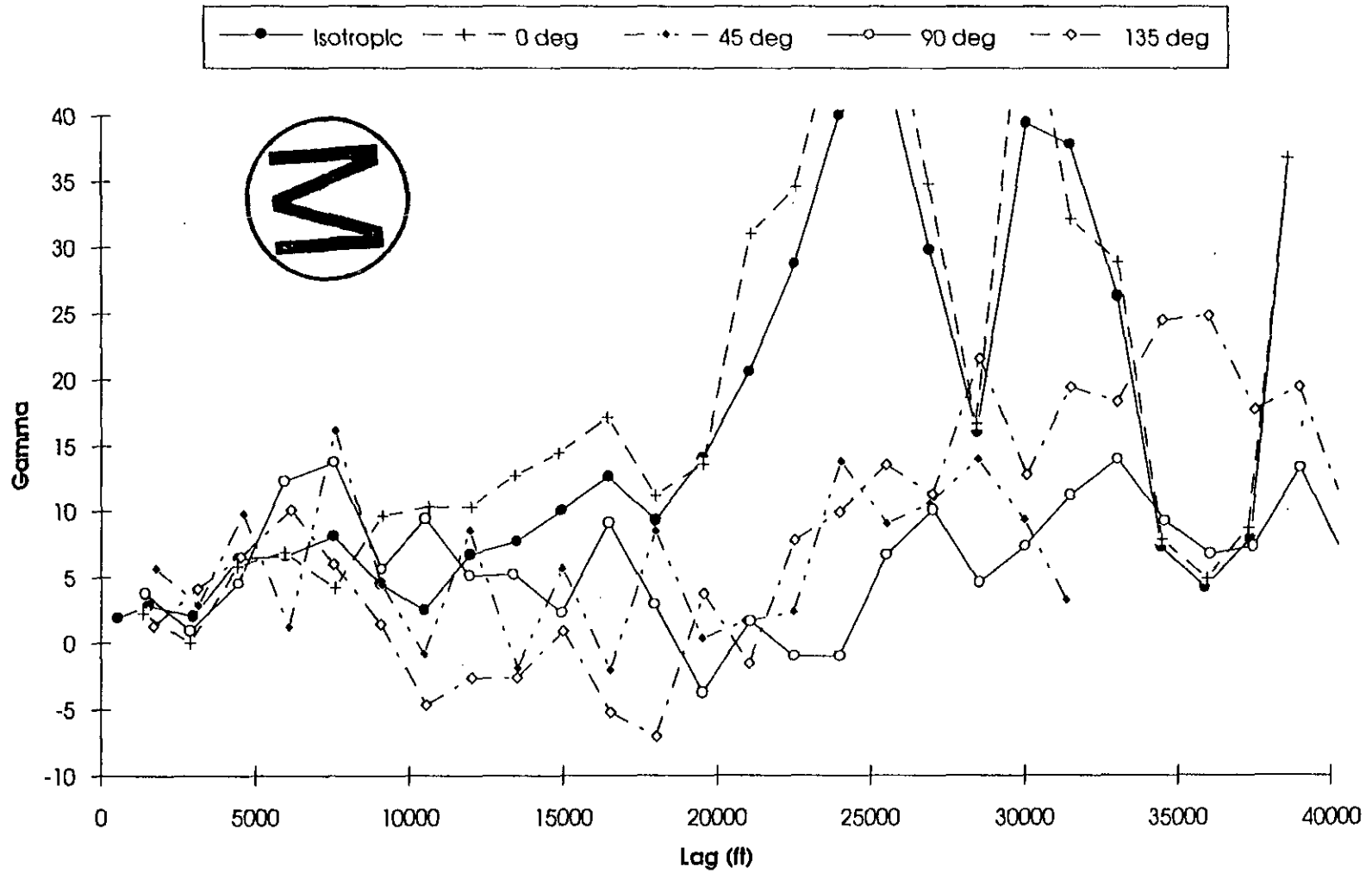
Cowden Isopach for Subset 2

Figure 7-99

Anisotropic Azimuth 160 deg.: Small-Scale Correlation

Model Parameters

Nest	Range	C	Model
1	3000	25000	Gaussian
Nugget		0	

Legend

- - - Variance
—— Model
• Experimental 1
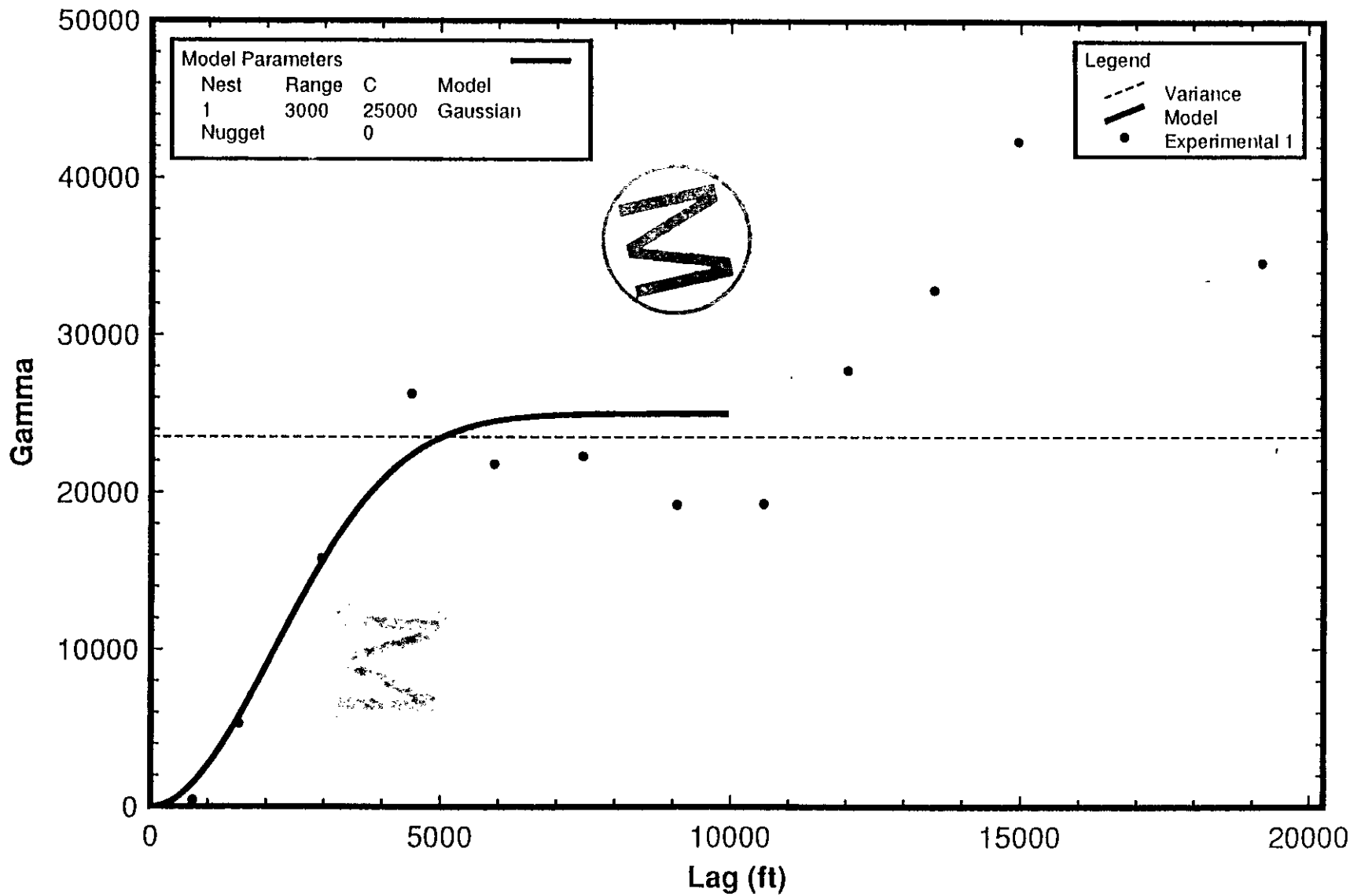
Cowden Isopach: icowr3

Anisotropic Azimuth 160 deg.: Small-Scale Correlation

Figure 1-96

Model Parameters —

Nest	Range	C	Model
1	6600	16000	Spherical
Nugget		0	

Legend
- - - - Variance
Model
• Experimental Az = 160 deg
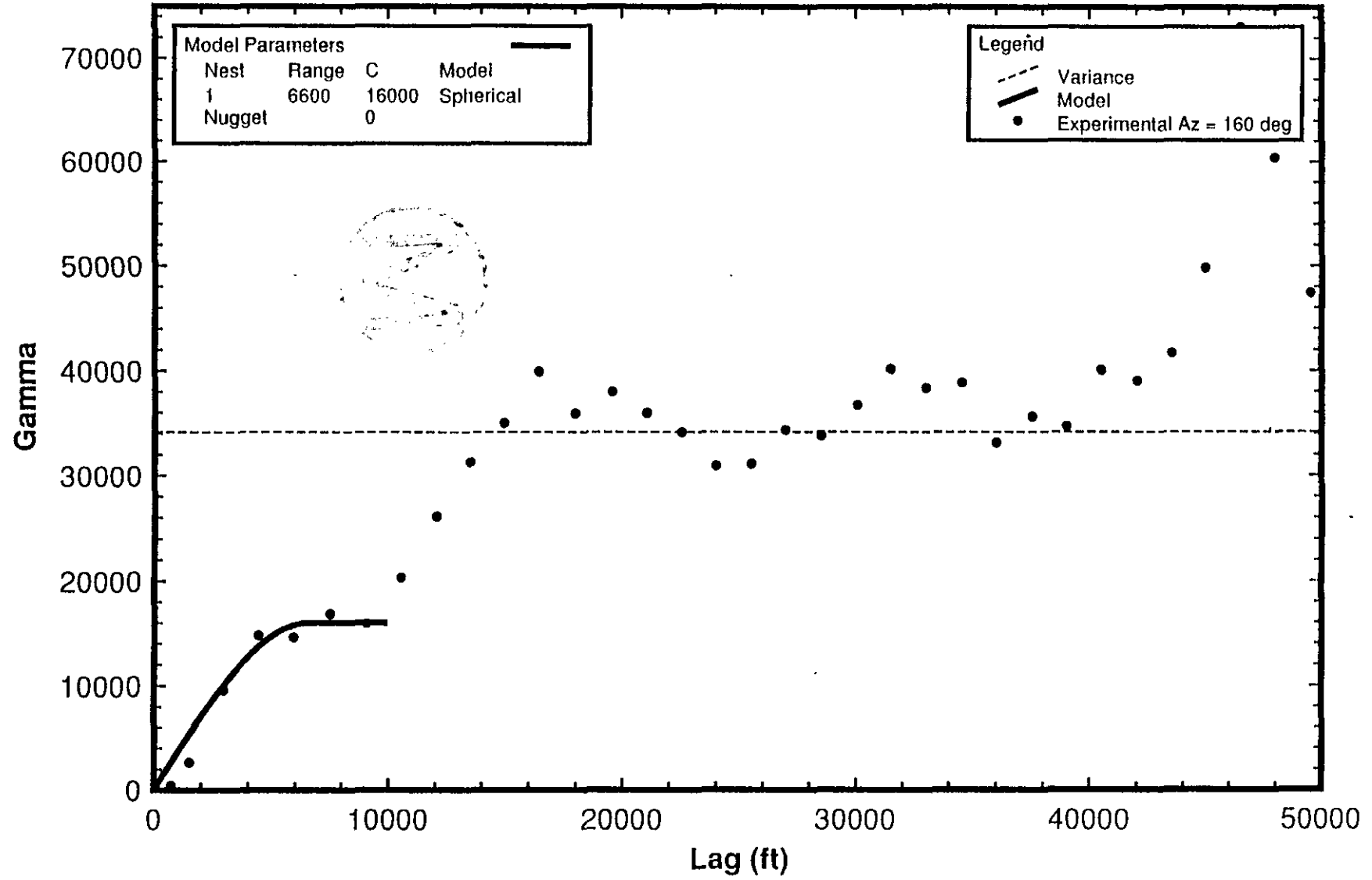
for all data and for Subset 2.   We fit a Gaussian model to the latter sample semi-variogram with an effective range of √3 x 3000 ft = 5200 ft (Figure 7-9a). The small-scale feature for the complete data set was fitted with a spherical model and an effective range of 6600 ft (Figure 7-9b).   These range values matched those estimated by eye for the small-scale correlation structure observed in the other sample semi-variograms. We focused solely on estimating effective ranges because we had no need of kriging the Cowden isopach variable.

7.4 SUMMARY

• The Bell Canyon to base of Cowden thickness (Cowden isopach) shows significant spatial correlation along several directions. Several directions demonstrate both small and large scale correlation structures.
• The observed large-scale spatial correlation had an effective range on the order of 10000 to 20000 ft.
• Small-scale spatial correlation, with effective ranges between 5000 and 7000 ft, was observed in the azimuth 160, 70, and 135 degree directions.
• The most consistent, significant correlation occurs in a range of azimuths from 135 to 160 degrees counterclockwise from north. These correlation structure does not appear to significantly influenced by data clustering and are consistent with the direction and correlation lengths observed for the brine intercept/no-intercept binary variable analyzed in Section 6.0
• Sample cross-semivariograms also appear to share the same small-scale correlation structure observed in the azimuth 160 degree sample semi-variograms.
• The geostatistical analysis results for the Cowden isopach are consistent with those for brine intercept/no-intercept.
• There may be a threshold Cowden isopach value, roughly 1670 ft, below which brine reservoirs do not occur.

8.0 INTEGRATION AND CONCLUSIONS

The geological information clearly outlines the area where evaporites have been greatly deformed to the northeast of the WIPP. Both structure contour and isopach data also give indications for certain horizons and intervals that areas at WIPP 12 and the Hudson Belco well differ from the surrounding areas. Drillholes east of the WIPP site differ structurally from regional trends as well, but are less deformed than the maximum for our study areas. The geological information strongly suggest that brine encounters are related to deformation of Castile evaporites.

The geostatistical analysis of brine intercepts alone demonstrates there is a directional anisotropy for brine reservoir intercepts along an azimuth of 160 degrees. This direction is in general agreement with the orientation of the major structures revealed by geological analysis. Further analysis of the spatial correlation of thickness data shows similar anisotropy, and is consistent with an association between the structural deformation of the upper anhydrite zones and the presence of brine reservoirs within the Castile Formation. Analysis of one interval shows also that known brine occurrences are in areas where the interval is thicker than estimated for the WIPP site; there may be a threshold thickness related to degree of deformation. Further analysis of this approach is warranted before concluding that this kind of information limits the probability of brine encounters under the WIPP site.

Two models of spatial correlation for brine encounters were observed: one isotropic with a range of 2500 ft and one anisotropic with a longer range of 5700 ft. We recommend conditional probabilities of encountering a brine reservoir intercept be estimated using the anisotropic model because it yields the larger estimate, though differences are small. Using the anisotropic model, the area-weighted average of estimated conditional probabilities at computational nodes located over the waste panel is 0.08.

9.0 REFERENCES

Anderson, R.Y., and Powers, D.W. 1978. Salt anticlines in the Castile-Salado evaporite sequence, northern Delaware Basin, New Mexico: Circular 159, Geology and Mineral Deposits of Ochoan Rocks in Delaware Basin and Adjacent Areas, G.S. Austin, ed., New Mexico Bureau of Mines and Mineral Resources, Socorro, NM, p. 78-83.

Bachman, G.O. 1984. Regional geology of Ochoan evaporites, northern part of Delaware Basin: Circular 184, New Mexico Bureau of Mines and Mineral Resources, Socorro, NM.

Borns, D.J. 1987. The geologic structures observed in drillhole DOE-2 and their possible origins: Waste Isolation Pilot Plant: SAND86-1495, Sandia National Laboratories, Albuquerque, NM.

Borns, D.J., and Shaffer, S-E. 1985. Regional well-log correlation in the New Mexico portion of the Delaware Basin: SAND83-1798, Sandia National Laboratories, Albuquerque, NM.

Borns, D.J., Barrows, L.J., Powers, D.W., and Snyder, R.P. 1983. Deformation of evaporites near the Waste Isolation Pilot Plant (WIPP) site: SAND82-1069, Sandia National laboratories, Albuquerque, NM.

Chaturvedi, L. 1984. Occurrence of gases in the Salado Formation: EEG-25, Environmental Evaluation Group, Santa Fe, NM.

Cressie, N. 1991. Statistics for Spatial Data. John Wiley and Sons, New York. 900 pages.

D'Appolonia Consulting Engineers, Inc. 1982. Data file report, ERDA-6 & WIPP-12 testing: Westinghouse Electric Corporation, Albuquerque, NM.

Deutsch, C.V., and Journel, A.G. 1992. GSLIB: Geostatistical Software Library and User's Guide. Oxford University Press, New York. 340 pages.

Gonzales, M.M. 1989. Compilation and comparison of test-hole location surveys in the vicinity of the Waste Isolation Pilot Plant site: SAND 88-1065, Sandia National Laboratories, Albuquerque, NM.

Griswold, G.B. 1977. Site selection and evaluation studies of the Waste Isolation Pilot Plant (WIPP), Los Medanos, Eddy County, NM: SAND77-0946, Sandia National Laboratories, Albuquerque, NM.

Holt, R.M., and Powers, D.W. 1988. Facies variability and post-depositional alteration within the Rustler Formation in the vicinity of the Waste Isolation Pilot Plant, southeastern New Mexico: DOE/WIPP 88-004, US Department of Energy, Carlsbad, NM.

Isaaks, E.H., and Srivastava, R.M. 1989. An Introduction to Applied Geostatistics. Oxford University Press, New York. 561 pages.

Jones, C.L. 1981. Geologic data for borehole ERDA-6, Eddy County, New Mexico:
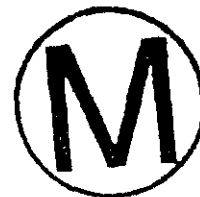
Open-file Report 81-468, US Geological Survey, Denver, CO.

Jones, C.L., Bowles, C.G., and Bell, K.G. 1960. Experimental drill hole logging in potash deposits of the Carlsbad District, New Mexico: Open-file Report 60-84, US Geological Survey, Denver, CO.

Journel, A.G. 1984. The place of non-parametric geostatistics. In G. Verly et al, eds., Geostatistics for Natural Resources Characterization, pages 307-355, Reidel, Dordrecht, Holland.

Journel, A.G. 1986. Geostatistics: Models and tools for the earth sciences. Math. Geology, v. 18, no. 1, p. 119-140.

Kehrman, R. 1994. Recent occurrences of pressurized brine in the Castile Formation: WS:94:03255, letter to W.D. Weart, Sandia National Laboratories, dated 7/20/1994. (Included as Appendix F)

Pannatier, Y. 1994. MS-WINDOWS Programs for Exploratory Variography and Variogram Modeling in 2D. In Statistics of Spatial Processes: Theory and Applications. Bari, Italy, September 27-30, 1993. V. Capasso, G. Girone, and D. Posa, eds., pages 165-170.

Popielak, R.S., Beauheim, R.L., Black, S.R., Coons, W.E., Ellingson, C.T., and Olsen, R.L. 1983. Brine reservoirs in the Castile Formation, Waste Isolation Pilot Plant (WIPP) project, southeastern New Mexico: WTSD-TME-3155, US Department of Energy, Albuquerque, NM.

Powers, D.W., and Holt, R.M. 1990. Sedimentology of the Rustler Formation near the Waste Isolation Pilot Plant (WIPP) site: Field Trip #14 Guidebook, Geological and Hydrological Studies of Evaporites in the Northern Delaware Basin for the Waste Isolation Pilot Plant (WIPP), New Mexico, D.W. Powers et al., eds., Geological Society of America (Dallas Geological Society), p. 27-32.

Powers, D.W., and Holt, R.M. 1995. Regional geological processes affecting Rustler hydrogeology: IT Corporation report to Westinghouse Electric Corporation (in review as SAND report). (Included as Appendix G)

Powers, D.W., Lambert, S.J., Shaffer, S-E., Hill, L.R., and Weart, W.D., eds. 1978. Geological characterization report, Waste Isolation Pilot Plant (WIPP) site, southeastern New Mexico: SAND 78-1596, Sandia National Laboratories, Albuquerque, NM.

Register, J.K. 1981. Brine pocket occurrences in the Castile Formation, southeastern New Mexico: TME 3080, US Department of Energy, Albuquerque, NM.

Sandia National Laboratories and D'Appolonia Consulting Engineers. 1983. Basic data report for drillhole AEC 7 (Waste Isolation Pilot Plant - WIPP): SAND79-0268, Sandia National Laboratories, Albuquerque, NM.

Sandia National Laboratories and US Geological Survey. 1983. Basic data report for drillhole ERDA 6 (Waste Isolation Pilot Plant - WIPP): SAND79-0267, Sandia National Laboratories, Albuquerque, NM.

Silva, M. 1996. Letter to P. Swift, Sandia National Laboratories, dated 3/20/1996,
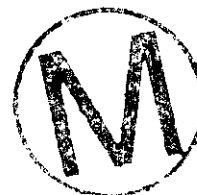
enclosing reports from petroleum companies regarding brine occurrences in selected wells. (Included as Appendix H)

Wingle, W.L., Poeter, E.P., and McKenna, S.A. 1994. UNCERT User's Guide. Colorado School of Mines, Golden, CO 80401.